ABSTRACT

Title of Dissertation:	ENGINEERING CELLULAR MICROENVIRONMENT FOR CARTILAGE REGENERATION
	Ting Guo, Doctor of Philosophy, 2018
Dissertation directed by:	Fischell Family Distinguished Professor, Department Chair and Director of NIH Center for Engineering Complex Tissues John P. Fisher, Ph.D. Fischell Department of Bioengineering

Articular cartilage defects, resulting from trauma or pathological change, affect a large population worldwide from adolescents to adults. The limited self-renewal ability of cartilage due to lack of blood vessels and cellular crosstalk makes it one of the most difficult tissues to regenerate. Common treatments to prevent the progression of critical cartilage defects involve surgical intervention such as microfracture and autologous chondrocyte implantation. Besides the time and cost involved in these clinical treatments, the quality of the regenerated tissue is not comparable to native tissue in regard to biological function; the cartilage synthesized at the defect region becomes fibrous and prone to failure over time, possibly due to the absence of required cellular microenvironment. To overcome the difficulties in cell expansion associated with chondrocytes, human mesenchymal stem cell (hMSC)

has been explored as an alternative cell source for its abundance and ability to differentiate into chondrocytes. The work presented here is aimed at recapitulating the complex microenvironment of cartilage tissue by guiding stem cell alignment and differentiation on a 3D patterned scaffold to improve the repair outcome. The first aim of this work examined cellular responses to the addition of mechanical preconditioning in an environment which incorporated signaling molecules and supporting matrices. Our developed compression-perfusion bioreactor provided a solution to enhance chondrogenic differentiation of hMSCs by providing mechanical stimulation that recapitulates the native environment. The second aim of the thesis extended the development of cellular environment to the use of 3D printed scaffold with controlled micro-patterns. During extrusion 3D printing, sheered polymer generated an organized micro-environment of aligned polymer molecules that had an impact on cell alignment and differentiation. The scaffold was then functionalized with aggrecan and applied to an in vivo model combined the standard approach of microfracture to evaluate the regenerative potential. The results demonstrated improved quality of the newly formed cartilage tissue. In this dissertation, we have investigated the cellular microenvironment that provides both mechanical and biological cues for cartilage regeneration. The acellular patterned scaffold that provides controlled cell behavior in combination with current surgical procedures will provide a cost-effective way to restore better cartilage function.

ENGINEERING CELLULAR MICROENVIRONMENT FOR CARTILAGE REGENERATION

by

Ting Guo

Dissertation submitted to the Faculty of the Graduate School of the
University of Maryland, College Park, in partial fulfillment
of the requirements for the degree of
Doctor of Philosophy
2018

Advisory Committee:
Professor John Fisher, Chair
Associate Professor Lijie Grace Zhang
Professor William Bentley
Associate Professor Ian White
Associate Professor John Cumings, Dean's Representative

Dedication

To my parents

To people who fight for their dreams like me

To people with a kind heart and try to make a better world

Acknowledgements

First of all, I would like to thank my advisor Dr. John Fisher for the opportunity to join the Tissue Engineering and Biomaterials lab, for guiding me with his wisdom and generously supporting me throughout the past five years. I would like to extend my appreciation to my committee members for their contribution in improving the outcome of this work. I am grateful to my friends and lab mates in the Tissue Engineering and Biomaterials Lab and in the BIOE department: their encouragement and friendship have made my time here bright and enjoyable. The completion of this work would be impossible without the tremendous help from all my collaborators. A special thank you to the four undergraduate researchers: Casey Lim, Timothy Holzberg, Julia Ringel, and Maeesha Noshin, who worked with me and contributed a lot in these projects. A big thank you to Dr. Feng Gao, for the 100,000 miles he drove and the technical support in programming. Lastly, I would like to thank my family and friends in China, especially my parents, who probably don't know what exactly I am doing here, for their love and care as always.

Table of Contents

List of Tables

List of Figures

Chapter 1: Introduction to Cartilage Microenvironment[1]

1.1 The Native Cartilage Niche

Articular cartilage is an elastic connective tissue that surrounds the surfaces of articulating joints. The primary function of articular cartilage is to bear the loads subjected to articulating joints during regular movement. The tissue accomplishes this function through fluid pressurization and a dense extracellular matrix (ECM) [1]. Articular cartilage is composed primarily of fluid and ECM and has a low cell content with a cellular density of less than 5% of the total tissue. The chondrocyte is the single cell type within articular cartilage, which functions to synthesize and maintain the ECM. The tissue overall is avascular, alymphatic, and not innervated. This contributes to a hypoxic metabolic environment for chondrocytes, and a limited capacity for intrinsic repair.

Collagen is the primary component of the matrix, and functions to resist compressive forces. Collagen makes up about 60% of the dry weight of the tissue, with type II collagen representing about 80% of the collagen component [1]. Due to its prevalence, type II collagen is the leading marker of the chondrocyte phenotype [2]. Other collagen isoforms are also present in the ECM, including type VI, IX, and XI. Collagens are critical to the organization of the ECM. It has been shown that mice lacking the type II collagen isoform are unable to form organized cartilage tissue, and suffer from an overall decrease in skeletal development [3]. Proteoglycans make up the second largest portion of the ECM, with a dry weight of 5-10%, followed by other non-collagenous proteins such as fibronectin, decorin, and biglycan. Aggrecan, the predominant proteoglycan present, is decorated with several types of sulfated glycosaminoglycans (GAGs), including chondroitin sulfate and keratan sulfate. Multiple

[1] Adapted from: Guo T, Ferlin K, Kaplan D, and Fisher J. Engineering Niches for Cartilage Tissue Regeneration. Book Chapter. Biology and Engineering of Stem Cell Niches: Elsevier; 2017. (531–546).

aggrecan molecules then bind to hyaluronic acid forming large aggregated proteoglycans which carry a negative charge, resulting in significant amounts of water being retained by the tissue [1, 4]. Water makes up approximately 65-80% of the overall weight of articular cartilage, and is critical to the mechanical properties of the tissue such as flexibility and viscoelasticity. GAG content allows the tissue to absorb fluid and distribute pressures during load cycles, a key factor to the overall function of articular cartilage tissue.

1.2 Zonal Organization

In addition to organization based on the distance from the cell surface, articular cartilage tissue has been divided into three zones based on tissue depth: the superficial or tangential zone, the middle or transitional zone, and the deep or basal zone [5]. The ECM organization, cell morphology, and metabolic activity of each zone are distinct and represented in **Figure 1.1**. Generally, the top 10-15% of the tissue, which contains the articulating surface, is defined as the superficial zone. The middle zone is defined as approximately the middle 60% of the tissue, and the deep zone is composed of the remaining 30% of the tissue [6]. The composition and organization of the ECM varies in each zone. The collagen content per dry weight is not significantly different in each zone; however, there are significant differences in the orientation of the collagen fibers and the number of crosslinks between collagen fibrils. It is suggested that the distinct collagen fiber orientation for each zone accounts for the depth dependent differences in stiffness and tensile strength [7]. These properties are highest in the superficial zone, and decrease with increasing tissue depth. In the superficial zone, collagen fibers are oriented parallel to the articulating surface and are found in tight bundles. This orientation provides tensile strength while also functioning to block unwanted molecules from diffusing into the articular cartilage from the synovial fluid [8]. In the middle zone, collagen fibers are oriented randomly in an arching pattern. Collagen fiber orientation shifts to become perpendicular to the articulating surface in the deep zone. The organization in the

middle and deep zones contributes to the compressive mechanical properties of these tissue zones [2, 5].

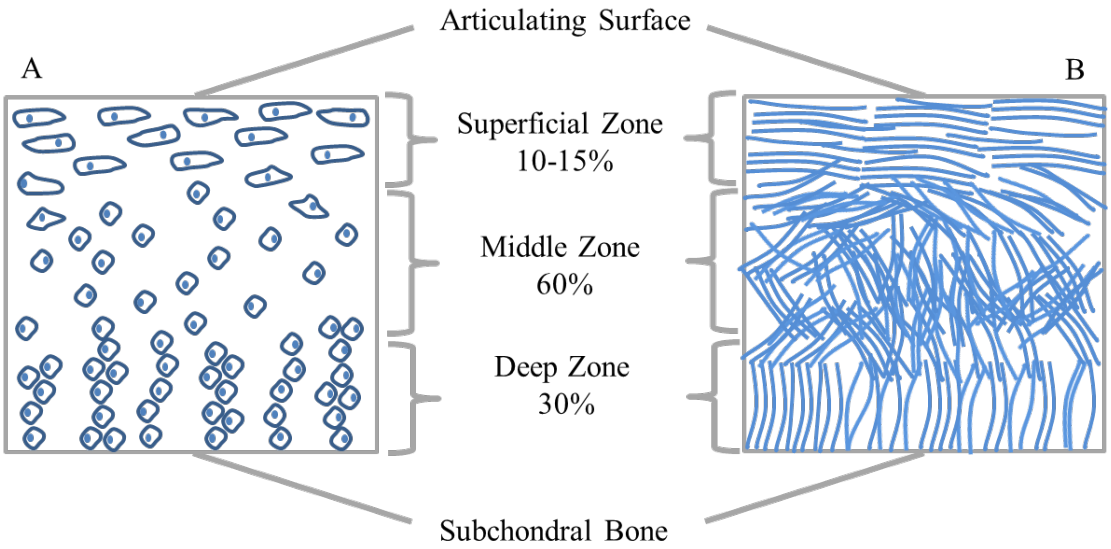

Figure 1. 1. Schematic representation of the zonal organization of chondrocytes and collagen fibers in articular cartilage. The superficial zone is the top 10-15% of the tissue volume and contains cells and fibers oriented parallel to the articulating surface. The middle zone is the middle 60% of the tissue and is marked by randomly oriented cells and collagen fibers. In the deep zone, which is the bottom 30% of the tissue, chondrocytes (A) are arranged in columns vertical to the articulating surface, and collagen fibers (B) are similarly oriented perpendicular to this surface.

There are also distinct changes in the proteoglycan content of each zone, with content increasing with tissue depth [9]. Increases in the proteoglycan content of the tissue correspond directly to increases in the compressive modulus of the tissue. Proteoglycans contribute to the hydration of the tissue, and therefore the superficial zone demonstrates the lowest water content of the tissue with approximately 65% of the water content residing in the middle and deep zones. Oxygen content also varies throughout the tissue depth, with the superficial zone containing the highest concentration of oxygen. This is likely due to the diffusion of oxygen from the synovial fluid and into the superficial zone. Concentration decreases with tissue depth, with the middle and deep zones having much lower oxygen concentrations [10].

Zonal differences in matrix organization and structure are due to variations in the cellular activity of each zone [11]. Chondrocytes in each zone differ in their morphology, density, and metabolic activity. Cells residing in the superficial zone are the smallest and occur in the highest density of the tissue. These cells have an elongated morphology and like the collagen fibrils in this zone, are oriented parallel to the articulating surface. Superficial zone chondrocytes are the predominant producer of proteoglycan 4 (PRG4), which is a large glycoprotein also known as lubricin, and contributes to the lubricating function of the synovial fluid [5]. Chondrocytes residing in the middle zone are larger and also less densely populated compared to the superficial zone. Middle zone cells do not have a defined orientation. Cells in the deep zone are similarly larger than the cells of the superficial zone, and are oriented perpendicular to the articulating surface. Deep zone chondrocytes are arranged in columns and function to anchor the articular cartilage tissue to the underlying osteochondral layer below. Unlike the cells of the superficial and middle zones which predominantly reside on their own, chondrocytes in the deep zone occur in clusters of five to eight cells [8].

Reconstruction of the zonal organization of the tissue is vital to the successful development of regenerative therapies for the repair of cartilage defects. While the importance of this structure is well understood, a majority of the current cartilage therapies treat the population as homogeneous. This has been shown to be inefficient, with the fibrous repair tissue forming after surgical interventions lacking the native zonal structure [2].

1.3 Engineering Cartilage Tissue

For cartilage engineering, it often refers to the repair of articular cartilage and the restoration of joint function. In particular, cartilage tissue has very limited ability to regenerate after

critical damage, so it brings a strong need and interest to the development tissue engineering treatments.

One way to make zonal cartilage constructs is to enrich and isolate chondrocytes from different regions [12]. After forming high density subpopulations of chondrocytes, cartilage constructs with different proteoglycan content and mechanical properties can be developed. Similarly, researchers have showed induced alignment from co-culture of MSCs with chondrocytes compared to chondrocyte-chondrocyte culture [13, 14]. Those results together suggested that the quality and sources of the cells could result in different differentiation outcomes such as matrix alignment, which is essential for forming zonal structure. For better regeneration results, highly purified subpopulations are needed with the help of zonal markers such as superficial zone protein (SZP) and developed purification procedures. However, it is also unclear if the chondrocytes would change their phenotype during the formation of 3D constructs.

Another direct method to tissue engineering zonally structured cartilage is to layer material by manipulating the hydrogel concentration in different layers. In a study using two-layer agarose gels to mimic the heterogeneity of the native cartilage, a potential to achieve zonal structure using this type of approach was demonstrated, but with concerns on the long term maintenance of the distinct zonal properties [15]. The culture conditions and the cell response can alter the original distinction of the engineered hydrogel constructs. Considering the easy crosslinking method using calcium chloride solutions, alginate is a possible candidate to form layered structures by attaching separately fabricated sheets [16]. Although these techniques show promise for the engineering of functional zonal cartilage, additional biological data and long term studies are required to better assess the possibility of these scaffolds for cartilage defect repair.

Interactions between cells and materials can influence each other. For example, cell behaviors can change the long-term properties of the scaffold material while the material can directly affect cell differentiation to generate zonally organized engineered cartilage. This allows for the use of a single source of progenitor cells to achieve this goal. For example, the addition of chondroitin sulfate (CS), matrix metalloproteinase-sensitive peptides (MMP-pep) and hyaluronic acid (HA) to PEG based hydrogels resulted in different expression of type II collagen and proteoglycans [17]. PEG:CS:MMP-pep hydrogel provided the highest levels of type II collagen expression with low expression of proteoglycans that mimics the superficial zone properties. As a comparison, a PEG:HA composite hydrogel showed high expression of proteoglycan but low expression of type II collagen, representative of the deep zone, while PEG:CS exhibited intermediate zonal properties. Correspondingly, the different compositions of hydrogels also have distinct compressive moduli that match the native cartilage properties.

The *in vivo* microenvironment is an important factor that contributes to the native cartilage structure. As a result, recapitulating the microenvironment such as oxygen levels and mechanical stimulation represents another strategy to create zonally structured cartilage tissues. One recent study developed a customized culture technique to create a gradient oxygen level for MSC chondrogenesis with additional dynamic compression to mimic the key aspects of the cartilage environment [18]. Another study demonstrated that gradient nutrient supply (e.g. glucose) also induces zonal differentiation of chondrocytes. A low glucose condition was also suggested as more suitable culture condition for chondrogenesis [19]. Results indicated that control of the microenvironment plays a role in differentiating 3D encapsulated progenitor cells to chondrocytes or modulating the chondrocyte phenotype and thus, forming depth-dependent cartilage structure.

The emerging technologies such as 3D printing will be beneficial to pursue the desired material structure to meet the physiological requirements by precisely controlling the fabrication process. The above techniques can be combined resulting in more complicated architectures with improved functional performance. Consequently, additional work is needed to optimize different conditions and detailed treatments.

Growth factors play an important role in determining the phenotype of both stem cells and differentiated cells. Considering the limited ability of cartilage tissue to self-renew, the use of growth factors as a treatment to modulate the regeneration process has been reported with positive results. In general, growth factors secreted by different cells can activate specific signaling pathways after binding to the cell surface [20]. The main drawback of the use of growth factors is their short half-life and rapid degradation once delivered *in vitro* or *in vivo*. The wide distribution of factors *in vivo* can also cause undesired reactions or cytotoxicity. The use of degradable vehicles provides a localized delivery and potentially stable release of the growth factor. In a study using natural polymer alginate as delivery vehicle for rabbit cartilage defects, the results indicated that targeted delivery to the injury site could prevent systemic side effects while improving cartilage repair compared to control group [21]. Other similar approaches have been investigated with materials such as chitosan [22] with similar conclusions; delivery using a chitosan material vehicle exhibited improved regeneration. In addition, these results pointed out that the release kinetics are influenced by the physiochemical characteristics of the encapsulated proteins. The material properties of the vehicles are critical in such applications. The process of making these protein-vehicle constructs may denature or deactivate the function of the growth factors. Despite the high expenses associated with these methods, long-term follow-up studies are needed to evaluate the safety and efficacy of treatment through growth factor delivery.

Acellular ECM that mimics the *in vivo* environment has been shown to be beneficial for both *in vitro* chondrogenesis of stem cells and cartilage regeneration in animal models. The success of acellular ECM is thought to be two-fold: first, ECM provides mechanical support for the damaged joint; and second, the similar structure may guide cell attachment, migration and behavior.

A direct approach is the use of decellularized cartilaginous or fibrocartilaginous tissue. The decellularization process can be achieved in a variety of methods. There are typically three categories of treatment—physical, chemical and enzymatic [23]. For all the methods, the purpose is to remove all of the cellular components while maintaining the integrity of the extracellular matrix. Physical processes such as thermal shock using freeze-thaw cycles and mechanical disruption are often used as an initial step prior to further processing. Chemicals such as detergents, solvents, acidic and alkaline solutions, and ionic solutions are commonly used in tissue decellularization including cartilage tissues [24]. The retention of bioactive molecules in addition to the mechanical and structural integrity make decellularized cartilage tissue an attractive strategy considering the intrinsic lack of growth factors and nutrient supply of cartilage tissues. However, the total performance of this treatment highly depends on the decellularization procedure. An insufficient decellularization process may cause severe foreign body reactions and cytotoxicity.

Another option is to use synthetic materials to mimic the ECM structure for functional cartilage tissue restoration. One way to pattern the ECM structure is to use nano-fabrication techniques, among others. For example, a low-density 3D nanofiber network composed of poly(vinyl alcohol) (PVA)-methacrylate (PVA-MA) and a composite of PVA-MA/CS-methacrylate (CS-MA) was fabricated to mimic the cartilage ECM [25] The authors hypothesized that the non-adhesive nature of PVA would reduce fibroblast invasion in vivo to

form hyaline-like cartilage, while the presence of CS would increase the expression of type II collagen. The biomimetic structure of the ECM made by synthetic polymers has a potential to solve the poor biological functions of these materials while providing desired mechanical strength in native cartilage range.

A major concern of using pure ECM treatment is the poor integration with native tissues due to a lack of cell-cell interaction. Therefore, modifications or bioactive molecules attached on ECM that help attract local cell migration and differentiation would strengthen the local regeneration. For example, the combination of ECM and growth factors as a treatment for cartilage defects has been reported. The researchers used injectable visible blue light inducible chitosan covalently conjugated with TGF-beta-1 for the regeneration of partial cartilage defects in a rat model [26]. Their results suggested that this combined therapeutic system promoted the cartilage regeneration in this challenging healing environment where limited native stem cells and growth factors are presented.

Although on some levels acellular ECM is a promising approach to treat cartilage dysfunction, the intrinsic low proliferation of chondrocytes remains a challenge for long-term success, especially for larger defects. Incorporation with native or transplanted cells is needed in many cases.

A growing field of work involves the combination of acellular biomaterials with clinical treatments such as microfracture to improve cartilage regeneration. Microfracture has been applied as a clinical treatment for decades; however, the long-term results vary significantly case to case. Often, repair tissue becomes fibrocartilaginous with increased amounts of type I collagen and decreased type II collagen. To improve upon the microfracture technique, many researchers have tried to combine the surgical procedure with the use of novel materials with

an acceptable biocompatible profile. Most of the materials are natural or contain similar components to the ECM. Applying hyaluronic acid (HA) after microfracture has been shown to promote thicker, hyaline-like cartilage compared to controls in a three-month study in rabbit model [27]. A recent stage 1 clinical trial using injected hyaluronic acid as postoperative treatment indicated improved clinical performance compared to microfracture alone [28]. Chitosan is a widely used biomaterial in tissue engineering. It is inexpensive, easy to handle and most importantly, has tunable mechanical and chemical properties. In a study combining chitosan-glycerol phosphate/blood clots with microfracture, the implants resulted in an increased filling of the defect, hyaline-like repair tissue, and restoration of normal glycosaminoglycan production [29]. There is a commercially available chitosan based matrix (BST CarGel by Piramal Healthcare), which can be mixed with whole blood to achieve improved quantity and residency of the blood clot. Alternatively, synthetic or mixed components are also popular because of their relatively low cost and tunable properties. ChonDux (Biomet) is a PEG based biomaterial that could be connected to the native tissue via biological glue such as chondroitin sulfate and is currently under clinical trials in Europe (ClinicalTrials.gov identifier: NCT01110070).

Although the mechanisms of the repair processes are not well understood, the common rationale behind the use of biomaterials in combination with microfracture is to guide the native cells and growth factors to the target sites by providing similar structures as native proteoglycans, which, in addition to collagen, can help to induce local chondrogenesis.

Therapeutic materials applied after microfracture for guided cartilage repair are also been modified with bioactive molecules such as growth factors for the purpose of improving the chondrogenic process. For example in one study, TGF-β3 infused bioscaffolds were proven to recruit significantly more cells than TGF-β free bioscaffolds [30]. However, researchers also

indicated that the addition of biologics may slow the regulatory process and result in weaker regeneration than delivery of the materials alone [31]. This might be due to the complicated cell responses occurring during the regeneration, and therefore, a fundamental understanding of the chondrogenesis process will further the combination of acellular materials and biologics such as growth factors.

Biomaterials can be modified to present biologically active signals to a cell population, including cell adhesion peptides and growth factors to facilitate cell adhesion and direct cell fate. Biomaterials are designed to mimic the ECM and local cellular environment to promote tissue infiltration and regeneration. Polymers used to make biomaterials can be naturally or synthetically derived, with natural polymers such as collagen or hyaluronic acid containing bioactive moieties to support cell attachment, proliferation, and differentiation. *In vivo* degradation rate is an important factor to consider when designing a scaffold since it affects the interactions between implanted tissues and native tissues. However, these natural materials are often hydrogels that cannot be tuned to a desired mechanical stiffness or degradation rate. Synthetic polymers such as poly (ethylene glycol) or PEG, offer the ability to control scaffold properties, but do not have any native biological activity. Synthesis techniques have been developed to incorporate biologically active domains into the structure of synthetic polymers, offering a means to control mechanical, degradation, and bioactive properties of the overall biomaterial scaffold.

The adsorption of ECM proteins onto the surface of biomaterials is one of the simplest means to improve cell attachment to a biomaterial, and is often employed as a means to combine synthetic and natural polymers [32, 33]. In addition to adsorption, bioactive molecules and growth factors can be covalently tethered to a material surface. A commonly used polymer for surface modification through covalent tethering is PEG, as it is known to resist cell

adhesion in its unmodified form and can be considered a “blank slate” prior to surface modification. PEG based polymers have been used extensively to control the interaction between chondrocytes and differentiating MSCs with the underlying material substrate, with results indicating that the inclusion of ECM molecules and growth factors contributes to increased mechanical properties, ECM deposition, and expression of cartilage-specific markers [25, 34, 35]. Sridhar et al. [34] functionalized PEG hydrogels with the growth factor TGF-β1, a known inducer of chondrogenesis. Chondrocytes encapsulated within modified hydrogels exhibited increased levels of DNA, GAGs and collagen over a 28 day culture period compared to samples that received soluble delivery of the growth factor in the media. PEG hydrogels have also been modified with matrix metalloproteinase (MMP) sensitive sequences to encourage scaffold degradation as a function of cell activity. MMPs are enzymes known to participate in the remodeling of the articular cartilage ECM, and therefore sequences sensitive to the activity of MMPs would be degraded as cells infiltrate and remodel the implanted material. PEG norbornene gels modified to include TGF-β1 and crosslinked with MMP cleavable sequences resulted in significant increases in GAG and collagen production following 14 days of coculture between MSCs and chondrocytes. Compared to non-degradable gels, MMP degradable hydrogels showed increased amounts of matrix deposition [36]. Recently, aggrecanase sensitive PEG hydrogels have been fabricated using similar methods and show sensitivity to aggrecanase over culture time and promotes the formation of hyaline-like cartilage tissue [37].

In addition to the use of PEG based hydrogels as a means to tailor the interactions between cells and materials, modified nanofibers have also been developed as a means to increase the ECM production and gene expression of cells seeded on the material surface. Coburn et al. [25] showed that the combination of PVA nanofibers with chondroitin sulfate nanofibers resulted in a significant increase in ECM deposition over the micromass pellet control, with modified

nanofiber scaffolds producing the highest levels of type II collagen *in vitro* and *in vivo*. Self-assembling nanofibers have been used as a means to promote *in vitro* chondrogenesis through surface modification with TGF-β1 binding epitopes [38].

Surface modification of natural polymers has also been utilized to promote cartilage tissue regeneration. Chawla et al. [39] showed that single amino acids of a saccharide based peptide copolymer could be modified to increase the modulus of the resulting cell-biomaterial construct following the induction of chondrogenesis. The modulus of the resulting tissue was also significantly upregulated in chitosan modified poly l-lactide-co-ε-caprolactone (PLCL) scaffolds when compared to unmodified scaffolds, with chitosan modified scaffolds resulting in double the modulus of the unmodified counterpart [40].

Finally, combinatorial modification of scaffolds has been shown to produce increased cartilage matrix production compared to single modification alone. The inclusion of the ECM proteins hyaluronic acid and chondroitin sulfate alone or in combination with the adhesion motif RGD was investigated by Kim et al. [41], showing that the combination of chondroitin sulfate and RGD resulted in the greatest degree of DNA, GAG, and collagen accumulation, while also promoting the production of lubricin, a key component of the superficial zone of articular cartilage. Similarly, the combination of mechano growth factor, or MGF with TGF-β3 on embedded silk fibroin scaffolds resulted in the combination group exhibiting a 1.8 fold increase *in vitro* and a 2 fold increase *in vivo* in type II collagen and aggrecan production compared to the TGF-β3 alone group [42].

A widely used natural material in tissue engineering area is chitosan, which originates from the exoskeleton of crustaceans. Its superior tunable material properties make it a popular material choice for scaffolds in cartilage tissue repair. Biologically, besides its high

compatibility, the similar structure to glycosaminoglycans attracts cells and growth factors, similar to the function of proteoglycans in native tissues. The cationic nature of chitosan makes it possible to trap anionic GAGs linked with biomolecules by electrostatic interactions [43]. Mechanically, the degradation rate and pore size could also be tuned during processing [44]. Chemically, the cationic nature of chitosan allows it to form insoluble composite with many anionic polymers [45]. Available amine groups facilitate the formation of composite scaffolds or copolymers with other natural materials such as HA [46], collagen [47], agarose and gelatin [48] and even synthetic materials such as poly(ε-caprolactone)[49]. The superior gelation property also gives the possibility to make injectable therapeutic materials [50, 51], which is beneficial for clinical applications to simplify the surgical procedures. One of the major concern of chitosan for cartilage regeneration is the low degradation rate *in vivo* will cause poor interactions with native tissues. Chemically modified chitosan with improved degradation properties has also been explored to solve this problem [52].

Alginate is a highly biocompatible material that has been used for cartilage tissue engineering for years. One of the unique characteristics of alginate is that it crosslinks in the present of calcium ions which makes it very easy to encapsulate cells and maintain their viability. The cells cultured in 3D alginate scaffolds can maintain good viability and phenotype [53]. By adding EDTA to sequester calcium ions, the scaffolds can be readily dissolved to retrieve cells. The major disadvantage is weak mechanical properties, in addition to a loss in scaffold integrity in regular cell culture media because calcium ions diffuse away during culture [54]. However, complete degradation *in vivo* still takes a significant amount of time, which may result in a negative effect on the regenerated tissues. As a relatively well understood material with multiple crosslinking possibilities, cartilage tissue engineering using alginate has been expanded to incorporate other advanced techniques for better repair outcome. For example, the use of a microfluidic device to produce highly organized 3D alginate scaffolds showed

improved chondrocyte proliferation and differentiation results [55]. This technique was also investigated *in vivo* using a mouse model showing upregulated type II collagen expression after two weeks in a follow up study [56].

Similar to alginate, agarose is another polysaccharide derived from seaweed that has been well characterized as a basic tissue engineering scaffold candidate. It has a gelling temperature of 34–38 °C and a melting temperature of 90–95 °C. Agarose also exhibits poor *in vitro* degradation properties, losing matrix integrity over time due to the loss of thermal factors through temperature change [57]. However, *in vivo*, agarose is not degradable in the physiological environment, which may cause undesired immune responses. Agarose alone has very limited ability to treat cartilage defects, but the continuous structure of agarose can deliver the mechanical stimulation in dynamic culture to the encapsulated cells to help maintain extended differentiation [58]. Recently, to overcome the disadvantages of using single agarose material, researchers have broadened their views on the combination of agarose and other materials.

Hyaluronan (also called hyaluronic acid) (HA) is a widely used anionic, nonsulfated glycosaminoglycan in chondrogenic applications as it also presents in native cartilage tissues and might contribute to cell behaviors [59]. It can be modified with methacrylic anhydride and photopolymerized into networks with a wide range of physical properties such as degradation rate and mechanical behavior [60]. The bioactive functions on chondrogenesis and unique nonsulfated properties makes HA possible for injectable clinical treatment, which has been applied for years [61].

Aqueous-derived silk fibroin is another natural material that has been reported to promote cell attachment, proliferation and differentiation in serum free media with additional TGF-β1 [62].

Briefly, when used to generate cartilage tissue engineered construct, the silk fibroin solution is first prepared from *Bombyx mori* silkworm cocoons. Then a salt leaching process is followed to create a porous structure [63]. The results also demonstrate a relatively high expression of type II collagen and chondrogenic genes compared to other materials. Notably, different extraction processes and concentrations can affect the resulting properties of silk fibroin and thus influence cell proliferation and matrix formation [64]. Another unique advantage of silk hydrogel scaffolds is improved mechanical support compared to other common natural materials such as agarose and alginate [64]. Silk fibroin can also been conjugated with other materials to form composite functional materials. For example, silk fibroin/chitosan blended scaffolds were introduced to provide ideal cell attachment and proliferation as well as similar structures as glycosaminoglycans, which are crucial for cartilage repair [65].

Compared to natural materials, synthetic biomaterials allow the researcher to modify physical and chemical structures to achieve known and controllable properties such as degradation rate, mechanical strength and porosity.

Poly-glycolic acid (PGA) is one of the most commonly demonstrated and used materials in cartilage tissue engineering. The degradation rate of PGA is relatively high, as compared to other synthetic biomaterials, with an expected *in vivo* residence time ranging from 4-12 months[66]. In terms of cartilage repair, mesh forms are usually used [67] to obtain highly porous structure that allows better nutrient transfer to the encapsulated cells. However, this design can cause weak mechanical properties. In a study using chondrocytes seeded onto PGA scaffolds for *in vivo* cartilage regeneration, new ECM produced by seeded chondrocytes acted as a cover to the original PGA fiber, preventing rapid degradation by the host tissue. Additionally, chondrocyte-seeded PGA scaffolds caused decreased inflammatory response

compared with non-seeded scaffolds, most likely due to seeded PGA scaffolds causing fewer degradation products which might cause local PH change and thus immune responses [68].

Another polyester that is being widely applied for tissue engineering strategies is poly-lactic acid (PLA), which has also been used in several different FDA approved or cleared devices. Its degradation products can be absorbed by the human body. The degradation of PLA is slower than PGA, which causes less inflammatory response, but the decreased mechanical properties when making highly porous PGA scaffolds still exists in such applications. A study suggests that the chondrocytes initially adhere more readily on the PGA surface compared to PLA although the final proliferation remains similar [69]. PLA has also been explored as a base material to combine with natural polymers such as collagen and chitosan to make hybrid scaffolds. With improved mechanical properties while adding additional cell attachment and invasion abilities, hybrid scaffolds are potentially more promising than those made by pure materials.

The copolymer poly(lactic-co-glycolic acid) or PLGA made of PGA and PLA monomer was developed to achieve tunable degradation rates combining the advantages of the two polymers. The hybrid scaffold composition determines not only the mechanical properties, but also cell responses such as adhesion and proliferation. It was reported that high PGA ratio would result in improved chondrocyte attachment and maintenance of a rounded shape [70]. A recent publication found that microtubular oriented PLGA can induce a more homogeneous structure and thicker cartilage formation *in vivo*. Briefly, microtubular oriented PLGA can be formed through a freeze dry process [71]. Together with other studies on the chondrogenesis effect caused by the microstructure of the material [72], the orientation and detailed structures of the scaffolds should be considered to develop biomimetic tissue engineered cartilage. The

tunable properties and well-characterized science behind PLGA makes it a good choice for further studies on specified material modifications.

Poly-caprolactone (PCL) based materials show improved mechanical integrity compared to PGA/PLA biomaterials with a longer degradation period, up to a few years. This will allow time for the regeneration of native tissues. An important application of PCL is the formation of nanofiber structured meshes, which can be achieved by using electrospinning techniques [73] or lyophilizing a water–dioxane–PCL solution to created micro and nano-pores [74]. The nano-structured PCL exhibited higher expression of chondrogenic markers *in vitro* and a higher histology score *in vivo* in comparison to a collagen based scaffold Chondro-Gide®.

Since biocompatibility and cell behavior are major concerns when using synthetic materials for regenerative medicine, materials that exhibit superior biological functions are being explored to solve these questions. The most common example is poly-ethylene glycol (PEG). Its high hydrophilicity prevents growth factors and proteins from being attracted by the material that could potentially cause immune response [75]. This advantage makes PEG very popular in combining with other materials to form composite structure. For PEG based gels, the degradation rate can be controlled and has been proven to affect the neo-cartilage growth. One study used non-degradable poly(ethylene glycol) dimethacrylate (PEGDMA) and a degradable triblock copolymer, poly(lactic acid)-b-poly(ethylene glycol)-b-poly(lactic acid) with acrylate end groups to fabricate a PEG hydrogel with tunable degradation rates by varying the weight percentage of the two macromers [76]. Gels with increased degradation rate resulted in higher type II collagen synthesis. Other tunable materials properties such as the crosslinking density of photocrosslinkable PEG also plays a role in chondrocyte morphology [77]. With more promising mechanical properties close to native cartilage, PEGDMA with

human chondrocytes has been considered to use for direct cartilage repair combining the 3D printing technology [78].

Considering that native cartilage is composed of more than one material, composite materials have become more and more popular in recent years to better functionally restore the damaged cartilage. In one study, porous elastomeric poly L-lactide-co-e-caprolactone (PLCL) was generated and crosslinked at the surface to chitosan [40]. Chitosan-modified PLCL showed improved chondrogenesis and an increased modulus of cartilage tissue. Increased expression of phenotypic markers and cell compatibility was also improved compared to unmodified PLCL. Research of this nature provides insight into the potential of combining natural and synthetic materials. Through combination fabrication technologies, we can compensate for the disadvantages of each material type while highlighting and maintaining the intrinsic advantages.

1.4 Dissertation Work Overview

In general, as stated by Langer et al., tissue engineering applies the principles of engineering and life sciences toward the development of biological substitutes that restore, maintain, or improve tissue function [79]. It requires the combination of biomaterials, cells, chemical factors and engineering methods to reach a solution for clinical problems.

Specifically, the aims of this work are as follows:

(1). Investigate the cellular responses to different culture conditions and mechanical stimuli.

a. Develop a compression bioreactor system with real time sensor to test the mechanical conditions

b. Evaluate the cell proliferation and differentiation potential in response to different culture conditions

(2). Design and fabricate a cartilaginous scaffold that mimics the complex structure of native cartilage

a. Exam the material composition and printing conditions for high resolution scaffold fabrication using extrusion-based 3D printing technology

b. Investigate the cell alignment and the induced cellular function on 3D micropatterned scaffold

(3). Establish a new treatment that combines microfracture with our bioactive scaffold to enhance the *in vivo* cartilage tissue regeneration

a. Characterize the aggrecan functionalization and evaluate the cell adhesion *in vitro*

b. Demonstrate the therapeutic effect of the scaffold in a lapine cartilage defect model

Chapter 2: Human Mesenchymal Stem Cell Proliferation and Chondrogenic Differentiation: Effect of Culture Conditions and Mechanical Stimulations[2]

2.1 Introduction

Articular cartilage formation begins in the mesenchyme with the condensation and differentiation of mesenchymal stem cells (MSCs) into pre-chondrocytes. Although autologous chondrocytes transplantation (ACT) has been clinically used as an advanced clinical treatment, healthy cartilage tissue is often very limited in human bodies. In this case, chondrocytes are harvested in an initial surgery from intact cartilage tissues that come from non-weight bearing parts of the joint [80], so the availability of autologous chondrocytes is further limited considering secondary osteoarthritis may develop as a result of the tissue removal. Recently, mesenchymal stem cells (MSCs) have been considered an attractive cell source for cartilage engineering. In addition to their availability and well documented isolation protocols, implanting undifferentiated MSCs may result in a better integration with *in situ* differentiated chondrocytes when compared to the implantation of differentiated chondrocytes[81-83]. MSCs are found in multiple tissues throughout the body including the bone marrow, adipose tissue and the synovial membrane.

However, the use of human MSCs (hMSCs) is limited as studies have shown the reduced formation of extracellular matrix, which is a major contributor to the mechanical function of cartilage. To improve upon current methods, mechanical stimuli can be introduced to

[2] Adapted from: Guo T, Yu L, Lim C, Goodley A, Xiao X, Placone J, Ferlin K, Nguyen B, Hsieh A, Fisher J. Effect of Dynamic Culture and Periodic Compression on Human Mesenchymal Stem Cell Proliferation and Chondrogenesis. Annals of Biomedical Engineering 2016;44(7):2103-2113.

engineered tissues to better mimic the natural environment of articular cartilage and to induce differentiation of MSCs in 3D scaffolds[84, 85].

It is well known that native articular cartilage is exposed to mechanical stimuli such as dynamic compression, fluid shear, and hydrostatic pressure. Considering the mechanical function of articular cartilage which transmits and distributes loads in joints, proper mechanical stimulation plays an important role in altering cell response for *in vitro* tissue culture [86]. Our laboratory previously developed a tubular perfusion system (TPS) that creates a dynamic environment for cell culture [87]. In this system, cells are encapsulated in 3D scaffolds and cultured in a tubular growth chamber. Nutrient and oxygen supply can be enhanced by perfusing media through the scaffolds. Concurrently, cells at the interface of the applied flow are exposed to shear forces. Previously published studies have demonstrated an improvement in osteogenic differentiation using the TPS. However, the influence of the TPS bioreactor on chondrogenic differentiation of MSCs still remains unclear [88]. To recapitulate the native mechanical environment that facilitates chondrogenesis, we have recently developed a new approach wherein both shear and compressive forces are applied to an engineered 3D cell-scaffold construct. Our design incorporates a metal roller, which applies mechanical compression in combination with the dynamic culture conditions provided by the TPS. The overall goal of this study is to develop an advanced *in vitro* chondrogenesis protocol with proper chemical and mechanical stimulation. We hypothesize that our compression perfusion bioreactor would enhance chondrogenic differentiation by providing mechanical stimulation that mimics the *in vivo* environment. There are three main objectives to comprehensively examine the proposed hypothesis. First, to evaluate the effect of dynamic culture on hMSC proliferation. Second, to evaluate the effect of dynamic culture on hMSC chondrogenic differentiation. Third, to evaluate the influence of an additional, periodic compression on hMSC differentiation.

2.2 Materials and Methods

2.2.1 hMSC Encapsulation and Culture

Primary hMSCs were purchased (Lonza) and expanded in a monolayer in high glucose Dulbecco's Modified Eagle Medium (DMEM) (Life Technologies) containing 0.1% penicillin/streptomycin (Life Technologies), 0.1 mM non-essential amino acids (Life Technologies) and 10% fetal bovine serum (Life Technologies). After two passages, hMSCs were trypsinized (Life Technologies) and counted using trypan blue staining and a hemocytometer. Two percent (w/v) alginate was prepared using protocols previously established by our laboratory [89]. Briefly, 2.0% (w/v) of alginic acid sodium salt from brown algae (Sigma-Aldrich) was dissolved in a 0.15 M sodium chloride and 0.025 M HEPES (Sigma-Aldrich) buffer, and then autoclaved and filtered for sterilization. The alginate solution was mixed with hMSCs (3 million cells/mL) and injected through a 21-gauge syringe into 0.1 M calcium chloride (Sigma-Aldrich) solution to induce crosslinking for 15 min. The diameter of the formed alginate spheres was approximately 2.5 mm. Alginate scaffolds encapsulated with hMSCs were loaded into the TPS bioreactor and cultured in chondrogenic media. Chondrogenic media contained: high glucose DMEM, 40 mg/mL proline (Sigma-Aldrich, St. Louis, MO), 0.1% penicillin/streptomycin (Life Technologies), 0.1% sodium pyruvate (Life Technologies), 50 mg/mL ascorbate 2-phosphate (Sigma-Aldrich, St. Louis, MO), 0.1 mM dexamethasone, 1% ITS+ premix (BD Biosciences, Bedford, MA), and 10 ng/ml TGF-β3 treatment (R&D systems, Minneapolis, MN).

The TPS bioreactor was set up as described previously [87]. Media flow was driven by an L/S Multichannel Pump System (Cole Parmer, Vernon Hills, IL) at a flow rate of 1 mL/min. The

media was changed every three days. For the study comparing static and dynamic culture, alginate scaffolds were fabricated and divided into two groups, one cultured in a petri dish (Fisher Scientific) and the other in TPS bioreactor. For the compression study, alginate scaffolds (N = 50-55) were loaded into five 12 cm growth chambers for collections at different time points. All scaffolds with encapsulated hMSCs were exposed to dynamic flow until the end of each time point. Scaffolds cultured for 7 days in one chamber were collected as a baseline for future assays. Two of the chambers were introduced to additional compression (group 1) while the other two were under dynamic culture only (group 2). The cyclic pressure was applied at 0.5 Hz frequency [90] . At each time point, hMSCs were isolated from alginate scaffolds by dissolution in ethylenediaminetetraacetic acid (EDTA) for 20 min at 37^{o}C. A cell pellet was formed by centrifugation and used for subsequent analyses.

2.2.2 Pressure Sensor Fabrication and Bioreactor Set-Up

Custom Fabry-Perot pressure sensors were constructed by adapting fabrication methods previously established [91]. A length of fiber optic cable (OD = 150 μm) was spliced at one end to a capillary tube (ID = 30 μm, OD = 150 μm) ensuring the fiber core was aligned with the hollow center of the capillary. The spliced capillary was cleaved approximately 15 μm from the fiber interface and a 500 nm thick, UV curable polymer layer was added to the freshly cleaved capillary thereby enclosing the capillary cavity. A titanium metal layer was sputtered onto the surface of the cured polymer to complete a flexible, water-resistant diaphragm atop the capillary cavity (**Figure 2.4A**). Pressure changes at the capillary terminus cause the diaphragm to mechanically deflect allowing for changes in cavity length to be recorded to quantify pressure at the sensor tip. All sensors were calibrated with a reference pressure gauge (SSI Technologies Inc, Janesville, WI) in a custom calibration chamber. A fiber optic system (USB-4000 Spectrometer and HL-2000 Light Source, Ocean Optics, Dunedin, FL;

Beam Splitter, Gould Fiber Optics) was used to record cavity length data at a frequency of 14.3 Hz in LabView 2012 (National Instruments, Austin, TX). Signal optimization and processing were completed using MATLAB R2012b (MathWorks, Inc., Natick, MA).
The TPS bioreactor was set-up as described previously [87]. Particularly, for the compression study, a customized metal roller was manufactured to apply cyclic compressive force onto tubular chambers that were confined in the supporting box (**Figure 2.3A**). We utilized a 3D printed reducing connector to connect the growth chamber to the supply line. Into this connector, we inserted the pressure sensor with a 21-gauge needle as a guide to insert the probe 1.5 inches from the connector into an alginate scaffold.

2.2.3 DNA Isolation and Quantification

Total hMSC DNA was isolated from scaffolds (alginate beads) using a DNeasy Blood and Tissue Kit (Qiagen, Frederick, MD). A Quant-iT PicoGreen dsDNA Assay kit (Life Technologies) was used to quantify DNA following the manufacturer's protocol. Total DNA was calculated as ng/bead.

2.2.4 RNA Isolation and qRT-PCR

The total RNA was isolated from the hMSCs using an RNeasy Plus Mini Kit (Qiagen, Frederick, MD) and then reverse transcribed to complementary DNA (cDNA) using a High Capacity cDNA Archive Kit (Life Technologies). Quantitative reverse transcriptase-polymerase chain reaction (qRT-PCR) was performed by combining the cDNA solution with a Universal Master Mix (Life Technologies), as well as oligonucleotide primers and Taqman probes for Sox 9, type I collagen (COL1A1), type II collagen (COL2A1), aggrecan (AGC), and the endogenous gene control glyceraldehyde 3 phosphate dehydrogenase (GAPDH; Life Technologies). The reaction was performed using a 7900HT real-time PCR System (Applied Biosystems) at thermal conditions of 2 min at 50°C, 10 min at 95°C, 40 cycles of 15 s at

95°C, and 1 min at 60°C. The relative gene expression level of each target gene was normalized to the mean of GAPDH in each group then the fold change was determined relative to the day 7 pre-culture gene expression in the bioreactor without compression. Fold change was calculated using the ΔΔCT relative comparative method as described previously [92]. Samples were completed in technical triplicates and mean ± standard deviations are reported.

2.2.5 Immunohistochemistry

Samples were fixed in 4% Paraformaldehyde on slides for 10 minutes. After washing, samples were blocked and then stained with the primary antibodies to detect Type I collagen, aggrecan or Type II collagen (Abcam, Cambridge, MA), respectively. Secondary antibodies were conjugated to Alexa488 or Alexa568 (Molecular Probes). Nuclei were visualized with of 200 μg/L DAPI (4′, 6-diamidino-2-phenylindole, dilactate) stain. Sections were mounted in Fluorescent Mounting Medium (DakoCytomation), and photographed using an Axioskop mot plus microscope (Zeiss, Thornwood, NY) with a digital camera (Axiocam) and Openlab software.

2.2.6 Live-Dead Assay

In order to assess cell viability, a live-dead assay was performed following standard protocols. The whole scaffolds were soaked in Hank's buffered saline solution (HBSS, Life Technologies) for 10 minutes to remove extra media and other active reagents. The beads were then incubated in a 2 μM ethidium homodimer and 4 μM calcein AM (Life Technologies) combined with HBSS for 30 minutes in the dark. The whole scaffold was visualized via fluorescence microscopy (Axiovert 40 CFL with filter set 23; Zeiss, Thornwood, NY) using a digital camera (Diagnostic Instruments 11.2 Color Mosaic, Sterling Heights, MI).

2.2.7 Histochemical Staining

All samples were collected and fixed in 4% paraformaldehyde in 0.1 M sodium cacodylate buffer containing 10 mM $CaCl_2$ (pH 7.4) for 4 h at room temperature and then transferred to 0.1 M sodium cacodylate buffer with 10 mM $CaCl_2$ (pH 7.4) for 24 h at room temperature to re-crosslink alginate. Then samples were dehydrated through a series of ethanol washes followed by two Citrisolv (Fisher Scientific, Pittsburgh, PA) washes. The samples were embedded in Paraplast X-tra Paraffin (Fisher Scientific) and sectioned to 5mm thick sections and placed on positively charged glass slides (Fisher Scientific). Prior to staining, sections were oven-dried at 37ºC for 2 h, deparaffinized in Citrisolv, and rehydrated in decreasing ethanol washes. Samples were stained using Alcian blue (Poly Scientific, Bay Shore, NY) for 30 min, followed by standard washes. Samples were counterstained under nuclear fast red (Poly Scientific) for 5 min. After dehydration and clearance, the slides were mounted and imaged.

2.2.8 Statistical Analysis

Data from all the studies were analyzed using analysis of variance and Tukey's multiple-comparison test. A significant level of 95% was chosen, and a p-value less than 0.05 was considered to indicate a significant difference between samples.

2.3 Results

DNA quantification of hMSCs in dynamic culture and static culture was performed to determine the effect of the TPS bioreactor on cell proliferation. By day 2, the total DNA content per scaffold in the dynamic group increased 2.7 fold in the dynamic group compared to the static group. For all remaining time points, hMSCs proliferation in the dynamic group

was statistically greater than that observed in static controls (**Figure 2.1A**). Fluorescent images showing viability of the whole scaffolds were obtained, and the majority of the cells appeared viable in both groups (**Figure 2.1B**). The cell distribution in dynamic group on day 21 appears more spatially homogenous than those in static groups. The increased cell numbers seen in the live dead assay of scaffolds under dynamic culture was consistent with the DNA quantification results.

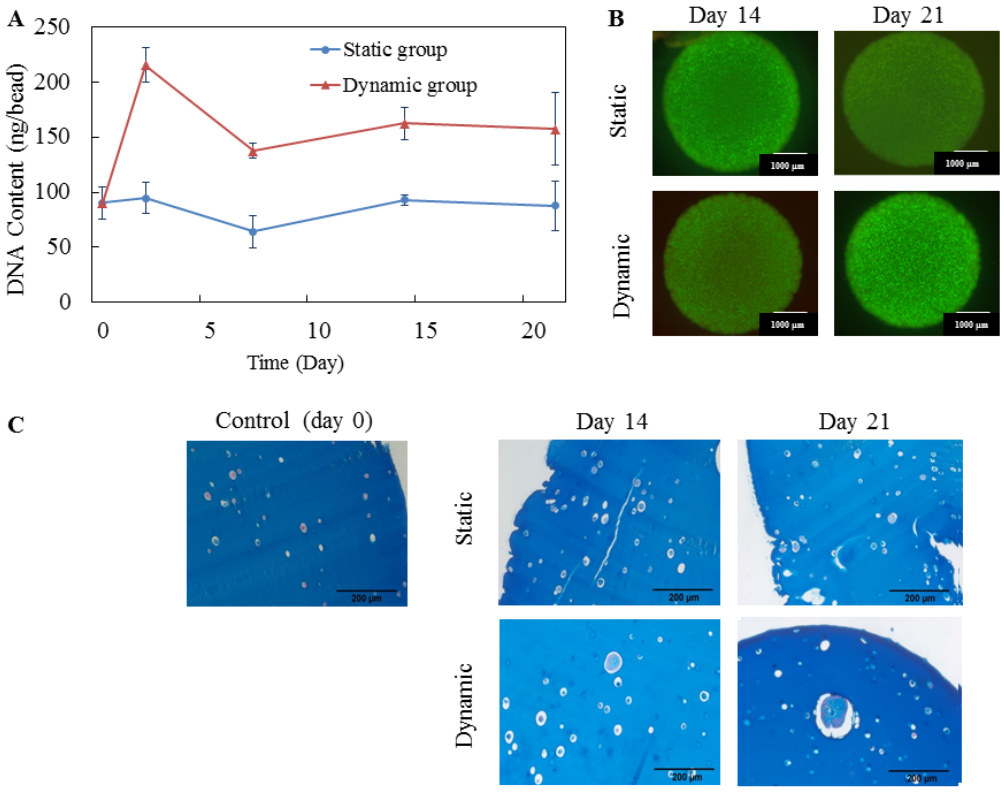

Figure 2. 1 . hMSC Proliferation and Proteoglycan Expression In TPS. A. The DNA contents in static and dynamic culture based on DNA quantification from PicoGreen assay. The cell population remained higher in the dynamic group than static group throughout the study. N=3. B. Live-dead images of beads in static and TPS culture throughout the study. The merged images showed that the majority of cells appear viable in all groups on each time point. All scale bars represent 1000 µm. C. Alcian blue staining of hMSCs in static and dynamic groups. Cell nuclei stain pink, and acidic GaG residues stain a light blue color (alginate scaffold stains a dark blue). After day 14, the lighter blue extracellular matrix was observed both groups with higher expression in the static group. All scale bars represent 200 µm.

Alcian blue staining was used to demonstrate the produced ECM contained glycosaminoglycans (GAGs). In these images, the nuclei and cytoplasm of the cells appear pink, while the GAGs appear light blue (the alginate stains a dark blue color). Increased GAGs production in both groups was observed after day 14, apparent by increased levels of light blue stain surrounding the cell nuclei. From the results, we noted an overall increased presence of GAGs in the static group. Additionally, hMSCs proliferated into large cell clusters in the dynamic group towards later time points (**Figure 2.2C**).

We also analyzed the gene expression of chondrogenic phenotype markers by the hMSCs in the dynamic and static groups at each time point. In general, three positive markers, aggrecan, type II collagen, and Sox 9 genes were expressed at higher levels in the static group when compared to the dynamic group (**Figure 2.2A**). On day 7, a burst of aggrecan and Sox 9 was observed in the static group and then was maintained at a similar level throughout the study. However, chondrogenic markers expression was not significantly increased in the dynamic group. Type I collagen is a negative marker of chondrogenic phenotype. For both groups, the expression of type I collagen decreased on day 2, but increased to the original level during the later time points in the static group.

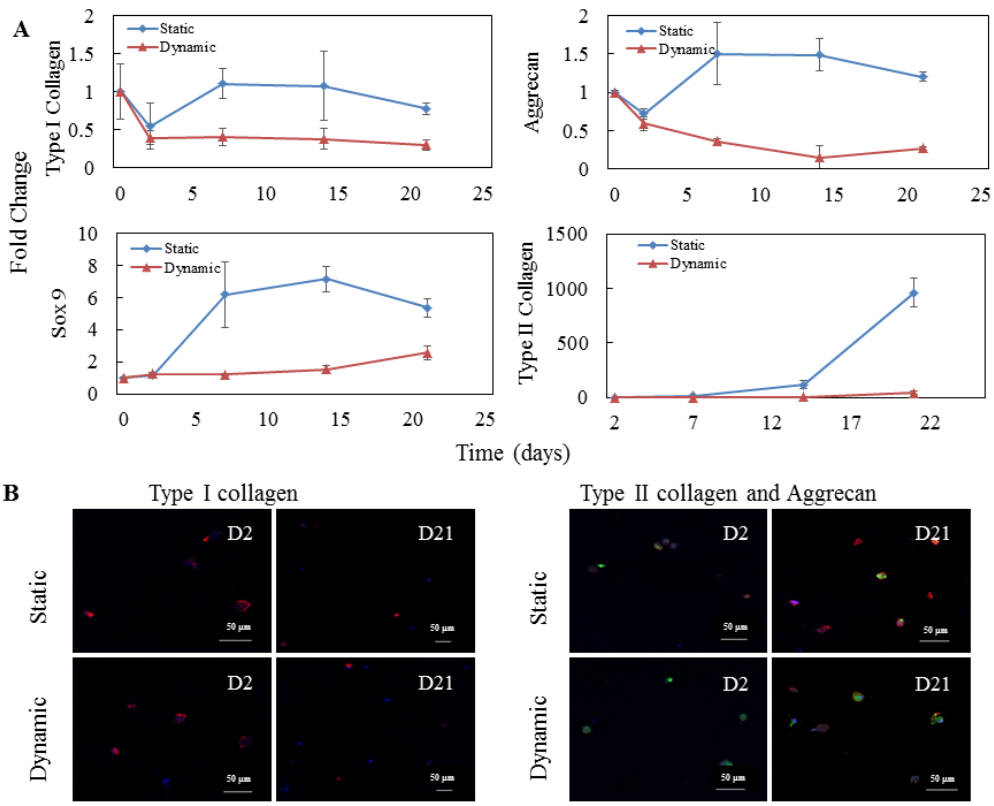

Figure 2. 2 mRNA Expression and Protein Expression of Chondrogenic Phenotype Markers. A. mRNA expression of positive chondrogenic markers including aggrecan, sox 9 and type II collagen. Type I collagen is a negative marker for chondrogenesis. For all genes, the expression level in static culture condition was higher than dynamic culture.* All samples were reported as average from technical triplicates plus standard deviation, although a few error bars were too small to visualize. All gene expressions were first normalized based on GAPDH, then normalized to the first time point. B. Fluorescent immunostaining for chondrogenic phenotype markers. Type I collagen expression decreased during culture in both groups while aggrecan and type II collagen expression increases. Both aggrecan and type II collagen showed higher level in static group compared to dynamic group. All scale bars represent 50 μm.

Immunostaining for type II collagen, type I collagen, and aggrecan in both groups was performed to evaluate expression at the protein level. The staining of type I collagen in both groups decreased in apparent expression with time, indicating chondrogenic differentiation was maintained throughout the study (**Figure 2.2B**). In agreement with the gene expression results, more intense type II collagen staining (red) was observed in static group on day 21 although both groups showed an increase of protein expression compared to the previous time

point. The aggrecan expression (green) in both groups appeared similar for all time points (**Figure 2.2B**).

The preliminary results brought us to the next set of experiments to investigate if the addition of compressive force could be beneficial to chondrogenic differentiation of hMSCs in the TPS bioreactor. The pressure changes while the roller moves across the tubular growth chamber and a peak pressure appears when the roller move onto the target scaffold containing the pressure sensor (**Figures 2.3A and 2.3B**). We recorded the peak pressure in each cycle and calculated the average peak gauge pressure at different conditions (**Figure 2.3B**). The pressure caused by dynamic flow was not detectable by the sensor. The addition of compressive force by the metal roller applied a peak pressure of 6813 ± 2195 Pa onto the scaffold and the encapsulated cells during movement.

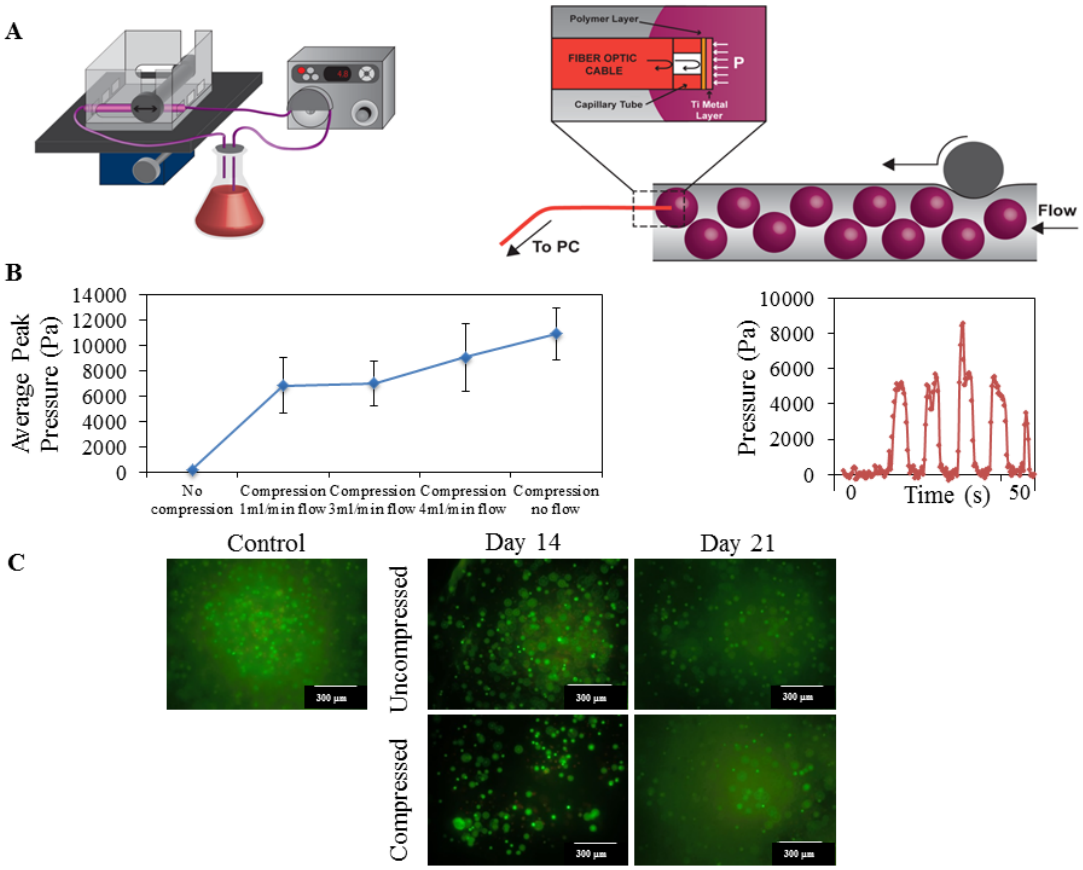

Figure 2. 3. Dynamic Compression TPS Bioreactor Set-Up and Results. A. Bioreactor assembly, the roller moves at a controlled speed provided by the rocker. The right picture shows the pressure detection experimental set up with a close look of the detailed sensor design. **B**. Gauge pressure measured inside the alginate scaffolds. The left figure shows the detected peak pressure at different conditions. Only the pressure change caused by compression was detectable. The right figure shows real time sensor response. A peak pressure appeared during each cycle of compression. **C**. Live-dead images of beads in static and TPS culture throughout the study. The bead cultured in dynamic flow for 7 days was taken as a control. The merged images showed that the majority of cells appear viable in all groups on each time point. All scale bars represent 300 µm.

A Live/Dead assay was used to investigate the hMSC viability under the combined mechanical stimuli including shear force and compressive force. The hMSCs cultured in the TPS bioreactor for 7 days in the presence of TGF-β3 were considered as a control group for the entire study. No significant difference of the cell viability was observed when applying additional compression to the encapsulated cells compared to the 7 days pre-culture control and the dynamic group (**Figure 2.3C**).

Gene expression of chondrogenic phenotype markers by the hMSCs in the uncompressed dynamic group and compression groups was analyzed (**Figure 2.4A**). To prevent unexpected cell apoptosis under mechanical loading, all hMSCs were culture in static environment for 7 days to allow for ECM production before loading. So the gene expressions in this study were specifically normalized to day 7. Sox 9 and aggrecan gene expression in the compression group significantly increased 15 fold and 7 fold on day 14 compared to day 7 pre-culture, respectively. Both Sox 9 and aggrecan expression remained low throughout the study for the uncompressed dynamic group. On day 21, the aggrecan gene expression decreased in the compressed group compared to day 14. The expression of Sox 9 maintained similar levels as day 14 until the last time point in the compressed group. We observed a delay of type II collagen gene expression in the compressed group during the study such that on day 14, the expression was higher in the uncompressed dynamic group compared to compressed group. However, on day 21, while the uncompressed group experienced a significant decrease of type II collagen expression, hMSCs exposed to mechanical compression showed an increasing trend when compared to the previous time point. Sox 9, type II collagen, aggrecan and type I collagen proteins were detected by Western blot.

Alcian blue staining was conducted to see the difference in ECM production between the compressed and uncompressed groups. We saw significantly increased GAG formation in both groups after day 14 by visualizing increased light blue staining around the pink cell nuclei (**Figure 2.4B**). When comparing the images from the two groups at each time point, a clear difference was observed. With additional compression, more GAGs were produced in the compressed group. In addition, cells were more frequently observed to aggregate into clusters and modify the surrounding alginate in the compressed group. The expression level of GAGs on day 21 was not significantly different than day 14 for both compressed and

uncompressed groups.

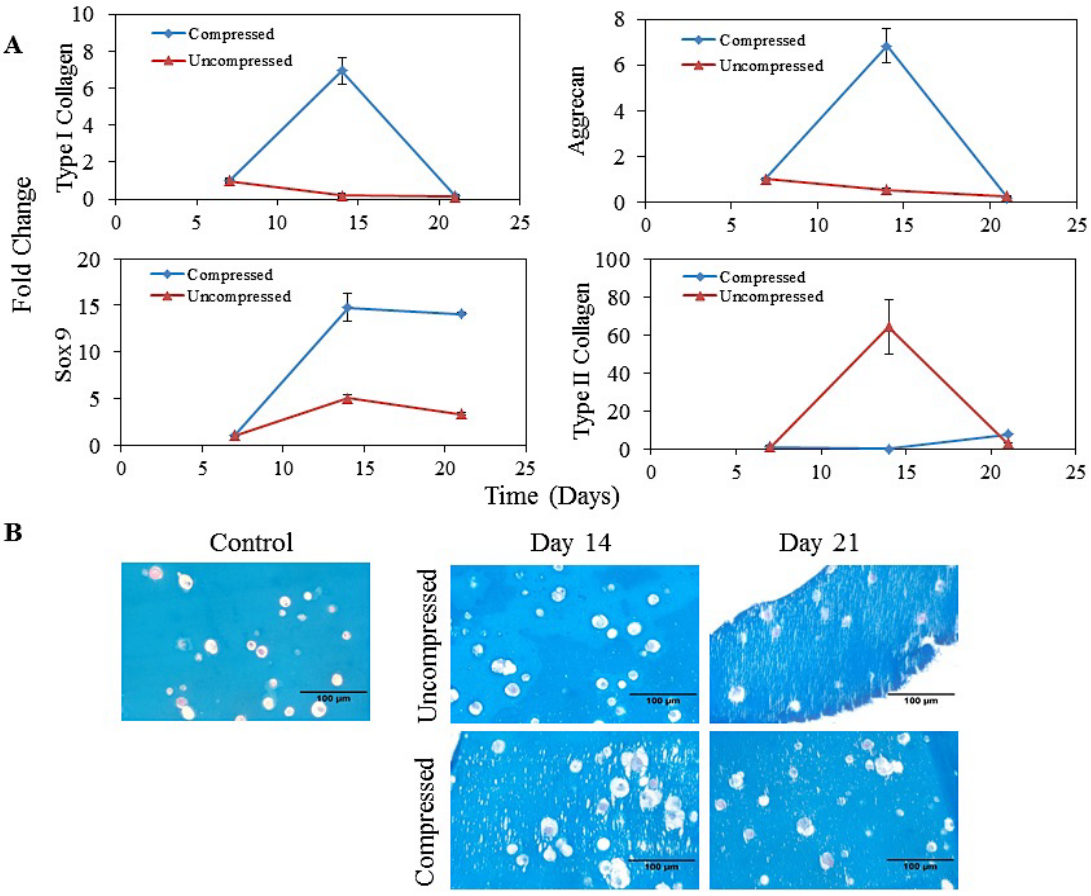

Figure 2. 4. Chondrogenic Phonotype Marker Expression in Compressed Group and Uncompressed Group During Dynamic Culture. A. mRNA expression of positive chondrogenic markers including aggrecan, sox 9 and type II colaggen. Type I collagen is a negative marker for chondrogenesis. For aggrecan and Sox9, the mRNA expression level in compression condition is higher than uncompressed condition. After day 21, Type II collagen gene expression in compression group is higher than uncompressed group. All gene expressions were first normalized based on GAPDH, then normalized to the first time point. **B**. Alcian blue staining of hMSCs in compressed and uncompressed groups. Cell nuclei stain pink, and acidic GAG residues stain a light blue color (alginate scaffold stains a dark blue). After day 14, the lighter blue extracellular matrix is observed both groups with higher expression in the compressed group. The expression level maintained similar through day 21. All scale bars represent 100 µm.

2.4 Discussion

As previously demonstrated, encapsulated cells in the TPS bioreactor experience shear forces in addition to increased nutrient and oxygen flow [87, 93]. Many studies have demonstrated the

positive effect of dynamic culture on hMSCs proliferation using other different types of bioreactors [94-97]. Our novel bioreactor can provide both shear and compressive forces at the same time to better mimic the natural environment of articular cartilage. Another advantage of this system is that by incorporating a customized sensor, the hydrostatic pressure inside the scaffolds can be directly measured as the compression is applied. In this study, we investigated hMSC proliferation during chondrogenesis and expression of hMSC chondrogenic markers in both static culture and dynamic culture in the TPS bioreactor. We also investigated the chondrogenic behavior of hMSCs under periodic compression.

Our first objective was to investigate the hMSCs proliferation during chondrogenesis process in the dynamic culture provided by the TPS bioreactor. Our DNA quantification results showed that a greater cell population in the dynamic group was maintained throughout the study than in the static group. This result is consistent with previous work demonstrating the importance of dynamic culture and 3D scaffolds in cell proliferation [98, 99]. Here we have demonstrated the ability to develop a platform that increases the *in vitro* expansion of hMSCs with satisfactory cell viability. The TPS bioreactor can provide an avenue to address this critical issue of initial cell population to allow for stem cell implantation and the treatment of articular cartilage defects. However, it is important to evaluate if the proliferated hMSCs are phenotypically stable for future chondrogenesis.

The second objective was to evaluate the effect of dynamic culture (shear force only) on hMSC chondrogenic differentiation. Our results revealed that in this study, static culture was more desirable for hMSCs chondrogenesis based on conclusions drawn from gene expression and histological data. For the mRNA expression, higher levels of chondrogenic markers including Sox 9, aggrecan and type II collagen in the static group were observed throughout

the study. Similar to our results, Kock et al. reported a reduced chondrogenesis in flow perfusion bioreactor with a rate of 1.22ml/min [100]. In fact, previous studies have shown the potentially negative effects of high oxygen level on chondrocyte metabolism [101, 102]. It has been indicated that the shear stress may play a negative role in regulating the mRNA expression for chondrogenesis with a shear stress range of 0.61-1.64Pa [103]. The shear stress that our TPS bioreactor provided is about 0.1Pa according to a previously developed computational model [87], which is relatively lower than the *in vivo* loading. As such, it is not likely to be a predominant factor in guiding the chondrogenic differentiation in this study. In another aspect, our bioreactor provides not only flow induced shear stress, but also significantly increased mass transfer (e.g., nutrients and oxygen). Several groups have demonstrated that a hypoxic environment can induce the increase of collagen II expression and proteoglycan deposition significantly for MSCs undergoing chondrogenic differentiation compared to normoxic conditions [101]. Therefore, although the mechanical stimuli could have played a role in enhancing chondrogenesis, the enhanced mass transfer might have potentially counteracted the positive effect, thus leading to the static culture being the preferred case for chondrogenesis in this study.

In articular cartilage tissue engineering, it has been well known that dynamic compression and hydrostatic pressure is crucial to the healthy development of chondrocytes or chondrogenic differentiation and phenotype maintenance [104, 105]. One study demonstrated that hydrostatic pressure enhances the cartilaginous matrix formation of mesenchymal stem cells during chondrogenesis [106]. Previous studies have shown the application of compression on chondrocytes and progenitor cells would induce apoptosis at early time points [90, 107, 108]. Particularly, Thorpe *et al*. pointed out that MSC seeded constructs should be first allowed to undergo chondrogenesis prior to transferring to a load-bearing environment [109]. Therefore cells encapsulated in alginate beads were cultured in TPS with TGF-β3 for seven days to

form ECM, which was shown by the Alcian blue staining, as a support against future mechanical loading.

Our third objective aimed to answer the question whether additional compression would enhance the chondrogenic differentiation of hMSCs in our TPS system. Our results showed that compared to hMSCs in dynamic culture in the TPS bioreactor, hMSCs exposed to additional periodic compression had higher expression level of aggrecan and type II collagen, the two main positive chondrogenic markers, at later time point after 14 days. The expression of transcription factor Sox 9 was maintained at higher levels in the compressed group throughout the study. Interestingly, one previous study reported that little ECM gene expression was observed by mechanical loading introduced on day 8, while significant ECM gene expression and matrix synthesis were induced by mechanical loading introduced on day 16 [110]. In our study, the aggrecan gene expression peak correlated with the observed GAG content in Alcian blue staining at day 14 in the compression group. Interestingly, type I collagen gene first increased in the compression study but deceased in later time points, indicating a transition from hMSCs proliferation to differentiation. These results may suggest that a mechanotransduction process occurred during chondrogenesis, where compressive stimulation induced higher metabolic activity of the cells. During early time points, hMSCs are balancing the response to dynamic culture that slows the chondrogenesis and periodic compression that improves the chondrogenesis. However, at later time points, the differentiation effect caused by compression becomes predominant. Based on the above results, we suggest expanding 3D encapsulated hMSCs in dynamic culture for a short period for proliferation, and subsequently the cells can be transferred to static culture for more desirable differentiation. Furthermore, the addition of compression applied to the 3D cell encapsulated construct may help prevent dedifferentiation. Overall, we suggest that a combination of dynamic and static culture to proliferate phenotypically stable hMSCs might

be preferred and necessary for future clinical cell treatment for articular cartilage defects with prominent outcome.

2.5 Conclusions

To solve the current problems associated with clinical cell-based treatments for articular cartilage defects, *in vitro* cell culture techniques must be improved. We have developed a bioreactor system that can enhance the *in vitro* proliferation of hMSCs encapsulated in 3D hydrogel scaffolds. We have also demonstrated that mechanical stimuli can alter the chondrogenic differentiation in different ways. In the first study, static culture was preferred for differentiation compared to dynamic culture. The second study showed that additional compressive force during dynamic culture can improve the chondrogenic differentiation of the hMSCs. The findings in this study suggest a combination culture conditions showing promise in producing clinically relevant amount of tissue through extended *in vitro* culture.

2.6 Acknowledgements

Ting Guo was responsible for the experiment design and execution. This study was funded by the National Institute of Arthritis and Musculoskeletal and Skin Diseases of the National Institutes of Health (R01 AR061460) as well as by the National Science Foundation (CBET 1264517). The metal roller box was designed by Dr. Yu Li, a visiting fellow in our lab. The pressure sensor was manufactured and calibrated by Addison Goodley.

Chapter 3: 3D Printing Articular Cartilage: Recapitulating the Complexity of Native Tissue[3]

In the past few decades, the field of tissue engineering combined with rapid prototyping (RP) techniques has been successful in creating biological substitutes that mimic tissues. Its applications in regenerative medicine have drawn efforts in research from various scientific fields, diagnostics, and clinical translation to therapies. While some areas of therapeutics are well developed, such as skin replacement, many others such as cartilage repair can still greatly benefit from tissue engineering and RP due to the low success and / or inefficiency of current existing, often surgical treatments. Through fabrication of complex scaffolds and development of advanced materials, RP provides a new avenue for cartilage repair. Computer aided design (CAD) and 3D printing allow the fabrication of modeled cartilage scaffolds for repair and regeneration of damaged cartilage tissues. Specifically, the various processes of 3D printing will be discussed in details, both cellular and acellular techniques, covering the different materials, geometries, and operational printing conditions for the development of tissue-engineered articular cartilage. Finally, this review concludes with some insights on future applications and challenges related to this technology, especially using 3D printing techniques to recapitulate the complexity of native structure for advanced cartilage regeneration.

3.1 Introduction

Tissue engineering has enabled the development of biological substitutes that restore, maintain, or improve tissue functions for therapeutic purposes in the past few decades [111]. For

[3] Adapted from: Guo T, Lembong J, Zhang L, Fisher J. Three-Dimensional Printing Articular Cartilage: Recapitulating the Complexity of Native Tissue. Tissue Engineering Part B-Reviews 2017;23(3):225-236.

cartilage in particular, the components do not require vascularization or multiple cell-cell interactions, making tissue engineering an attractive method for cartilage regeneration. Previous studies in cartilage tissue engineering using various materials are presented in **Table 3.1** [12, 15-18, 45, 112-126]. Nevertheless, the organized zonal structure adds difficulties in terms of recapitulating the mechanical properties of the native cartilage. A few studies have revealed attempts at creating multilayered structures that mimic the zonal zone with varying levels of collagen II, e.g. lamination of multiple material layers with varying properties [15, 16, 112], application of gradient in mechanical environment [18, 127], and chemical modification of materials [17].

Source	Materials	Advantages
Natural	Alginate [12, 16, 128], agarose [15, 18], hyaluronan [115, 129], silk fibroin [117, 118], chitosan [45]	Presence of bioactive moieties to support cell attachment, proliferation, and differentiation
Synthetic	Poly-glycolic acid (PGA) [119], Poly-lactic acid (PLA) [120, 121], Polyethylene glycol (PEG) [17, 112, 127, 130], Poly(lactic-co-glycolic acid) (PLGA) [123, 124], Poly-caprolactone (PCL) [125, 126]	Control over mechanical and degradation properties; incorporation of biologically active domains into the synthetic polymer structure enables bioactive properties of the scaffold.

Table 3. 1. Tissue engineering approaches for cartilage tissue engineering applications

Even with the advancement in tissue engineering, the intrinsic properties of the cartilage create barriers and challenges for a satisfactory solution to cartilage repair. For example, relatively isolated chondrocytes have low proliferation rate and experience dedifferentiation rapidly after expansion [131]. To maintain desired cell phenotypes and to guide the cells to form functional tissue structure, 3D scaffolds have been frequently used in the field of tissue

engineering [132, 133]. Numerous studies have demonstrated the importance and success of using 3D scaffolds in supporting chondrogenesis of mesenchymal stem cells (MSCs), indicating early formation of articular cartilage [134, 135], thus justifying the need for a method to fabricate precise and accurate 3D structures for cartilage regeneration applications.

With the development of computer-aided design (CAD) techniques and the understanding of biomaterials, solid free-form fabrication (SFF) or what we recognize today as rapid prototyping (RP) has become a popular and advantageous way to create 3D scaffolds with complex structures or simultaneously distributed cells [136, 137]. A more general term which evolved from RP concept called 3D printing has been commonly used for applications in tissue engineering, which will also be used in the content of this review. The technology allows the fabrication of three-dimensional objects of any shape constructible in a CAD digital model, layer-by-layer using 2D slices of the computer model. 3D printing provides many advantages including highly reproducible, well-controlled architecture (size, shape, inter connectivity, branching, geometry and orientation) and materials compositional variations [138]. The tunability of the mechanical property, biological effects, and degradation kinetics of the printed scaffolds [137, 139, 140] is also an attractive quality for yielding desired biomimetic structures.

In tissue engineering, the ideal 3D-printed structures would provide structural, mechanical support, and sufficient nutrient supply, therefore enabling growth and migration of cells to form a functional tissue that can actively remodel once implanted. This is where the concept of 3D printing can be utilized to recapitulate the complex properties of native cartilage. Topographically correct structures in the different zones achieved by 3D printing can provide the right cues to guide cell growth and alignment, induce cell differentiation, consequently affecting the deposit of extracellular matrix, thus ultimately forming a functional tissue. The

development of materials for 3D printing also enables the fabrication of structures that ultimately exhibit relevant properties of articular cartilage, and can recapitulate the complexity of the ECM that is present *in vivo* due to influence of biomechanical load and the microenvironment [141]. Overall, 3D printing provides a solution to engineer cartilage tissue while capturing both the biochemical and mechanical complexity, that are otherwise difficult to achieve with conventional cartilage regeneration using zonal chondrocyte subpopulations [142]. Combined with imaging techniques, 3D printing serves as a powerful tool to produce customizable scaffolds for particular applications or for specific patients [143, 144].

Various 3D printing techniques have been developed, each associated with its own range of operating parameters and compatible selection of materials. The desired qualities of the 3D printing process typically include the high resolution of the printed scaffold, small processing time, and compatibility with cells [143]. Parameters to be considered in 3D printing process for tissue engineering include materials degradation rate, mechanical strength of the printed structures, morphology and topography of the printed products, and the capability of vascularization of the formed tissue. One of the biggest challenges of 3D printing techniques is the limited types of materials that can be used, which have led to thorough research on the development of materials for 3D printing.

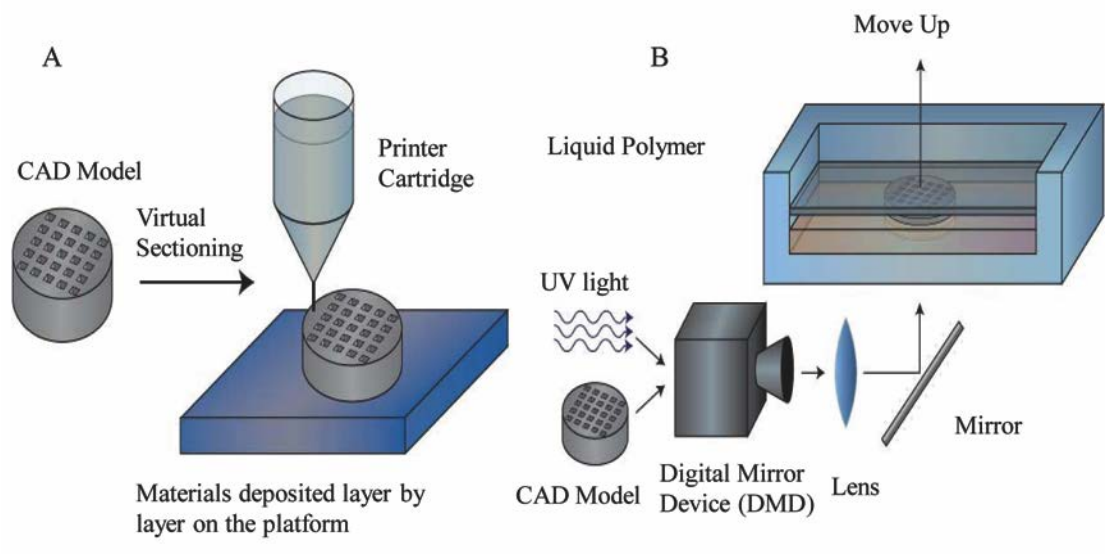

Figure 3. 1. Commonly used printing techniques for cartilage regeneration applications. **A.** Extrusion-based printing. After virtually sectioning the CAD model, the material will be deposited onto the platform to form 3D construct. Various curing methods can be used with this technique. **B.** Light polymerization printing. The CAD model with designed pattern is sent to a DMD and projected for fabrication. Photocrosslinkable polymer with initiator is loaded in the reservoir, along the platform movement, the layer contacted light will solidify due to crosslinking and thus form a 3D construct consistently.

While extensive studies have been conducted on 3D printing for other tissue engineering applications [145-147], such applications for cartilage tissue engineering, while growing, are still relatively rare due to the difficulties associated with the complex nature of the tissue. For the first time, in the review, we discuss recent advances in the development of 3D printing techniques, specifically for applications in articular cartilage regeneration. We focus on the most widely used techniques for cartilage regeneration among the many in 3D printing technology, namely extrusion-based printing and light polymerization [136, 148, 149] (**Figure 3.1**). In extrusion based printing, materials are loaded into cartridges that are typically made of plastic or stainless steel depending on the process condition, and then fed into an attached nozzle or needle. The loaded material is maintained at a certain temperature to allow formation of continuous jet onto a platform. Different solidification methods such as photocrosslinking, temperature change, and pH change can be applied during material

deposition [150, 151]. Light induced polymerization generates solid constructs from a reservoir, where liquid material that has photocrosslinkable groups are pre-mixed with a photoinitiator and exposed to light on the platform. As the platform vertically moves, the 3D construct is built with increased height. We will discuss choices of materials for each technique that will address major obstacles in cartilage tissue engineering. The two approaches to create cell-scaffold structure aiming at repopulating the zonal cell distribution using printing technology will also be discussed. One is to seed cells directly on the printed scaffolds, and the other one is to directly print materials with encapsulated cells for homogeneous cell distribution (**Figure 3.2**). Lastly, we conclude with some design consideration, future challenges and applications of this technology.

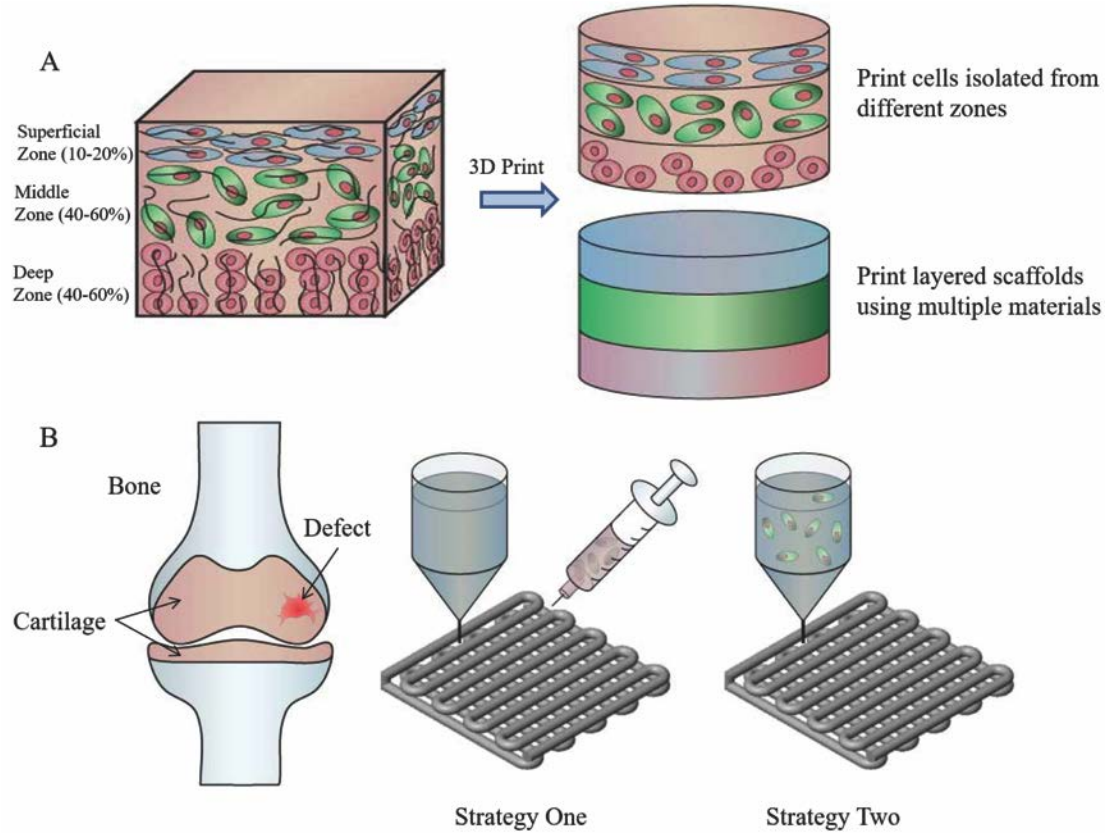

Figure 3. 2. Zonal property of native cartilage and current 3D printing approaches for cartilage defect repair. A. Chondrocytes and collagen fiber zonal distribution in native cartilage. With 3D printing technology, one attempt to recapture the structure is isolate chondrocytes from different zones and seed them into layered scaffold; the other is to use altered material to form different regions. **B.** Fabrication of cartilaginous construct for repairing the defect. For an extensive choice of material and printing condition, the first

strategy is to print acellular scaffold then seed cell onto it if needed for applications. To achieve a more homogenous and controlled cell distribution and encapsulation, cells can be pre-mixed with the printing resin to form a cell-laden construct.

3.2 Acellular Cartilaginous Scaffolds: Microstructure to Create the Complexity

The cartilage regeneration field has benefited from the advancement of fabrication of acellular scaffolds. From the engineering aspect of 3D printing, the acellular scaffold allows more choices of materials and processing conditions. The unrestricted fabrication process supports the potential of generating scaffolds with complex structures, which will benefit the cartilage tissue structure recapitulation at a small scale. Since the printing of acellular cartilage scaffold does not require suitability for bioactive components during the fabrication, the choice of material has more flexibility and is often based on different application specifications and desired printing techniques. For example, common synthetic thermoplastic material such as poly(caprolactone) (PCL) can be chosen for an easy melt fabrication process [152]. Materials that can be modified with photocrosslinkable side chains such as gelatin-methacrylamide are good candidates for UV-based gelation process.

The use of acellular scaffolds is attractive for clinical cartilage repair applications because it can avoid the potential immune response from transplanting allogeneic cartilage tissue and extra maintenance of autologous chondrocytes associated with the current treatments. One method to fabricate these scaffolds is extrusion-based printing, which is the most popular method to fabricate cartilage tissues. Using this method, complex 3D structures can first be virtually sectioned to layers using an associated software, and then created layer by layer, as materials are deposited on the printing platform. The fabrication time usually ranges from minutes to hours depending on the material extrusion efficiency and construct dimensions. There are different options to solidify the materials, such as photo-crosslinking, temperature,

or pH change. Compared to casted gels, extrusion-based printing offers another advantage for the cartilaginous scaffold, which is to provide additional interconnected pores at the scaffold level that supports local cells growth with the help of the CAD model [140, 153].

During the scaffold building process, various input parameters such as different patterns and curing methods can be tuned to give rise to a range of mechanical properties for the printed fibers, which can be applied to create zonal structures in the cartilage scaffolds, considering that native chondrocytes have unique response to the mechanical signal to regulate their metabolic activities and phenotypes [154]. The fiber dimension and orientation can be controlled precisely, with a resolution limit (the minimum width of the fibers) of around 100 μm. These parameters greatly influence the mechanical properties of the fibers [155]. Notably, although the yield resolution is in theory mainly dependent on the extrusion needle size, a needle size below 100 μm often brings practical problems such as extreme printing environment where conditions such as extremely high temperature and pressure may be harmful to the material or beyond the capacity of the machine.

One category of the extrusion-based methods, fused deposition manufacturing (FDM) or melt extrusion has been used as a convenient fabrication method for thermoplastic material. The main components include a computer that controls the scaffold model and nozzle motion with condition parameters, a heater that can be set to the desired temperature to melt the loaded material and a compressed gas supply to apply pressure for injection. The melted material can be deposited onto a platform with room or lower temperature to solidify and form 3D structures. PCL is a commonly used thermoplastic material in 3D printing scaffolds for cartilage and bone repair. Different architectures can be manufactured with clean fibers with different yield mechanical strength. Notably, as a reference to the future applications with controlled mechanical properties, it was demonstrated that the stress-strain behavior mostly

depends on the porosity, rather than the lay-down pattern and channel size [156]. The stable polymer structure makes PCL very resistant to high temperature during melt extrusion, but this could be an obstacle for *in vivo* cartilage regeneration because of the low degradation rate in the order of magnitude of years [157], which further creates barrier for the integration in native tissues. To overcome this problem, biocompatible thermoplastic materials that have relatively faster degradation rates have been explored. Polylactic acid (PLA) has been commonly used in cartilage tissue engineering for a favored degradation property [69, 158]. However, although printing temperature is molecular weight dependent, PLA in general requires a higher processing temperature than PCL.

While synthetic polymer with 3D printing allows fabrication of cartilage scaffolds with desired architecture that better mimics the native tissue, the ultimate goal is to achieve desired cellular response. The first matter to consider would be the effective cell attachment. For instance, Hsu et al. indicated that the printed PLA scaffolds with less complex structure and small interval of fibers allow better cell adhesion and proliferation, which might be due to easier cell trapping and larger surface for cell attachment [159].

Although commonly used thermoplastic materials such as PCL or PLA yield a relatively high resolution when building a cartilage-like structure, the lack of elasticity remains a potential disadvantage in cartilage regeneration since the difference in mechanical modulus also plays a role on cell activity. Therefore, block-copolymers such as polyethyleneoxide-terephtalate (PEOT) and polybutylene-terephtelate (PBT) have been investigated as a printing material due to their viscoelastic properties that mimic the native cartilage tissues. Different mechanical properties can be achieved by varying the internal structure of a scaffold [155]. The main advantage of PEGT/PBT as a biomaterial is that it is amphiphilic by combining

hydrophilic PEGT and hydrophobic PBT, allowing tailored swelling and mechanical strength. A similar study utilized and characterized 3D poly(ethylene glycol)-terephthalate-poly(butylene terephthalate) (PEGT/PBT) co-polymer scaffolds fabricated using fiber deposition technique [113]. The additional glycol in the compound prevents the material from crystallizing and becoming breakable. This class of material has been proven to promote chondrogenesis both *in vitro* and *in vivo* after being seeded with chondrocytes. As a follow-up study, scaffolds fabricated with pore-size gradients were further evaluated as a model to recapitulate the zonal structure of native cartilage [160]. Despite the improved mechanical strength of PEGT/PBT, the required high processing temperature (>200ºC) does not make this type of material attractive for printing. Taking into account the practical pressure and temperature the printer can apply, printing with small diameter needle that yields a more detailed cartilage structure can be even more challenging. Considering the high processing temperature required for the above materials, these printed scaffolds can only be coated with additional natural ECM components for better biological function such as chondrogenesis for cartilage tissue engineering.

Common thermoset synthetic materials usually require a heating temperature higher than 100°C for extrusion. Interests in low temperature printing have grown considering the potential to incorporate natural proteins or live cells in the printing process to add biological functions to the cartilage scaffold. Since chondrocytes have limited cell-cell interaction compared to most of the cell types, the sustained release of bioactive components becomes very important in chondrogenesis. To ensure the activity of growth factors after printing, a temperature below 70°C is recommended although different proteins may have various responses and resistance to temperature [161]. The addition of solvent is one of the most widely used methods to reduce the printing temperature. A low temperature 3D printing method using dioxane was developed to form scaffold in a refrigerator [162]. While typical printing

processes for commonly reported materials such as PCL, PLLA, and PLGA involve high temperatures (>120°C) [163], significantly reduced temperature (<60°C) for printing these materials can be achieved using dioxane as a solvent [164, 165]. Extra solvent can be evaporated by freeze drying process so a porous structure can be formed. The obvious drawback of the solvent printing includes the required vent system connected to the printing setup considering most of the solvents used to dissolve polymer is toxic, and the potential cellular toxicity if extra solvent remains. Since the addition of solvent also significantly reduces the viscosity of the resin, the outcome quality is usually lower than the result of printing polymer directly through FDM.

In addition to solvent-based printing, water-based printing system using synthetic material has also been recently developed as a modification to regular synthesized polymer. For example, water dispersion of polyurethane (PU) nanoparticles can first be synthesized, and then printed with the presence of polyethylene oxide (PEO) as a viscosity enhancer [166]. The hydrophilic surface of the polymer provides good cell adhesion and a non-toxic environment for chondrocytes proliferation. The water-based system could also allow incorporation of bioactive molecules such as growth factors for future cartilage tissue fabrication applications. However, one of the drawbacks of this current water-based system is that the printing process requires more synthesis steps and thus increases the complexity of the fabrication process.

In cartilage tissue engineering field, hydrogels have been considered as a promising scaffold material for cell encapsulation because it offers better diffusion of hydrophilic substrates such as growth factors and nutrients for living cells. However, the intrinsic diffusion is limited by distance so that a macro-scale printed porous structure is usually required in a 3D scaffold. Traditional fabrication methods such as molding and casting paste to create hydrogel block are not capable of fabricating patterned internal porous structure to support successful

chondrogenesis. RP-based thermoreversible hydrogel scaffold production using 3D dispensing techniques was first introduced in year 2000, using agar and gelatin [150]. This study, incorporating agar as the plotting material and gelatin as the plotting medium, demonstrated the feasibility of such printing technique, although some level of deformation was observed due to gravity for a $1cm^3$ scaffold as a result of the low mechanical strength.

Chemical modification of the hydrogel is a common way to improve or expand its suitability for 3D printing cartilaginous tissue by enabling the materials to crosslink with other materials, therefore improving its mechanical strength or biological potential. Chemical modification to make photopolymerizable and thermosensitive PEG gel was reported by synthesizing thermosensitive short copolymer chains and methacrylated groups onto the PEG polymer [167]. In addition, Skardal et al. developed a photo-crosslinkable hyaluronan-gelatin hydrogel for bioprinting [168]. By adding the methacrylate group, the hyaluronan-gelatin formed an extrudable gel solution, and therefore the fabrication can be completed in a two-step printing. Both cell free and cell laden printed scaffolds showed good biocompatibility and cell viability, demonstrating the potential to use this type of synthetic material for chondrogenesis in combination with different cell sources and other techniques. Although chemical modification expands the methods to solidify the hydrogels and makes various hydrogels suitable for printing, it usually has no or very limited impact on improving the weak mechanical strength of hydrogel scaffolds. Future studies aiming to solve this intrinsic problem of hydrogel may consider new material synthesis that provides much stronger mechanical strength while maintaining the cell-friendly environment [169] or the utilization of synthetic material with favored mechanical properties as a supporting component in the 3D cartilage construct.

While extrusion-based printing has been a popular method of 3D printing due to its flexibility with materials and curing options, stereolithography has been a well-developed and utilized printing technique considering the high resolution that can be achieved, i.e. less than 10 μm [170] and the relatively less labor involved fabrication process compared to extrusion based printing. However, the adhesion process in which the cured material attaches to the rising platform during polymerization requires certain material strength, which makes it a less popular method in developing soft tissues such as cartilage. In such applications, the materials used are often specially established or modified. For example, a photo curable polymer trimethylene carbonate/trimethylolpropane (TMC/TMP) was used to develop 3D cartilage regeneration scaffolds using microstereolithography. Its biocompatibility and favored mechanical strength give the fabricated scaffolds a potential to be seeded with chondrocytes. A pilot study showed a high yield scaffold resolution of around 100 μm with different cellular responses to different inner structures [171]. Similar approach was also reported using methacrylated poly TMC [172]. Other advanced modifications of the system such as incorporating two-photon polymerization were reported to improve the spatial resolution of the printed cartilage scaffold (<1 μm) using microstereolithography fabrication [173].

3.3 Bioprinting Cell-Laden Cartilage: Controlled Cell Distribution and the Potential to Incorporate Bioactive Molecules for Chondrogenesis

Considering the relatively isolated behavior and low metabolic activity of chondrocytes in native cartilage tissue, 3D bioprinting cell-laden scaffold brings attractive advantages, including the control of cell distribution in desired location and the possibility to incorporate growth factors. In order to achieve satisfactory cell viability, the choice of materials used to encapsulate the cells for printing is restricted. The most commonly used materials are natural hydrogels such as alginate [174, 175]. Since chondrocyte is the only cell type in native articular

cartilage tissue, it is the most popular cell source to apply to the cell laden printing trials. A study has demonstrated the possibility of printing engineered cartilaginous scaffold with arbitrary geometry using alginate solution containing chondrocytes [176]. The constructs were produced by an open-architecture computer-aided manufacturing system incorporating rapid prototyping techniques. Printed disks were proven to result in relatively homogenous cell distribution and satisfactory cellular response after culture. However, the formed alginate hydrogel may have limited ability to form inner structure and more complex structures considering the intrinsic poor printing resolution of soft hydrogels. Higher concentration of more viscous alginate solution (10% w/v) would improve the integrity of the printed porous cell laden scaffolds, however, the improvement is limited compared to the native tissue [177]. One disadvantage of the calcium mediated alginate gelation is that it usually requires additional set up or manual handling during the printing process. In addition, the very high concentration of gel solution may have a negative impact on cell response.

Despite the previously mentioned advantages of hydrogels as a material for cell printing, the weak mechanical property that does not match the native tissue is always one of the major concerns in cartilage engineering. Normal healthy human cartilage tissue has a compression modulus ranging from 9-13 MPa [178], while hydrogels usually provide a mechanical modulus in kPa magnitude [179]. One simple way to solve the weak mechanical properties of pure natural hydrogel construction is to combine the stiff synthetic material and hydrogel in a single scaffold, usually accomplished by printing one layer of stiff material followed by another layer of hydrogel with or without cells. These approaches not only provide an enhanced mechanical strength for the cartilaginous scaffold, but also add the complexity of the 3D construct for better mimicking the zonal cartilage tissue. Several studies introduced the production of hybrid constructs by a layer-by-layer deposition of polycaprolactone (PCL) and alginate containing cells [180, 181]. Their results showed improved control over mechanical

characteristics as well as favored biological function such as viability and cell morphology maintained in the hydrogel following printing. Because of the low handling temperature of hydrogel printing in those hybrid printing cases, it not only provides a way to directly print cells, but also a potential to print growth factors with cells. For example, another PCL-alginate-chondrocyte bioprinting study showed that the addition of TGF improved ECM formation after 4 weeks of culture [182]. Since hydrogel in these hybrid print application play the most important biological roles, the hydrogel concentration also affects the cellular response of the scaffolds. Notably, the yield mechanical properties are the structural property, not the material property. The cellular response could be different and affected by the connection boundaries of different materials as a result of distinct mechanical and biological cues.

Other than building a construct with different materials at scaffold level, hybrid materials have been explored as an advanced approach to 3D printing cartilage. Materials made out of thermoresponsive polymer poly(*N*-isopropylacrylamide) grafted hyaluronan (HA-pNIPAAM) with methacrylated hyaluronan (HAMA) were introduced as a novel bioink [183]. Hyaluronan (HA) is a natural component existing in native cartilages and it has been proven to promote chondrogenesis as a biofunctional material. As a result, using HA as a bioink is an attractive alternative for 3D printing of cell-friendly tissue engineered cartilage. However, similar to other unmodified natural hydrogels, HA has a low viscosity and slow gelation process which makes it difficult to fabricate scaffolds with satisfactory structures. Thus, chemical modification to HA is often required for a high resolution print. In this study, HAMA showed promising properties as a printing ink for cell encapsulation with good viability as a preliminary biological test. On the aspect of printing resolution, large needle of 3 mm diameter was used to extrude viscous HA solution with a 2 mm spacing. Future

improvements on the material to obtain scaffold structure on the micron scale level might be beneficial for chondrocytes morphology maintenance or stem cell differentiation.

In another study aiming at improving the mechanical strength of natural hydrogel, 3D printing bioink composed of alginate and nanofibrillated cellulose (NFC) was developed for desired printability [184]. The scaffolds were printed with low pressure and crosslinked using $CaCl_2$ at room temperature. The addition of NFC significantly improved the mechanical properties of the hybrid material, and resulted in a better resolution of the printing system. With the optimized formula of the bioink, human chondrocytes showed a promising viability after printing and during culture.

Synthetic hydrogels have demonstrated the ability to have tunable mechanical properties that match the native human cartilage. For example, poly(ethylene glycol) (PEG) is a widely used macromers in soft tissue engineering. Its solubility in water and well-documented protocols to synthesize photocrosslinkable products make it an attractive material for directly printing cells in 3D constructs. Printing poly(ethylene glycol) dimethacrylate (PEGDMA) with human chondrocytes onto a osteochondral plug using thermal inkjet printer was reported [78]. One concern with PEG in cartilage regeneration field is that the macromers are not biodegradable. However, such approach leads to a precise and maintained cell position after printing as a result of simultaneous photo-polymerization. As the integration of the implanted tissue into the surrounding native tissue remains one of the major challenges in cartilage repair, similar approaches with fast crosslinking will create the possibility to establish a one-step repair surgery by directly printing material and cells onto the defect site to treat damaged cartilage. This potential treatment will provide an improved integration during *in vivo* tissue regeneration, especially considering this is an intrinsic obstacle for regenerating non-vascularized cartilage tissue.

While chondrocytes seem like a natural choice of cells for cartilage repair, MSCs are proven to be promising cell types in cartilage tissue engineering. They are more abundant in human body than primary chondrocytes. In the past years, various methods and *in vitro* expansion techniques have been well documented. Gao et al. developed a printing system using gelatin methacrylate (GelMA) PEGDMA mixture to simultaneously print hMSCs, which was photocrosslinked during layer by layer manufacturing [185]. Taking into account the advantages MSCs have over chondrocytes, including more rich sources and higher proliferation, forming cartilaginous tissue through differentiation requires mechanical and biological signaling cues involved in the design. Addition of bioactive molecules such growth factor in the printing resin might be one of the future avenue to successful chondrogenesis using 3D printing MSC encapsulated scaffolds. In this case, the low-temperature processing printing techniques will help trap the growth factors in the scaffold for sustained and control release over chondrogenesis. Furthermore, although greatly increasing the complexity of the manufacturing and requiring more fundamental knowledge on cell signaling, loading different growth factors with stem cells in each cartilage zonal region may be a way to reproduce a functional and healthy cartilage tissue in the future.

The major intrinsic challenge in simultaneously printing scaffolds and cells is to balance the material properties and printing condition that favor the scaffold fabrication and biological functions. The choice is typically depending on the specifications of each study. In general, the development of materials that provide superior biocompatibility and advanced mechanical strength will greatly benefit the bioprinting area.

In cartilage tissue engineering field, in order to achieve a similar structure of the native cartilage tissue, 3D printing techniques can also be combined with other advanced techniques

to achieve superior mechanical properties, preferred cell environment, or to reduce the fabrication difficulty and cost. For example, a study introduced an inkjet printing/electrospinning system to create PCL and hydrogel hybrid constructs for engineering cartilage tissues [186]. The sheet of electrospun PCL fibers was alternated with inkjet printed chondrocytes suspended in a fibrin–collagen hydrogel to fabricate layered scaffolds. Besides the enhanced mechanical strength compared to normal hydrogel printing, the deposition of type II collagen and GAGs helped enhance the formation of cartilage-like tissues in both *in vitro* and *in vivo* experiments. As a summary, different materials have distinct advantages and disadvantages **(Table 3.2)**. The mechanical and biological properties need to be balanced depending on the specification of a design and the expected outcome.

		Material properties	Advantages	Disadvantages
Synthetic	PCL	temperature curable, degrades in vivo in years	inexpensive, well developed fabrication procedure	degrades very slowly, hard for newly formed tissue to integrate
	PLA	temperature curable, degrades in vivo in months	faster degradation than PCL, which is more favored by cartilage regeneration	higher temperature (~150°C) is required for printing
	PLGA	temperature curable, degrades in vivo in months	tunable mechanical and degradation properties	polymer is easy to degrade at high processing temperature
	PEOT/PBT	temperature curable, biodegradable and degrades faster than normal PEG product	viscoelastic mechanical properties	low mechanical strength
	PU/PEO	temperature curable, biodegradable	water based system favored by cell seeding	more complex synthesize/process

				required for printing
	PEG	the polymer is not biodegradable although the network can be modified to be biodegradable, photocrosslinkable	well-developed chemical modification to allow multiple crosslinking methods	PEG polymer is not biodegradable
Natural	Gelatin	photocrosslinkable with modification, degrades in vivo in months	denatured protein favored by cells	low mechanical strength
	Alginate	ionically crosslinking or photocrosslinking after modification, degrades in weeks	cell friendly, inexpensive hydrogel	weak gel, degrades fast
	HA	chemical crosslinking with crosslinkers, degrades in days to weeks	natural component in native cartilage that supports cell function	chemical crosslinkers are usually required for crosslinking, long gelation time

Table 3. 2. Summary of commonly used materials in 3D printing cartilage applications.

3.4 Advanced Technology incorporating 3D Printing Enables More Complex Structures Similar to Real Cartilage Tissue

As discussed in the introduction, cartilage is a highly organized tissue. Each depth zone has a unique biological, chemical and mechanical environment. Many approaches simply consider cartilage as a uniform piece of tissue ignoring the complexities for easy fabrication. However, recapitulation of the zonal structure is important for the functional restoration of the damaged cartilage. 3D printing is a preferred way to achieve the complex structures. Many experiments

have demonstrated the possibility of harvesting cartilage tissue and cells from different zones [187]. Chondrocytes located in different zones have distinct phenotype in terms of matrix formation and gene expression [188, 189]. Printing chondrocytes isolated from different zones within hydrogels layer by layer has been attempted, resulting in good cell viability and cell localization [13]. Notably, the derived zonal chondrocytes are not pure, although showing different behaviors. Therefore, future evaluation of long-term chondrocytes phenotype maintenance and surrounding matrix formation are still required to bring similar concept to real applications. In fact, 3D printing technology incorporating the chondrocytes repopulation into 3D hydrogels with accurate control will improve the outcome of zonal approaches using regionally isolated chondrocytes [142]. A recent publication utilized a combination of 3D printing and directional freezing to create micro-pores inside the printed macro-pores with hydrophilic chitosan-alginate solution [190]. Due to the mechanical limit of the material, 3D printed mold with macro pore was used instead of direct printing in this pilot study, but the idea of creating both macro and micro level pore may benefit the bone marrow infiltration *in vivo* and thus stimulate more effective chondrogenesis. With the knowledge of complex biological constituents at different scales in native cartilage tissue, fabricating biomimetic construct with the help of novel printing techniques becomes a popular focus to direct cell adhesion and differentiation. For example, a recent study demonstrated the possibility of using table-top stereolithography to generate nanocomposite scaffold with different distributions of nanocrystalline hydroxyapatite and TGF-β1 as bioactive factors to repair osteochondral defects [191]. This pilot study provides an idea of printing bioactive graded scaffold to guide cellular response. With improvement of the material and more detailed distribution of bioactive molecules, similar future approaches can be applied into creating zone specific cartilage with desired cell morphology and ECM formation, therefore achieving more effective chondrogenesis.

Compared to other 3D scaffolds fabrication, 3D printing technology offers the possibility to engineer not only porous scaffolds in a 3D tissue level, but also complex structures at organ level. For example, Goldstein et al. introduced a 3D printed laryngo-trachea using poly-lactic acid as an alternative to autologous cartilage in order to address the donor site mobility issue [192].

Moving forward, 3D printing technique also provides a way to incorporate multidisciplinary fabrication techniques to create functional biological components. For example, as an advanced application, 3D printing live cells together with electronic components inside a scaffold leads to a new direction in tissue engineering at organ level. In one study, alginate hydrogel mixed with chondrocytes was 3D printed along with conducting (AgNP infused) and non-conducting silicone solutions using a syringe head to form a cyborg cartilaginous ear [193]. This conceptual design provides an insightful idea of combining 3D printing, tissue engineering and nanomaterials technologies for future complex organ reconstruction.

Despite the above 3D printing studies particularly targeting on cartilage repair, other pilot researches on advanced materials and new concept of complex printing may enlighten the future development of cartilage scaffold incorporating RP. Although in the past years, printing technology has been significantly expanded to create finer structure and have the ability to perform bioprinting, fabrication of 3D anisotropy microstructures still remain challenging, especially with the most commonly used extrusion method. However, novel fabrication process can be applied to compensate the limitation of the current manufacturing technology. For example, using thermoreversible bath as supporting material to maintain anisotropy structure during fabrication, researchers have demonstrated the possibility of creating complex organ-level structure using hydrogels with normal syringe extrusion printer [194]. Individual ECM components such as collagen and fibrin have been attempted for the

reason that they provide biological support to the cells, but in fact, native ECM regulates cellular response as an integrated structure. Therefore, designing biomimetic scaffolds using derived whole ECM has become a popular method in tissue regeneration. Engineering ECM bioink will help bridging this new concept with the benefits that 3D printing would offer. Many ECM components have the natural ability to form a gel by controlling temperature or adding photo initiator, making them even more attractive to serve as printing resin. The general processing procedure to develop ECM bioink includes decellularization, tissue homogenization and pH adjustment from the native tissue samples [195, 196]. Despite the promising biological advantages ECM printing provides, several issues need to be addressed for effective cartilage tissue regeneration. ECM components vary a lot between different types of tissues. There are no current established standards to characterize the isolated ECM (including the chondrocytes ECM) bioink. It might be necessary for future studies to understand whether the processing alters the function of the natural components in cartilage ECM. Besides, due to the unknown chemical components and the possible crosslinking methods, it is often challenging to optimize the gelation of the ECM bioink. Therefore, for many applications, addition of other supporting materials that provides strong network (e.g. mixing ECM with photocrosslinkable hydrogel) may be required to obtain a solid structure at current stage.

Following the printing process and the biomaterial development, challenges also originate from translating this process to patients during implantation. Current approaches involve constructing the scaffolds in a laboratory setting and implanting them in patients. Although 3D printing is capable of fabricating complex shapes, these laboratory scale studies take on simple geometries, such as disks, while real defects in patients are often irregular. Advanced imaging techniques allow for recognition of defect shapes in patient, which consequently allows custom, patient-specific scaffold shapes to be fabricated. Even then, the reconstructed

structures are often incapable of perfectly matching the defect shape [197]. In the future, there needs to be an *in situ* repair method, where materials can be printed directly into the patient's defect. This is a large challenge to be tackled, which will involve the development of a printing system that is mobile and can possibly be integrated with surgical equipment in an operating room.

3.5 Conclusion

As cartilage tissue function relies on the complex structures such as the zonal distribution of collagen fibers and chondrocytes, traditional treatments fail in mimicking such complexity of the native cartilage. With the development of 3D printing technology to fulfill the needs of developing constructs that can recapitulate the complex structure of native cartilage for effective regeneration, 3D printing of cartilaginous tissue has opened a new direction to achieve desired cartilage tissue regeneration or joint functional restoration. Future advancement of novel materials with robust mechanical strength and favored biological functions, and new fabrication technologies will further broaden the applications of 3D printed cartilage for effective tissue regeneration. The emerging RP technology combined with other functional additions will complement current existing therapies for cartilage defects, and thus benefit future clinical treatments for diseases such as osteoarthritis.

Chapter 4: 3D Printing Cartilaginous Construct: A Quantitative Examination of the Effects of Polymer Composition and Printing Parameters on Print Resolution[4]

4.1 Introduction

Tissue engineering has successfully enabled the development of biological substitutes that restore, maintain, or improve tissue function for therapeutic purposes [111]. However, the complexity of the native tissue environment creates challenges to successfully promote tissue regeneration. In order to maintain desired cell phenotypes and guide the cells to form functional tissue structures, 3D scaffolds have been applied and proven to have positive impact in the field of tissue engineering [132, 133]. Numerous studies have demonstrated the importance and success of 3D scaffolds to maintain appropriate cell morphology and promote differentiation [134, 135].

While cell therapy for tissue engineering needs further consideration and regulation on source selection, and cell phenotype stability, which slows the development of effective treatment, acellular approaches have been explored in regenerative medicine [159]. In the field of engineering scaffolds utilizing 3D printing technology, the acellular scaffolds approaches have much more choices in terms of materials and processing conditions compared to the cell laden approaches. For clinical applications, the acellular scaffolds can avoid the potential immune response from allogeneic cells and extra maintenance of the cells on the shelf.

One of the challenges that the conventional molded acellular scaffold has is the difficulty to capture the tissue structure. Recently, the advancement of 3D printing technologies provides

[4] Adapted from: Guo T, Holzberg TR, Lim CG, Gao F, Gargava A, Trachtenberg JE, Mikos AG, Fisher JP. 3D printing PLGA: a quantitative examination of the effects of polymer composition and printing parameters on print resolution. Biofabrication 2017;9(2):024101.

new avenues for the fabrication of scaffolds with detailed structure to recapitulate the desired organization of native tissue or organ. In particular, for the fabrication of scaffolds to treat osteochondral defects, extrusion-based printing is one of the most popular fabrication methods due to its favored layer-by layer features with multiple solidification ways such as pH, temperature change or photocrosslinking [150, 151], and its relatively fast fabrication process compared to stereolithography. During manufacturing, complex 3D structure can be virtually sectioned to layers by associated software first, and then created layer by layer, as materials are deposited on the printing platform. With this technique, another advantage is the high quality of the interconnected pores as defined in the computer-aided design (CAD) model [153, 198]. During the scaffolds building, the fiber orientation can be controlled precisely with a resolution of around 100 μm. The mechanical properties of the printed scaffold can be greatly influenced by the fiber orientations [155].

While many different materials have been assessed for 3D printing, due to the lack of systematic research on the printing procedures, the reported fabrication methods are specific and case-dependent. Our present study utilizes an advanced evaluation process incorporating microCT scanning and computational statistic modeling to investigate the correlation between printing parameters and the resulting printing resolution. Previous work on printing poly(propylene fumarate) has offered a conceptual method to evaluate the effects of material composition and printing parameters on scaffold architecture [199]. Our current study used poly(lactic-co-glycolic acid) (PLGA) as the printing resin and extrusion-based 3D printing to fabricate scaffolds. Although PLGA has been widely used as a biocompatible material in the tissue engineering field [200-202], 3D printing PLGA with direct melt method has not been well developed. Most reported attempts require solvents or binders during the fabrication process [138, 203], with significantly increased complexity of fabrication and risk of solvent residue remaining in the printed scaffolds. Therefore, we are interested in using PLGA as a model

material – with no additional ingredients needed – to develop a systematic procedure for direct melt extrusion 3D printing. In addition, although the effect of PLGA composition on the degradation rate and mechanical properties have been investigated, how these material properties contribute in 3D printing quality or affect the printing conditions are not well known. We also demonstrated how material properties affect the printing outcome and evaluated the printed scaffold. Therefore, this study would be a suitable guide for researchers want to 3D print PLGA for a particular application, but not sure which type and what quality they could obtain. In this study, five different types of PLGA with various molecular weights, lactic acid (LA):glycolic acid (GA) ratios, and end caps were chosen to investigate the dependence of the extrusion process on the polymer composition. In the process of 3D printing thermoplastic material, it is essential to understand how material properties and printing parameters (such as temperature and pressure) correlate with each other. Therefore, our first objective was to determine the material rheology and temperature range suitable for high quality printing. Our second objective was to use a statistical model to investigate how printing parameters, polymer composition, and scaffold fiber orientation correlate with each other and affect the 3D printing quality. Overall, we demonstrated success of printing scaffolds with precise structures, and quantitatively evaluated the material and printing parameters effects on printing quality when using different needle sizes. We also investigated the effect of PLGA compositions on the scaffold degradation, mechanical and water adsorption properties.

4.2 Materials and Methods

4.2.1 Materials

PLGA with different compositions (LA:GA ratio, molecular weight, and end cap) was purchased from Lactel (Birmingham, AL) (PLGA 0.5-10kD-ester) and PolySciTech (West

Lafayette, IN) (other four compositions). We selected five different types of PLGA to systematically investigate the impact of material composition on the quality of 3D printed scaffolds. **Table 4.1** details the five material compositions and assigns a code to each composition.

Composition Code	Polymer	LA:GA ratio	Molecular Weight (kDa)	End Cap
0.5-10kD-ester	PLGA 1	50:50	9.73	ester
0.5-30kD-ester	PLGA 2	50:50	30.3	ester
0.6-42kD-ester	PLGA 3	60:40	42.6	ester
0.6-34kD-acid	PLGA 4	60:40	33.8	acid
0.85-62kD-ester	PLGA 5	85:15	61.9	ester

Table 4. 1. Summary of different PLGA compositions. Different types of PLGA were investigated in this study, and we refer to their composition code in the figures and manuscript. For the composition code, the first term is the lactic acid percentage, the second term is the rounded molecular weight, and the last term is the end cap type of the co-polymer. *LA:GA = lactic acid : glycolic acid

4.2.2 Differential Scanning Calorimetry

Modulated differential scanning calorimetry (mDSC) was performed to determine the glass transition and thermal energy at the printing temperature using TA DSC Q100 (TA Instruments, New Castle, DE) to obtain the potential printing temperature range. Five different types of unprocessed PLGA were sealed in hermetic aluminum pans (TA Instruments, New Castle, DE). Materials were quickly equilibrated at the highest temperature and kept isothermal for 5 minutes. The temperature was ramped at 10 ºC /min to -20ºC, and then a scan from -20ºC to 200ºC at a rate of 10ºC/min was conducted and recorded.

4.2.3 Rheology

The rheological studies were conducted on a strain-controlled RDA III rheometer (Rheometric Scientific Inc. Piscataway, NJ). All experiments were conducted using 25 mm flat plate geometry. Samples were maintained at the safe temperature according to the DSC results in closed oven. Each temperature was given a soak time / equilibration time of 15 min before experiments were conducted. Strain sweep was first performed to identify the linear viscoelastic region (LVR). Subsequent tests were performed at 10% strain within the LVR. Frequency sweep (0.1 rad/sec - 100 rad/sec) was performed at each temperature starting from 80^{O}C at 10^{O}C increments. Frequency sweep was performed instead of strain-rate sweep to make sure the sample was in LVR. Strain sweep was also performed (0.1/sec – 100/sec) for comparison. Data was recorded and analyzed using TA orchestrator software (TA Instruments, New Castle, DE).

4.2.4 Gel Permeation Chromatography

The molecular weight of the unprocessed PLGA and printed PLGA was determined by gel permeation chromatography (GPC) using a Waters Alliance Separations Module e2695, Waters 2414 Refractive Index Detector, and Waters HSPgel columns in series (HR MB-L and HR 3.0 columns, 6.0 mm ID × 15 cm) (Waters, Milford, MA) [204]. For printed PLGA, scaffold was fabricated using conditions summarized in **Table 4.2**, then a small piece of the printed scaffold was cut and dissolved in tetrahydrofuran for the test. Polystyrene standards were used to report the relative molecular weights. The standard curve was generated from a 10-point calibration using Agilent EasiCal polystyrene standards. The data analysis was performed using Waters Empower 3 Chromatography Data software. Three samples of each composition were performed for statistical analysis.

4.2.5 Scaffold Printing

3D square models with a dimension of 4 mm (length) × 4 mm (width) × 1.5 mm (height) were designed in SolidWorks (Waltham, MA). According to the manufacturer's (EnvisionTEC, Gladbeck, Germany) instruction, the model scaffold was sliced into layers with a slicing thickness equal to 80% of the needle inner diameter (ID) before printing. For 0.2 mm and 0.4mm ID stainless steel needles, we used 0.16 mm and 0.32 mm slicing thicknesses, respectively (Bioplotter RP, EnvisionTEC). Scaffolds were printed under various conditions including: needle size, temperature, pressure, printing speed, fiber spacing, and inner fiber pattern. The scaffolds were printed on double-sided tape for better adhesion. The platform temperature was kept at 15 ^{O}C. Three patterns were fabricated for the quality assessment: 1. Parallel strands with 0.2 mm fiber spacing, 2. 0º/90º crosshatch where the printed layers are alternatively perpendicular to each other with 0.2 mm fiber spacing. 3. 45º/45º crosshatch with 0.4 mm fiber spacing). Each combination with different printing parameters for different types of PLGA was printed for further evaluation and statistical analysis. For degradation and mechanical testing, 0°/90° crosshatch pattern was used to test the scaffold properties.

4.2.6 Micro-Computed Tomography

Micro-computed tomography (microCT) was used to noninvasively image and characterize the printing quality of the scaffolds. Scanning was performed on a microCT 100 (SCANCO Medical, Brüttisellen, Switzerland) operated at 55 kVp (peak kilovoltage), 9 mm voxels, and 200 mA. The resulting 3D datasets were segmented using thresholds (lower: 60, maximum: 1000), with gauss sigma (0.8) and support (1) values to separate 3D printed pores and pores within the polymer [205]. We used a peak histogram approach to determine the threshold segmentation values so that the 3D scaffold can be identified from the background visually. The 3D images were evaluated for fiber diameter, fiber spacing, and porosity using Scanco's

Image Processing Language (IPL). After processing, each fiber diameter of the whole scaffold was automatically calculated. These numbers were used to report the average yield fiber diameter of scaffold printed with different PLGA and various printing conditions.

4.2.7 Statistical Analysis

For GPC results, data were analyzed using Student's t test. A significant level of 95% was chosen, and a *p*-value less than 0.05 was considered to indicate a significant difference between samples.

Statistical models were utilized to: (1) evaluate the effects of different experimental factors, including LA:GA ratio, end cap, molecular weight, temperature, pressure, speed, and fiber pattern, on the error of 3D printing (ε), defined as

$$\varepsilon = \frac{|d_{fiber} - d_{needle}|}{\mathrm{d}_{needle}} \times 100\% \qquad \textbf{Equation 1}$$

where d_{fiber} is fiber diameter and d_{needle} is needle diameter; (2) build a model to predict the error/accuracy of 3D printing under given experimental conditions (i.e. material composition and printing conditions, listed in Figure 3a). The experimental data were separated into two groups based on d_{needle} (0.2 mm or 0.4 mm). For the group with d_{needle} = 0.4 mm, all experimental factors were used in the linear model. Pressure was excluded in d_{needle} = 0.2 mm group since the values were kept constant for all experimental groups (9 bars). A linear regression was performed using statistical package R. The *p*-values of β coefficients in the linear models were used to determine if the experimental factors significantly impacted ε. An experimental factor was considered significant if its *p*-value < 0.05. To evaluate the predictive performance of these linear models, root mean squared error (RMSE) was used to

compare the predictions from the linear regression model ($\hat{\varepsilon}_i$, predicted error) and the actual 3D printing error (ε_i), for a sample size, *n.*

$$RMSE = \sqrt{\frac{\sum_{i=1}^{n}(\hat{\varepsilon}_i - \varepsilon_i)^2}{n}} \qquad \textbf{Equation 2}$$

4.2.8 In Vitro Degradation

Scaffolds printed with a 0º/90ºcrosshatch pattern (0.2 mm fiber spacing) were chosen as an example in the following scaffold characterization tests. The scaffolds were placed in 5ml of PBS (Sigma-Aldrich, St. Louis, MO) and shaken at 37ºC at 65 rpm for *in vitro* degradation. The original weight of each scaffold was recorded. The pH of each sample was measured and PBS was changed every 7 days to make sure it was maintained at 7.4. Before measuring the wet weight, the scaffolds were removed from the PBS and then dried with a paper towel. After measuring wet weight, the scaffolds were lyophilized to determine the dry weight [206]. To measure the wet scaffold mass, scaffolds were removed from PBS, dried with a paper towel, and then the weight was measured. For water adsorption statistical analysis, percentage water uptake was compared between each two groups.

4.2.9 Compression Mechanical Testing

Compression mechanical testing was performed on degraded scaffolds using an Instron mechanical testing system (33R/4465) (Norwood, MA). At each time point, fully hydrated scaffolds were removed from PBS and immediately tested in air (days 7, 14, and 21). Five scaffolds of each PLGA composition from each time point were tested (0º/90º crosshatch pattern was chosen as a standard pattern for testing). The compressive mechanical properties during degradation were evaluated. Samples that lost the shape due to significant degradation

were excluded from the measurement and indicated by "-" in **Figure 4.4B**. A 50N load cell was applied to all samples. Samples were compressed at a displacement rate of 0.5 mm/min and values were recorded every 10 ms. A pre-load of 0.05N was applied to all samples reduce the noise of the measurement. The compression was maintained until a drop of at least 10% in force was observed or it reached the machine protection distance. Engineering stress and strain were calculated based on original cross-sectional area and height of the wet scaffolds measured before testing. For each time point, compressive stress and strain was recorded. Compressive modulus was calculated using R software to determine the linear region and the slope of the stress-strain curve. The program found the linear region (which determines the compressive modulus based on definition) that contained more than 100 data points and searched for the longest valid region for the calculation, which has $R^2 \geq 0.95$. The slope of the region is the calculated as compressive modulus.

4.3 Results

It is important to understand the basic material behavior before 3D printing. In particular, when using a high temperature extrusion technique, it is essential to quantify the thermal response of the material. First of all, we studied the heat flow of the five types of PLGA when temperature changes **(Figure 4.1A)**. Based on the plot, we observed a glass transition temperature around 35°C to 60°C. By comparing the glass transition temperature for the various material compositions, it was indicated that the glass transition temperature largely depends on the molecular weight. PLGA 0.5-10kD-ester with a low molecular weight has a dramatic lower temperature compared to other PLGA. Although each composition had a different LA:GA ratio and end cap, the glass transition starting points were similar among groups with comparable molecular weights. The PLGA 0.85-62kD-ester group (with the highest LA:GA ratio and molecular weight) exhibited the highest glass transition temperature around 57°C. The energy of the materials was stable without a significant energy wave in the

temperature range that includes the printing temperature, which demonstrates that the high temperature printing conditions do not break down the polymer.

The rheology plot was presented as viscosity versus temperature for all five PLGA compositions **(Figure 4.1C)**. The temperature range includes all extrusion temperatures. Viscosity decreased linearly with increasing temperature for all samples. At a given temperature, for ester end capped-PLGA groups, the viscosity was higher for compositions with higher LA:GA ratios and/or higher molecular weights. In particular, the acid end cap-PLGA group showed a significantly lower viscosity compared to the ester end cap-PLGA groups. The viscosity at the optimized printing temperature for each group also depended on the selected needle size. For effective extrusion, the viscosity of the polymer was observed in the range of 0.1-10 Pa•s.

Gel permeation chromatography was performed to compare the molecular weight of different types of PLGA before and after printing. In general, other than the PLGA 0.85-62kD-ester group, the molecular weight of printed PLGA and the unprocessed PLGA were significantly different **(Figure 4.1A)**. By comparing 0.5-10kD-ester and 0.5-30kD-ester, the PLGA with lower molecular weight has a relatively lower percentage molecular weight loss. We observed that the ester end cap is more resistant to the temperature increase, which is consistent with the results observed in rheology. Notably, in the rheology test, the ester end cap PLGA also showed greater resistance to high temperature. As the LA:GA ratio increases from 50:50 to 85:15, the molecular weight loss is inversely related to the increased LA ratio.

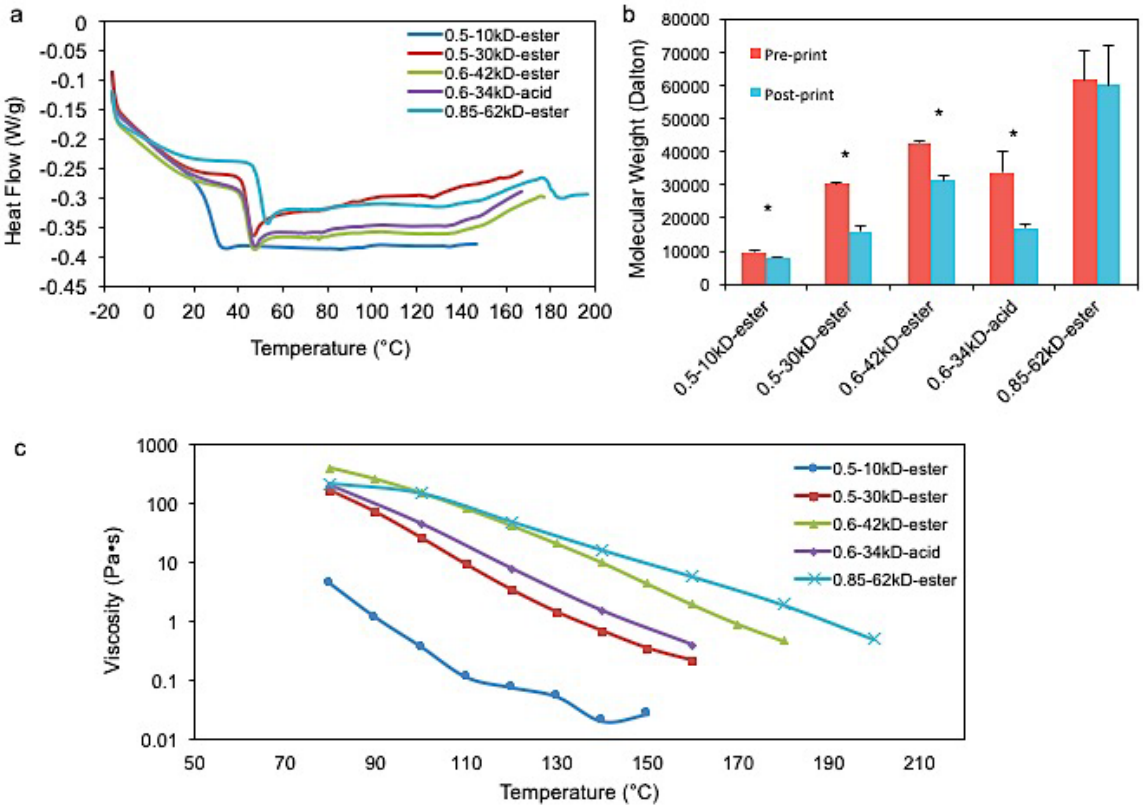

Figure 4. 1. Evaluation of PLGA Material Properties Before and After 3D Printing. A. Differential scanning calorimetry assay showed normalized heat flow as temperature increases. PLGA glass transition was observed between 35°C to 60°C, which is significantly lower than extrusion temperature. **B.** Comparison of molecular weight of five PLGA compositions before and after printing. * Indicated significant difference in each group (*p*-value < 0.5). **C.** Complex viscosity of different types of PLGA as a function of temperature. Viscosity generally decreased with increasing temperature. The complex viscosity was measured at a fixed frequency of 10 rad/s.

Scaffolds with designed patterns were successfully fabricated using direct melt extrusion **(Figure 4.2)**. Based on the designed dimension, scaffolds with 9 layers were built layer-by-layer, and the printer camera took images of single printed layers. The programmed spacing of the adjacent fibers for the parallel and crosshatch patterns is 0.2 mm. The programmed spacing of the adjacent fibers for 45° crosshatch pattern is 0.4 mm. (In Figure 4.3, “pattern” is simplified to the spacing between adjacent fibers in mm to transfer this categorical factor to numerical factor). The printed scaffolds had a comparable pattern to the CAD model for each layer. MicroCT was performed to reveal the details of the complete 3D printed scaffolds.

This non-destructive technique can further quantify the scaffold structural properties, such as fiber diameter, which was used as a metric to assess printing quality.

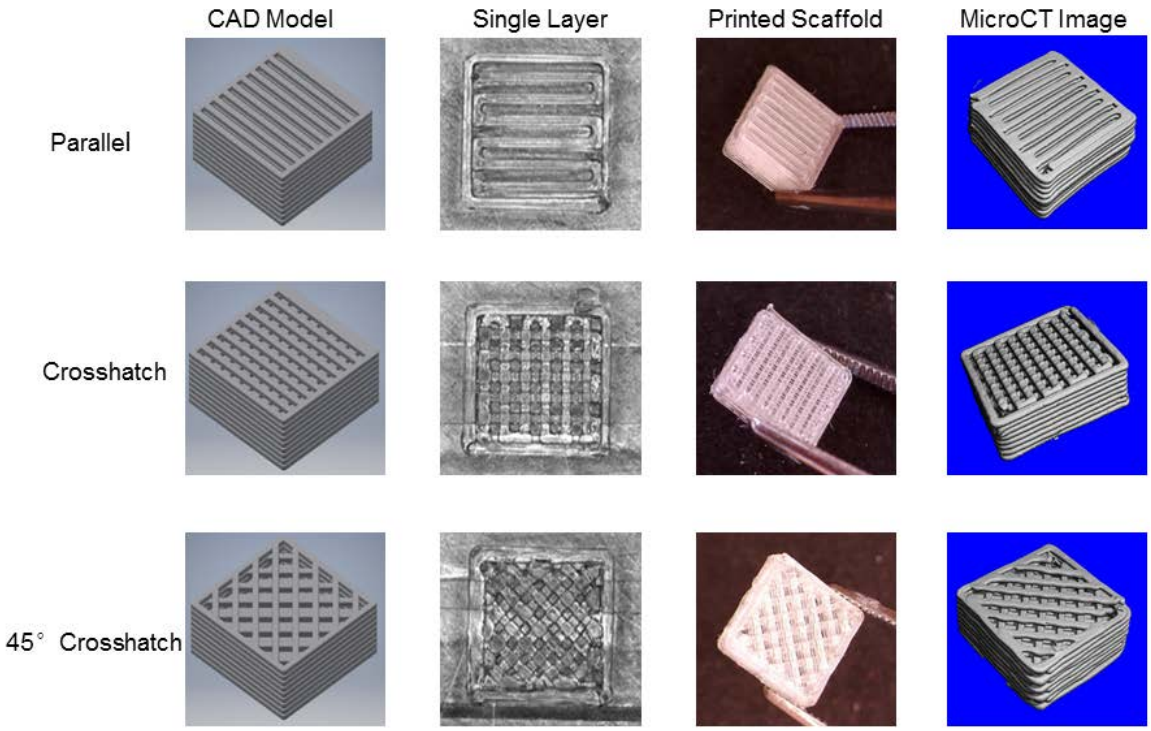

	0.2mm ID	0.4mm ID
Mean fiber diameter	0.18±0.04 mm	0.30±0.04 mm
Mean fiber error	19.26%	25.16%

Figure 4. 2. Scaffold Design and Image Analysis. 3D printed PLGA scaffolds with distinct patterns (from top to bottom: parallel, $0^o/90^o$ crosshatch*, and $45^o/45°$ crosshatch) were printed in a dimension of 4 mm × 4mm ×1.5 mm. From left to right column: the CAD model design, a single layer picture recorded by the printer camera, a 3D view of printed 9-layer scaffold, and a microCT-reconstructed image are shown. The table summarizes the average fiber diameter and printing accuracy (mean fiber error) of printed scaffolds using different needle sizes. A smaller needle size resulted in higher printing resolution with a smaller error. *Crosshatch means that the printed layers are alternatively perpendicular to each other (in a $0^o/90^o$ or a $45^o/45^o$ alternating pattern, where the angle is measured between inner structure and outer contour). SEM image of the printed scaffold showed smooth surface and clean fibers.

The printing conditions to form fine fibers that will yield the programmed fiber diameter ($\pm$0.01 mm) are listed in **Table 4.2**. Notably, since the three main printing parameters are

not independent of each other, other combinations, such as higher temperature with higher speed, can also be applied to achieve similar printing quality. However, in order to minimize the degradation that could be caused by extreme temperature, the conditions summarized in **Table 4.2** were set at a lower temperature with a reasonable printing speed. As the needle inner diameter is reduced by half, the required temperature and pressure for extrusion increased significantly. For the 0.2mm ID needle, the pressure was kept at 9 bars, which is the safe upper limit our printer could provide. Comparing PLGA with different compositions, the temperature required for extrusion depends strongly on the molecular weight, although LA:GA ratio and end cap also play a role in determining the printing conditions. In general, higher molecular weight, higher LA:GA ratio, and an ester cap demand more extreme processing temperatures and pressures.

	0.2 mm ID*			0.4 mm ID		
Composition Code	Temperature (°C)	Pressure (bar)	Speed (mm/s)	Temperature (°C)	Pressure (bar)	Speed (mm/s)
0.5-10kD-ester	110	9	1.5	95	7.5	1.5
0.5-30kD-ester	135	9	0.7	125	8	1.5
0.6-42kD-ester	165	9	0.7	140	9	0.5
0.6-34kD-acid	150	9	1.5	130	8	1
0.85-62kD-ester	170	9	0.5	145	8	0.5

Table 4. 2. Printing conditions for PLGA with different compositions. Printing conditions such as temperature, pressure, and speed were optimized to print fine fibers for each composition. * Two syringe needles were used to print PLGA fibers, ID = inner diameter.

In order to understand how material properties and printing parameters determine the extrusion fabrication accuracy, PLGA compositions with different LA:GA ratios, molecular weights, and end caps were printed at various temperatures, pressures, speeds, and patterns. Each combination was printed and then imaged and analyzed using microCT and the

supporting software. From the 3D reconstruction results, the fiber diameter as a function of different printing parameters is listed in **Figure 4.3A.**

We evaluated the printing accuracy based on different extrusion needle sizes **(Figure 4.2)**. The printing error (or fiber error) was calculated from **Equation 1**. The statistical results summarized from different types of PLGA gave an average fiber diameter of 0.1773 mm when using a 0.2mm ID needle and an average fiber diameter of 0.2993 mm when using 0.4 mm ID needle. The calculated error when using 0.2 mm ID is lower than the 0.4 mm ID. These interesting findings indicate that a smaller needle size requires more extreme processing conditions (i.e. higher temperature and pressure) but also produces more precise fibers since the conditions are more restricted and more close the optimized case.

A linear regression model was applied to the experimental data to determine the impact of each material and printing parameter on the printing accuracy **(Figure 4.3B)**. In the results, factors with a *p*-value less than 0.05 were considered as significantly impactful on the printing error (**Equation 1)**. Since the same pressure was applied during fabrication using the 0.2 mm ID needle, this factor was not considered in the 0.2 mm statistical model. With the 0.2 mm needle size, the material parameters including LA:GA ratio (ratio), molecular weight (Mw), and end cap, and printing parameters, such as temperature, speed, and pattern (simplified as the fiber spacing for the parallel, 0º/90º crosshatch, and 45º/45º crosshatch patterns) , all played a significant role in determining the precision of printing. The small p-value associated with the material parameters indicated them as significant factors for the 0.2 mm needle. However, when using a larger needle with 0.4 mm ID, we observed that the printing accuracy relies more on the printing parameters, and some printing parameters became less significant. In both groups, the designed pattern did not have a significant impact

on the printing accuracy, indicating the feasibility of using this technique for broader applications containing complex structures.

0.2 mm Needle Linear Regression

$$Error = 2.79 - 3.54 \times \text{ratio} + 6.561 \times 10^{-5} \times \text{Mw} - 0.326 \times \text{endcap} - 0.00217 \times \text{temperature} + 0.5539 \times \text{speed} - 0.0555 \times \text{pattern}$$

Equation 3

0.4 mm Needle Linear Regression

$$Error = 0.6648 + 0.0846 \times \text{ratio} - 1.36 \times 10^{-5} \times \text{Mw} - 0.3756 \times \text{endcap} + 0.013 \times \text{temp} - 0.1555 \times \text{pressure} - 0.2947 \times \text{speed} - 0.0237 \times \text{pattern}$$

Equation 4

The linear models showed an R^2 of 0.76 for the group with d_{needle} = 0.2 mm and 0.74 for the group with d_{needle} = 0.4 mm. Both groups exhibited significant linear relationships between the experimental conditions and the resolution of 3D printing (p-value = 3.21×10^{-4} for the 0.02 group and 1.81×10^{-4} for the 0.04 group)(for linear model in Figure 3b). The RMSEs are 5.52×10^{-3} and 3.75×10^{-3} for the 0.2 mm and 0.4 mm group respectively, suggesting that our linear models performed well in prediction in both scenarios.

a

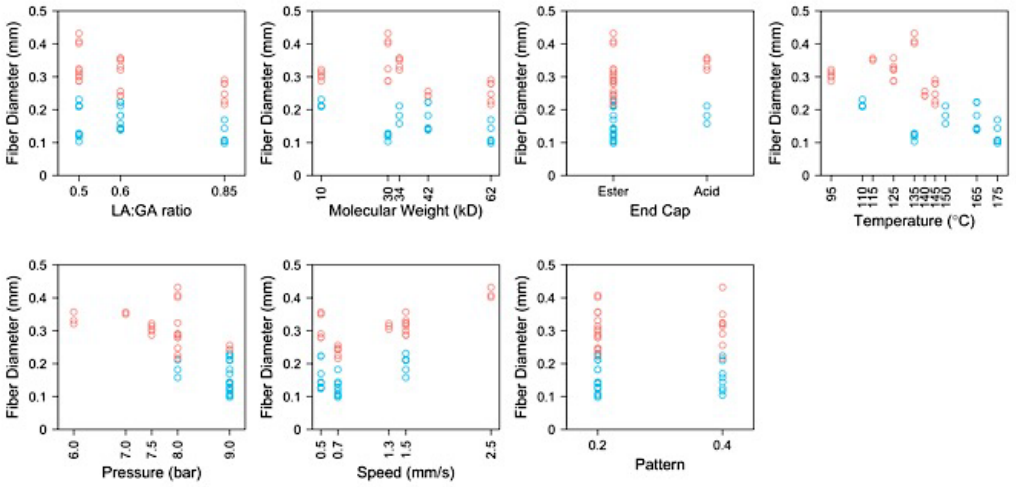

b

	0.2 mm ID			0.4 mm ID	
	Interaction coefficient	p-value		Interaction coefficient	p-value
LA/GA ratio	Significant	0.0017	LA/GA ratio	Not significant	0.91
Molecular weight	Significant	0.00019	Molecular weight	Not significant	0.22
Endcap	Significant	0.028	Endcap	Significant	0.010
Pressure	N/A	N/A	Pressure	Significant	0.048
Temperature	Significant	0.000068	Temperature	Significant	0.025
Speed	Significant	0.022	Speed	Significant	0.0025
Pattern	Not significant	0.78	Pattern	Not significant	0.88

c

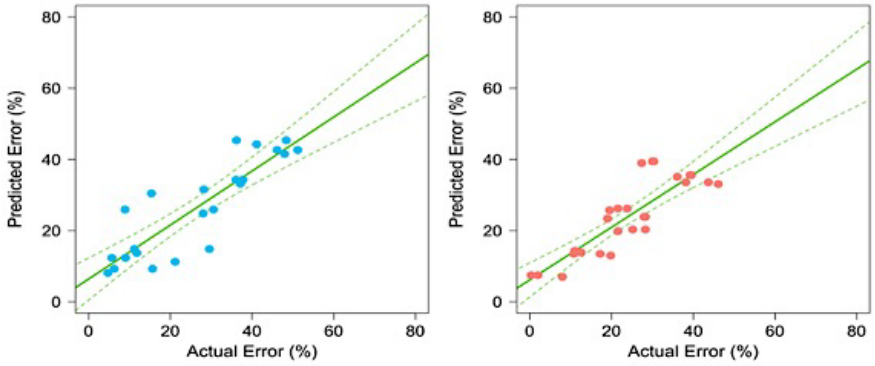

Figure 4. 3. Statistical Analysis of Printing Resolution. A. Fiber Diameter Distribution with Different Material Properties and Printing Parameters. Data points associated with 0.2 mm ID needle were shown in blue, while data points associated with 0.4 mm ID needle were shown in red. X-axis includes material and printing control parameters, and y-axis shows measured fiber diameter calculated from microCT scanning. **B.** Main effect analysis of the material parameters and printing parameters impact on printing accuracy. Two significant digits were applied in p-value analysis. A p-value < 0.05 is considered to be statistically significant. **C.** Evaluation of the Accuracy of the Predicted Model. Linear regression of predicted error using equation 5 & 6 and actual error calculated from microCT evaluation (Left: 0.2 mm ID needle, Right: 0.4mm ID needle). Both models showed strong linear relationship between the predicted error and actual error, indicating a precise prediction potential of our model.

We further investigated if our predicted values using **Equation 3** and **Equation 4** were capable of representing the actual error **(Figure 4.3)**. Linear regression was performed to evaluate the relationship between the actual errors and the errors predicted from the linear models.

0.2 mm Needle Linear Regression Error

$$\text{Predicted Error} = 0.75855 \times \text{Actual Error} + 0.06384 \qquad \textbf{Equation 5}$$

$$p\text{-value} = 6.45 \times 10^{-8}$$

0.4 mm Needle Linear Regression Error

$$\text{Predicted Error} = 0.73987 \times \text{Actual Error} + 0.06151 \qquad \textbf{Equation 6}$$

$$p\text{-value} = 8.88 \times 10^{-9}$$

Both cases suggest that there is a significant linear relationship between the actual errors and the predicted errors because the p-value is much less than 0.05. Based on statistical precision of our model, we believe this model could provide a good prediction of printing outcome.

In order to use the printed PLGA scaffold for osteochondral defect repair, the scaffold properties were also investigated **(Figure 4.4)**. The scaffolds were kept on shaker at 37°C for *in vitro* degradation and the scaffold morphology and mechanical properties were evaluated. As expected, PLGA with a 50:50 LA:GA ratio experienced fast degradation with significant mechanical strength loss over 21 days [207]. Both 50:50 groups lost about 50-60% mass during the 21-day incubation **(Figure 4.4A)**. In particular, the acid end cap played a significant role in accelerating the degradation and resulted in weaker compressive modulus. The acid end capped PLGA scaffolds lost around 80% mass after 21 days at 37 °C. The compressive modulus of PLGA 0.5-10kD-ester was not measurable due to the structural loss during its rapid degradation. With a 85:15 LA:GA ratio and moderate molecular weight, PLGA 0.85-

62kD-ester showed a steady degradation during early time points **(Figure 4.4B)**. In the water adsorption test, the wet mass at each time point was compared with the initial scaffold mass **(Figure 4.4C)**. The printed scaffolds with different polymer composition all demonstrated the ability to adsorb water. In general, PLGA with a lower LA:GA ratio and an acid end cap was able to uptake water more readily during *in vitro* incubation. Based on the statistical analysis comparing significance between each two groups, by day 7, the acid end capped PLGA adsorbed significantly more water than the ester end capped PLGA.

a

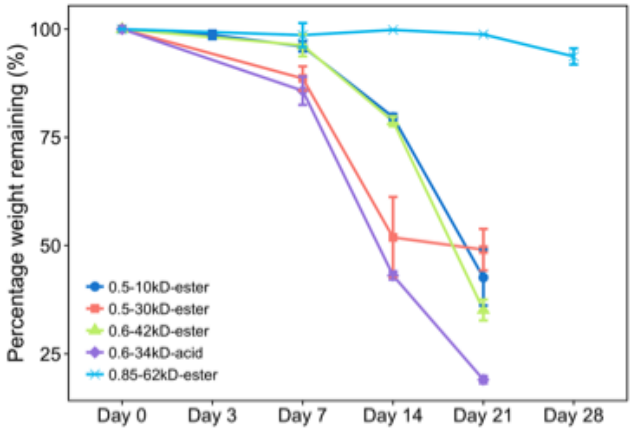

b

	0.5-10kD-ester	0.5-30kD-ester	0.6-42kD-ester	0.85-62kD-ester
Day 7	0.0015±0.0005MPa	0.34±0.1MPa	0.017±0.008MPa	1.79±0.8MPa
Day 14	-	0.0019±0.0004MPa	0.0033±0.0002MPa	4.44±1.8MPa
Day 21	-	-	-	1.72±0.3MPa
Day 28	-	-	-	1.82±0.7MPa

c

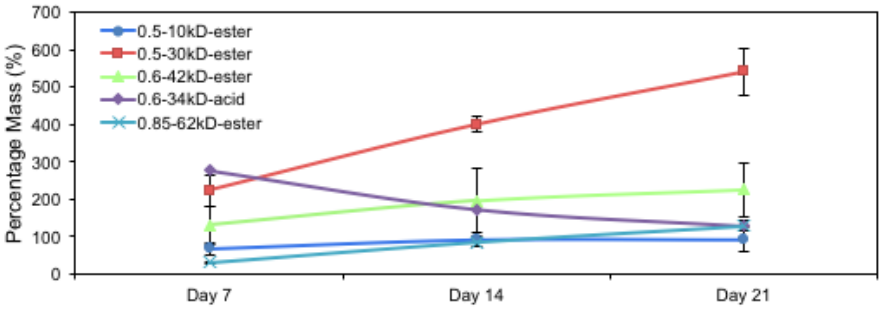

Figure 4. 4. Printed scaffold properties. A. Degradation profile of scaffolds printed with different types PLGA. The mass remaining of different types of PLGA was recorded. PLGA with lower molecular weight and acid end cap experienced faster degradation. **B.** Compressive modulus of scaffolds with different compositions during *in vitro* degradation. PLGA with moderate molecular weight and an ester end cap showed stable compressive mechanical properties during the study. **C.** Water adsorption of the printed scaffold. The printed scaffolds showed ability to uptake water. Scaffolds printed with an acid end and more

PGA content adsorbed more water during the course of study because the material is more hydrophilic.

4.4 Discussion

In this study, we evaluated the feasibility and impact factors of using a direct melt extrusion printing method to process PLGA, a thermoplastic material. At first, mDSC was performed to determine the glass transition and thermal energy at the printing temperature. The stable thermal energy at our desired printing temperature confirms that the high temperature processing is not likely to break down the material. Therefore, DSC may serve as an initial step to consider the processing temperature for new material printing. In order to prevent breakdown of the material, the printing temperature should be kept at a range higher than the glass transition temperature but lower than the thermal molecular decomposition temperature. Particularly in extrusion printing, rheology is an important factor to evaluate, which can be utilized as a further guide to determine the fabricating conditions [208]. The rheological properties of five types of PLGA were analyzed. In this case, the plot of complex viscosity at certain frequency equals to the viscosity at certain shear rate according to Cox-Merz rule. To protect the material under shear, the experiment was conducted under oscillatory setting so the complex viscosity was measured. We observed effective extrusion and an optimal printing resolution when the viscosity was within the range of 0.1-10 Pa•s, which is consistent with documented ranges using other materials [199, 209, 210]. Specific viscosity at certain extrusion condition depends on the needle size, where smaller needle requires lower viscosity for effective extrusion. The linear relationship between viscosity and temperature confirmed that a high temperature extrusion technique would not harm to the polymer structure during printing. However, the GPC data comparing the molecular weight between unprocessed PLGA and printed PLGA revealed a molecular difference. This could be a result from the lower printing temperature since the melting temperature mostly relies on the

molecular weight. This indicates that for actual applications, we may take account the molecular weight change after printing if it is a critical factor to consider in the further studies. These results indicate that although the direct melt extrusion procedure does not seem to drastically alter the polymer structure, the printed scaffolds may still have different mechanical and degradation properties as casted scaffolds, which should be considered in the future applications.

We performed a linear regression model to systematically investigate the effects of material composition and printing parameters on printing accuracy. In general, we found that using a smaller needle results in a smaller error. The printing conditions are unlikely to have a linear relationship with the viscosity or the resulted printing error. An exponential relationship between the temperature and viscosity would be one reason that when using smaller diameter needle, the fiber diameter change is more resistant to the printing condition parameters change. The Hagen-Poiseuille Law **(Equation 7)** [211] provides the connection between the viscosity, needle size and volume of plotting material. Due to a proportional fourth power in needle size in the equation, the needle diameter affects the dispensed material at a given time dramatically, which makes the fineness of extruded fiber harder to control. An interesting finding we learned from the main effect analysis of the control parameters and fiber accuracy is that the printing error is more material-dependent when using a small diameter needle while more printing condition dependent when using a larger diameter needle.

By comparing the significant factors between printing using small needle and large needle, we observed that when using smaller diameter needle, the material properties play a more important role in the resulting printing quality. In contrast, when using a large diameter needle, the printing parameters such as pressure, and speed became more significant to determine the fiber quality. One explanation could be that when the needle diameter is very

small, the printing conditions are strict and extreme without much flexibility. As a result, the printing outcome most depends on the material itself. However, when the needle diameter increases, multiple 1st order factors in the Hagen-Poiseuille Law can be considered as predominant factors to compensate the material property difference.

$$V = \frac{\pi \times \Delta p \times \Delta t}{8 \times \eta \times L} \times r^4 \qquad \textbf{Equation 7}$$

where V is the volume of the plotting material, η is the dynamic viscosity, p is pressure, t is dispensing time, L is needle length and r is the needle diameter.

In the statistical analysis, the small RMSEs values, 5.52×10^{-3} and 3.75×10^{-3} for the 0.2 mm and 0.4 mm group, respectively, suggest that our linear models **(Equation 3 and 4)** performed well in the prediction of yield printing accuracy. We also demonstrated that our prediction model has a strong linear relationship relating to the actual accuracy, which further confirmed the power of this established prediction model. However, statistically, a new set of experimental data with new input material and printing parameters is needed to test the true power of our model in future applications and analysis.

In terms of printed scaffold properties, from the mechanical properties of the scaffolds during degradation, PLGA scaffolds with a low LG:GA ratio quickly lost their compressive strength and morphology in the first two weeks. In addition, an ester end cap is beneficial to stabilize the material during both the printing process and degradation. Since glycolic acid is more hydrophilic than lactic acid due to the presence of methyl side groups in LA, scaffolds with a lower LA:GA ratio were more capable of adsorbing water [212]. An acid end cap also decreases the hydrophobicity, in addition to accelerating the degradation. Therefore, for 3D printed scaffolds, PLGA that has a high LA:GA ratio and ester end cap may serve as a suitable scaffold for cartilage regeneration, considering the relatively slow degradation rate and similar compressive mechanical strength to native human cartilage [213]. For future

applications, a wide variety of PLGA compositions can be combined with direct melt extrusion to design 3D printed implants requiring unique chemical, mechanical, and degradation properties.

4.5 Conclusions

In conclusion, for the applications of 3D printing thermoplastic material using direct melt extrusion, it is important to first understand the material properties and use the analysis as a guide to determine optimal printing conditions. For applications that prefer to maintain scaffold structure and mechanical strength over a relatively long period, it is recommended that a high LA:GA ratio is chosen for the printing process. PLGA with an ester end cap also demonstrated a better structural stability in 3D printing for tissue engineering applications. These well-characterized PLGA scaffolds with high resolution can be used in many tissue engineering applications. Although the techniques and discovery in this study are not restricted to a specific type of tissue or certain applications, our research mainly focuses on optimizing printing procedures and scaffold characteristics to repair osteochondral defects. This systematic study will contribute to developing standards for the 3D fabrication procedures in tissue engineering and regenerative medicine.

4.6 Acknowledgements

Ting Guo designed and carried out the majority of this study. The authors would like to Dr. Maureen Dreher from Food and Drug Administration for microCT training. The statistical analysis codes were mostly written by Dr. Feng Gao from Cornell University. Timothy Holzberg contributed significantly in running microCT for the scaffold samples. This work was supported by National Science Foundation grant CBET 1264517 and CBET 1604742.

Chapter 5: 3D Extrusion Printing Induces Polymer Molecule Alignment and Cell Organization within Engineered Cartilage[5]

5.1 Introduction

Recognizing the relatively more flexible fabrication process and reduced labor and cost of acellular scaffolds compared to cell-laden approaches, the tissue engineering field has advanced to develop scaffolds that can better support biological functions for cells introduced *in vitro* or *in vivo*. [214] Among many cell types that have been combined with acellular scaffold to form an engineered tissue construct, stem cells are the most commonly used due to the advantages of multipotency and more abundant cell sources. [215-218] Besides widely used chemical cues such as growth factors to control stem cell lineage commitment, material cues including stiffness and geometry have been shown to contribute in stem cell differentiation.[219-222]

Therefore, cell-surface interactions with extracellular biomaterials are an important consideration when constructing tissue regenerative devices as such interactions can influence cellular attachment, alignment, proliferation, and differentiation when using multipotent cells such as mesenchymal stem cells (MSCs). The basement membrane in vertebrates is composed of a complex mix of ECM proteins with varied pore and fiber size and orientation serves as the substrata for supporting cellular structures. [223] Although the process is not well understood, it is generally accepted that the surface topography of the basement membrane or synthesized material provides cues to influence cellular function and differentiation, through activation of plasma membrane integrin receptors. [224, 225] Surface features at the microscale influence cell adhesion, alignment, morphology, proliferation and

[5] Adapted from: Guo T, Ringel JP, Lim CG, Bracaglia LG, Noshin M, Baker HB, Powell DA, Fisher JP. 3D Extrusion Printing Induces Polymer Molecule Alignment and Cell Organization within Engineered Cartilage. *Journal of Biomedical Materials Research: Part A.* In Press.

differentiation; having an even greater impact at the nanoscale. [226, 227] For example, topographically influenced MSCs showed similar efficiency when differentiating into bone lineage as to MSCs treated with osteogenic media. [228] In another study, nanotopography also showed a stronger effect on the upregulation of neuronal markers than biochemical cues alone on unpatterned surfaces. [229] In general, the presence of surface features on the scaffold such as ridges, steps or spaces affects cell attachment and proliferation by as the cells increase their complement of filopodia and microspikes, which are known to be the "sensing" organelles. [230]

Articular cartilage tissue exemplifies the impact of cellular organization on tissue function. It is composed of 3 zones: the superficial or tangential zone, the middle or transitional zone, and the deep zone, each with different biological functions. Cartilage in the superficial zone provides high tensile properties by having parallel collagen fibers and chondrocytes to the surface of the cartilage.[231] Cartilage in the middle zone provides a transition between the superficial and deep zones. Collagen fibers and chondrocytes in this zone are randomly organized to provide a functional bridge between the superficial and deep zones. The deep zone collagen fibers and cells are arranged perpendicular to calcified cartilage and bone, which allows it to adhere to bone tissue and provide resistance to compression. Zonal differences in matrix organization and structure are due to variations in the cellular activity of each zone. For example, proteoglycan 4 (PRG4), which is a large glycoprotein contributes to the lubricating function of the synovial fluid, is predominantly produced by the superficial zone chondrocytes.

The dysfunction of articular cartilage affects millions of people of all ages. The prevalence of clinical osteoarthritis had grown to nearly 27 million by 2007 with trends indicating this

number will continue to increase every year. [232] A limited self-renewal capacity owing to lack of blood vessels and low cellularity makes cartilage one of the most difficult tissues to regenerate. A few of the most frequently employed treatments include microfracture, autologous chondrocyte implantation (ACI), but these strategies have limited success. [233] To significantly reduce the potential immune response from transplanting allogeneic cartilage tissue and the cost and time associated with ACI, the use of biomimetic acellular scaffolds which provide zonal biological and mechanical cues to stimulate seeded stem cell differentiation is an attractive alternative for functional cartilage regeneration.

Our present study investigated the impact of 3D printing induced surface properties on MSC adhesion and chondrogenic differentiation, both at a scaffold pattern (~100 μm) and polymer molecule level (nano scale) so that cell distribution as a population and cell alignment at the single cell level were observed. Unlike the complicated nanofabrication process used in previous studies to achieve desired surface patterns, the polymer molecule and cell alignment we observed was a result from the 3D extrusion without any additional processing. The objective of this study is to demonstrate effect of polymer molecule alignment and induced cell alignment caused by extrusion based 3D printing. The cell alignment was revealed and quantified both in *in vitro* and *in vivo* models. Finally, the chondrogenic differentiation of MSCs on scaffolds printed with different patterns was evaluated.

5.2 Materials and Methods

5.2.1 Scaffold Fabrication

PLGA with LA:GA ratio of 85:15 and molecular weight of 35kD was purchased PolySciTech (West Lafayette, IN). The 3D printed scaffold was fabricated using 3D Bioplotter (EnvisionTEC, Gladbeck, Germany) with direct melt extrusion technique. The scaffold was

programmed with inner patterns using the provided EnvisionTEC software. For printing, the material was loaded into the printing cartridge and melted at 165°C and extruded at 9 bar with an average speed of 1.5 mm/s using a 0.2 mm inner diameter needle based on previously established methods [234] . Parallel pattern scaffold has fibers diameter of 0.2 mm parallel to each other with 0.2 mm edge-to-edge spacing of two adjacent fibers. For random pattern, the angle to the contour and the spacing of each layer were randomly selected using a random generator package in R software. All scaffolds have a dimension of 4 mm (length) × 4 mm (width) × 1.5 mm (height). The casted PLGA was made by melting the raw PLGA material and shape to the same size as the printed scaffold.

5.2.2 Small Angle X-Ray Scattering

SAXS has been used to determine the material internal structure as the interference pattern is characteristic to the molecule orientation in the material. Therefore, by recording the scattered pattern or signal distribution on each direction, the intrinsic molecule alignment of the material can be interpreted. SAXS measurements were performed with Xenocs Xeussat system at the X-ray Crystallographic Center, located at Department of Chemistry & Biochemistry, University of Maryland. The system was equipped with 5 Meter system with CuKα sealed 30W tube high brightness micro-focus source at a constant X-ray energy of 10 keV. The samples were taped on a metal holder in the experiment chamber. The exposure time to collect each scattering profile was 600 s. The sample-to-detector distance was set at 2514.72 mm for all samples. The incidence angle between x-rays and the sample surface was fixed at 0.14°. Scattering profiles were recorded on a Pilatus 1M 2-D area detector.

5.2.3 Cell Culture and Seeding

Primary hMSCs (P2) were purchased (Lonza, Basel, Switzerland) and expanded in a monolayer in high glucose Dulbecco's Modified Eagle Medium (DMEM) (Life Technologies, Carlsbad, CA) containing 0.1% penicillin/streptomycin (Life Technologies), 0.1 mM non-essential amino acids (Life Technologies) and 10% fetal bovine serum (Life Technologies, Carlsbad, CA) (MSCs growth media). After reaching the desired amount, cells were lifted with trypsin to form a cell pellet. Approximately 1 million cells were seeding onto each scaffold by dropping 100 μL concentrated cell solution covering the entire scaffold. Before adding fresh MSCs growth media, seeded scaffolds were kept in 37 °C for 4 hours to allow attachment. Cell culture media was changed every the other day during maintenance.

5.2.4 Live/Dead Staining

Live/Dead assay was performed to show cell viability and morphology. The scaffolds were washed in Hank's buffered saline solution (HBSS, Life Technologies, Carlsbad, CA) for 5 minutes to remove extra media and other active reagents. The cells on the scaffolds were stained in a 2 μM ethidium homodimer and 4 μM calcein AM (Life Technologies, Carlsbad, CA) combined with HBSS for 30 minutes in the dark.

5.2.5 Confocal Imaging

Cells were imaged using Zeiss LSM 710 confocal microscope (Carl Zeiss Microscopy, Jena, Germany). Separate channels of lasers were applied, A488 for green, A594 for red, and a DAPI channel. Images were taken at frame scanning mode, with a size of 1024 × 1024 at medium speed to achieve desired resolution. Each laser power was kept in consistent for comparable results.

5.2.6 Cell Alignment Quantification

The degree of cell alignment was quantified using an Image J plugin Orientation J following a series of steps. First the image taken from Zeiss software was converted to 8 bit in Image J. The region of interest (ROI) was defined by circling cells along their shape. Orientation J automatically measured the alignment angles to the horizontal axis. By extracting the printed fiber orientation, the angle to the printed fiber can be calculated. Images were taken from three different regions to calculate average orientation. All cells on each image was counted to eliminate the biased choices. Single-blinded experiment was conducted to analyze the images.

5.2.7 Animal Surgery

The scaffolds pre-seeded with rat MSCs were implanted subcutaneously in rats. Three rats were used with 6 implantations per rat, 3 dorsal and 3 ventral. The scaffolds were UV sterilized and seeded with rat MSCs (R&D systems, Minneapolis, MN). The cell-laden scaffold was prepared one day before the implantation and was allowed to culture and maintained at 37 °C until the surgery. After induction and maintenance with isoflurane, a small dorsal incision was made in the skin. Subsequently, a subcutaneous pocket was created cranially and caudally to the incision by blunt dissection and then the scaffolds were placed into the created space. The wound was closed by subcuticular suturing along the incision lines using 4-0 C-14 reverse cutting resorbable sutures. After 7 days of implantation, the rats were euthanized and the implants were collected for analysis. Using both histology and confocal microscopy, cell alignment was examined within the scaffolds. This animal protocol was approved by University of Maryland College Park Institutional Animal Care and Use Committee (IACUC) (Project 955010-1).

5.2.8 RNA Isolation and qRT-PCR

Toal RNA was isolated from the hMSCs using an RNeasy Plus Mini Kit (Qiagen, Frederick, MD) and then reverse transcribed to complementary DNA (cDNA) using a High Capacity cDNA Archive Kit (Life Technologies, Carlsbad CA). The cDNA solution was then combined with a Universal Master Mix (Life Technologies, Carlsbad CA), as well as oligonucleotide primers and Taqman probes for Sox 9, type II collagen (COL2A1), aggrecan (AGC), and the endogenous gene control glyceraldehyde 3 phosphate dehydrogenase (GAPDH) (Thermo Fisher Scientific, Waltham, MA) to perform quantitative reverse transcriptase-polymerase chain reaction (qRT-PCR). A standard protocol at thermal conditions of 2 min at 50°C, 10 min at 95°C, 40 cycles of 15 s at 95°C, and 1 min at 60°C was applied. The relative gene expression level of each target gene was normalized to the mean of GAPDH in each group then the fold change was determined relative to the first time point baseline gene expression. Fold change was calculated using the ΔΔCT relative comparative method as described previously [235].

5.2.9 Statistical Analysis

Student t-test was performed to compare cell orientation between two groups. To assess gene expression, data were analyzed using analysis of variance and Tukey's multiple-comparison test. A significance level of 95% was chosen, and a p-value less than 0.05 was considered to indicate a significant difference between samples.

5.3 Results

5.3.1 Polymer Alignment

We scanned our printed scaffold and a casted PLGA scaffold using small angle X-ray scattering to investigate the polymer molecule organization between casted and printed

scaffolds. Differences in molecular organization of materials results in different scattering maps due to the different paths traveled by the X-ray. Therefore, the distribution of scattering signals on each direction carries structural information of the molecular alignment in each direction. The scattering intensity map here shows homogeneous scattering in each direction for casted PLGA polymer samples, which indicates the polymer molecules were randomly distributed in the material. However, the scattering of printed PLGA was compressed to one direction as a result of constructive interference, which indicates a polymer molecule orientation exists in the printed sample (**Figure 5.1A**). Notably, the scaffold was printed in solid construct without spacing and the X-ray beam diameter was smaller than the printing nozzle diameter to avoid structure interference. The intensity was presented as an arbitrary detector unit so that the value itself does not carry any structural information; only the ratio of distribution of the scattered signal in each direction indicates the intrinsic polymer molecules organization.

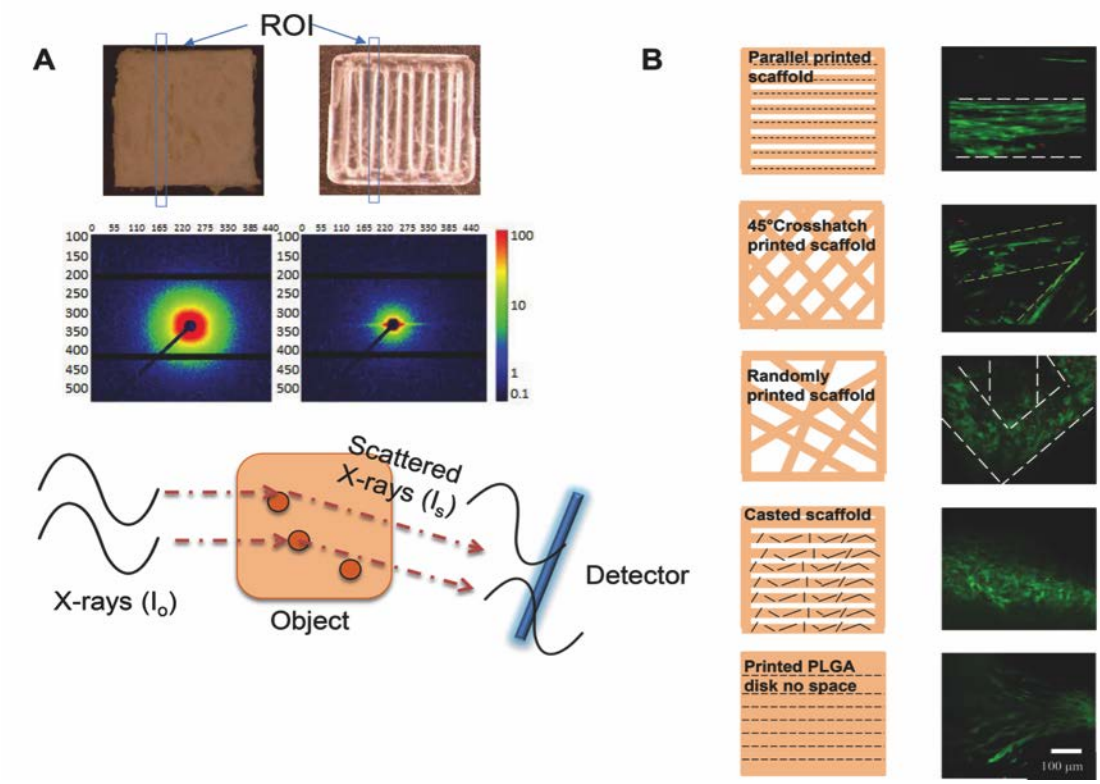

Figure 5. 1. 3D printing induced polymer molecule alignment and resulted cell alignment. A. SAXS set up and results comparing casted and printed PLGA scaffolds. Scattered X-ray waves arrive at the detector at different time to form signals as a result of material intrinsic structure. X-ray scattering shows uniform scattering in all directions of the casted scaffold, which indicates random polymer molecule organization. However, scattering shows higher intensity on the horizontal direction of the printed scaffold, which indicates vertically oriented polymer molecule existing after printing. Blue boxes indicate regions of interest (ROI) upon incoming x-ray. **B.** Cell alignment on scaffolds printed with different patterns. Confocal microscope image showed hMSCs aligned differently on printed patterned scaffolds. Live cells were shown in green and dead cells were shown in red. Short black lines indicates the polymer molecule alignment.

5.3.2 In Vitro Cell Alignment

hMSCs were seeded on the 3D printed PLGA scaffolds with different patterns. Confocal microscopy was used to reveal the cell organization followed a quantitative analysis using ImageJ. We observed different cell alignment levels when seeded on scaffolds printed with different patterns (**Figure 5.1B**). Since the polymer molecules on each single printed fiber were aligned due to the extrusion processing, cells seeded on scaffolds with parallel fibers showed an induced alignment along the extrusion direction. As a control group, hMSCs were

also seeded on casted PLGA scaffold (melt and shaped with parallel pattern), where cells appeared randomly ordered on each fiber. As another control, printed solid scaffold without spacing was seeded with cells to exclude structural cues. Without spacing, cells were still observed to be aligned on the printed direction. For a 45° crosshatch pattern, the printed fibers were less ordered compared with the parallel fibers considering the interactions at the crossed regions. As a result, the cells appeared less ordered than cells seeded on the parallel scaffold. For the random patterned scaffold, with multiple connection points for cells to migrate, cells appeared more randomly aligned compared to the previous two cases. In particular, cells on scaffold corners appeared to be bridging into different directions. In order to test if the cells were encouraged to align due to high concentration, cells were also seeded on the parallel printed scaffold at 10X and 100X diluted concentration. The yield cell attachment efficiency on the scaffold was approximately 15% according to hemacytometer counting. At different seeding concentration, the cells appeared similar degree of alignment, where the majority of the cells attached with an angle less than 30°. Although limited cells can be detected were seen at 10^4 cells/scaffold seeding density after attachment, the detected cells showed positive alignment along the printed fiber direction (**Figure 5.2A**).

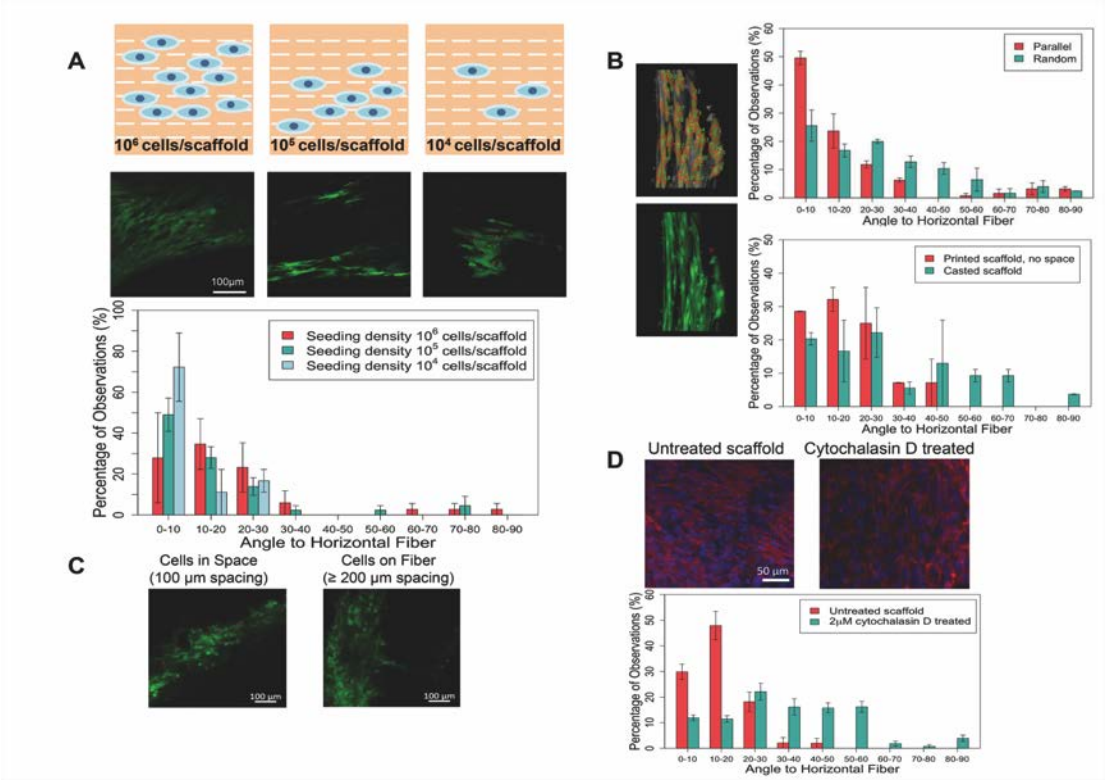

Figure 5. 2. Cell alignment quantification and the impact of different factors on cell attachment. A. Cell alignment and quantification for different seeding densities. Cells seeded at various concentration all showed aligned pattern, with more than 80% of the total population had an angle to the fiber less than 30 degree. **B.** Cell alignment quantification for scaffolds with different patterned and fabrication methods from Figure 1. Individual cells were selected manually in ImageJ, then the angles were automatically calculated by the built in Plugin OrientationJ. Cells on scaffolds with parallel pattern mostly aligned along the fibers, by displaying an alignment angle to the printed fiber of less than 30°. As a comparison, cells on random printed fibers aligned with less order, displaying more evenly distributed angles. As a control, cells on casted scaffold showed evenly distribution of attachment angles. In a nother control using printed solid disk without any patterns, cells showed directional alignment along the printed fibers. All cells from the captured images were included for analysis. **C.** Preferred adhesion with different scaffold spacing. With a 200 μm printed fiber, when the width of the spacing is smaller than the fiber, most cells appeared in the gap spacing rather than attached on the surface of the scaffold. However, when the spacing was larger than the diameter of the fiber, cells tended to attach on the scaffold surface instead. **D.** Phalloidin staining of actin fibers and comparison of cell alignment before and after cytochalasin D treatment. After cytochalasin D treatment, the attached cells completely lost their organized direction due to loss of focal adhesion.

The quantified cell alignment revealed that the cells on parallel patterned scaffolds were more organized. The general trend distribution showed that the majority of cells seeded on parallel scaffolds had a smaller contact angle to the horizontal fiber compared to the random

patterned scaffold. 50% of cells on the parallel patterned scaffold showed a contact angle less than 10° while only 26% of cells on the random patterned scaffold had contact angles less than 10° (**Figure 5.2B**).

The above results suggested that not only the aligned polymer molecules determines the how the cell would adhere, but also the pattern of the printed fibers contributes to the overall cell distribution. Taking account this effect, we conducted experiment on how the orientation of the fiber influence the cell adhesion. We found that when the spacing was 100 μm or less, cells tend to fill the gaps rather than grow on the printed fibers. On the contrary, for spacing larger than 200 μm, cells would choose to attach on top of PLGA fibers (**Figure 5.2C**).

The phalloidin staining revealed aligned actin fibers in the ECM of aligned hMSCs. However, after treating the attached and aligned cells with 2μM cytochalasin D, a known inhibitor of actin polymerization, the cells were disassembled and completely lost their organized direction due to loss of focal adhesion. The quantified resulted showed significant different angle distribution between the untreated group and the cytochalasin D treated group (**Figure 5.2D**).

5.3.3 In Vivo Cell Alignment

We then conducted an *in vivo* study using a rat model by subcutaneously implanting the scaffold to see if the cell alignment can be maintained (**Figure 5.3A**). After retrieving samples from the rats, the scaffold was visually intact with clear preserved patterns. The whole scaffold was stained and imaged, where cell nuclei were stained blue using DAPI and actin was stained red using phalloidin to show the cell morphology and orientation. While cells appeared randomly distributed on the casted scaffolds, on the printed scaffolds cells

were aligned along printed fibers (one fiber marked with dashed line) (**Figure 5.3B**). Cell orientation (angle to the fiber) was quantified using ImageJ and the Plugin OrientationJ by manually selecting individual cells and automatically calculating the angles. A total of 178 cells from three images of the casted group and 118 cells from three images of the parallel were included in the single blinded quantification study. Most of the cells on the parallel printed implant displayed an angle less than 50°, with 37% having an angle to the fiber of less than 20°. However, the cells attached on the casted scaffold showed an evenly distributed orientation. In terms of cell morphology, the MSCs on parallel printed scaffolds also appeared more elongated or star shaped compared to those on the casted scaffold.

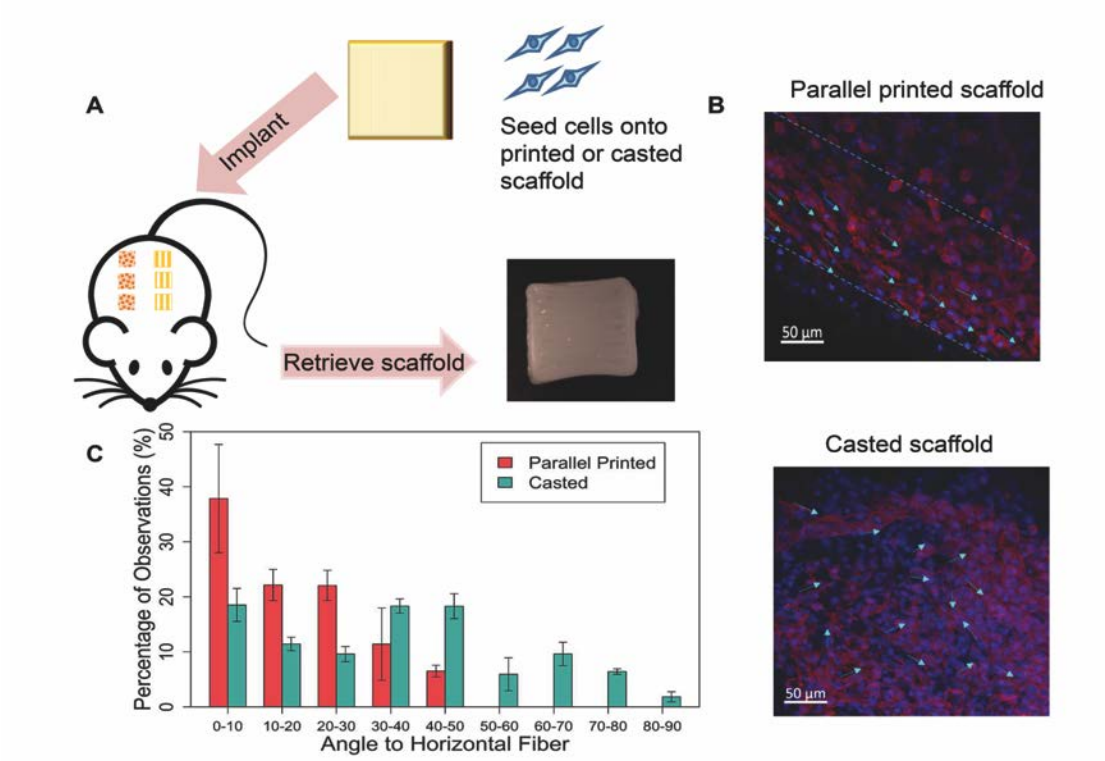

Figure 5. 3. ***In vivo*** **cell alignment evaluation and quantification. A.** Experimental flow of the animal study. Rat MSCs were seeded on parallel printed or casted scaffolds, then scaffolds were implanted subcutaneously in rats. After 7 days, retrieved scaffolds showed intact structure and printed patterns. **B.** Cell alignment was maintained after *in vivo* implantation. Cells appeared mostly aligned on the parallel patterned scaffold, while cells were more randomly distributed on the casted scaffolds. **C.** Quantification of cell alignment *in vivo*. The average number was calculated from three different images.

5.3.4 Chondrogenesis Response

Finally, we investigated the chondrogenesis as a response to different scaffold patterns and the induced cell alignment. Positive markers aggrecan (main proteoglycan in articular cartilage), type II collagen (composes main part of chondrocyte ECM), Sox 9 (transcription marker) and PRG4 (superficial zone marker) were evaluated. Generally, increased expression of positive markers was observed in parallel patterned scaffolds, which indicates a potential to engineer zonal scaffolds with a controlled cellular response. Expression of aggrecan on both day 14 and day 21 was significantly higher for the MSCs seeded on parallel patterned scaffolds. Similarly, approximately 2.5 folders higher expression of type II collagen was observed in the parallel group compared to the random pattern group. In particular, the superficial zonal marker expression was 7 fold increased for cells on parallel aligned scaffolds, and the increased expression was maintained throughout the 21 day study.

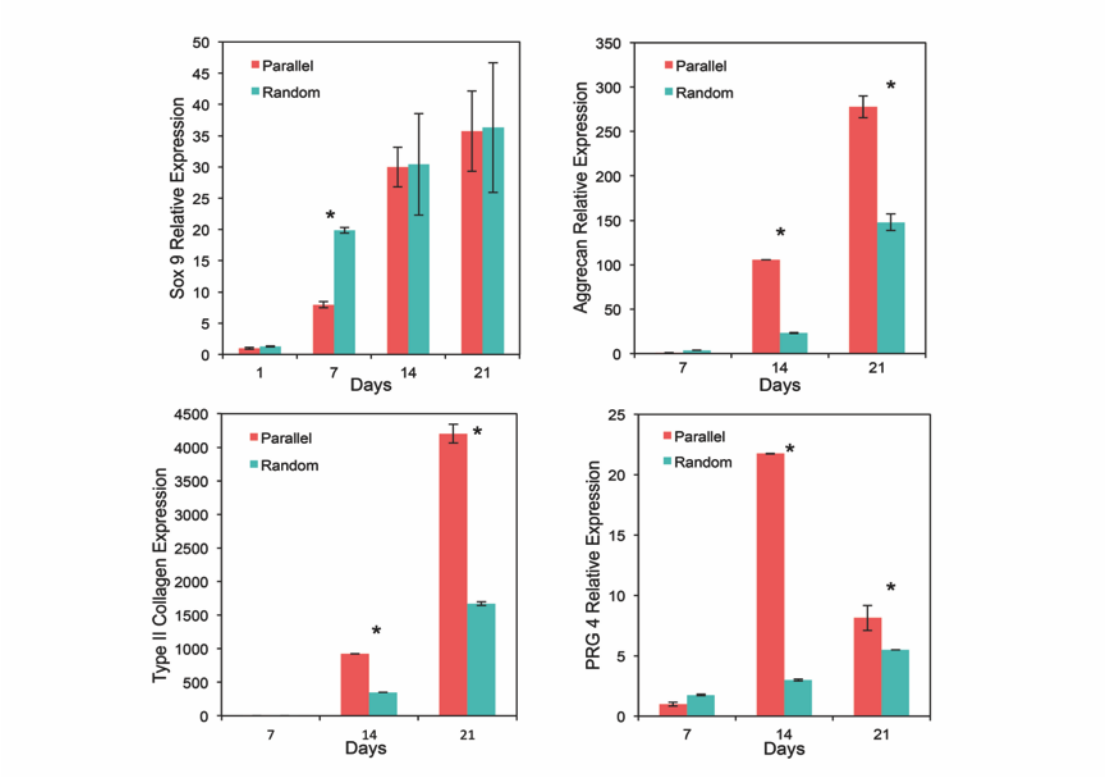

Figure 5. 4. Comparison of chondrogenic gene expression for cells grown on scaffolds with different patterns. All chondrogenic markers showed different levels of expression as a response to different scaffold patterns and induced cell alignment. In general, positive

chondrogenic markers aggrecan and type II collagen expression were up-regulated for the parallel pattern group. Superficial zonal marker PRG4 expression was significantly higher when hMSCs were parallel aligned.

5.4 Discussion

In this study, we investigated the impact of polymer alignment as a result of extrusion-based 3D printing at high pressure and temperature. Most of the reported PLGA printings use solvents or adhesives combining with an ink jet printer. [236, 237] Because of the more extreme processing conditions required, only few direct fusion extrusion on PLGA printing has been attempted. As a result, detailed cell-material interactions such as cell attachment or alignment under such fabrication ways have not been studied. In fact, as a result of sheared polymer "solution" under high pressure (9 bar) through a fine needle (0.2 mm), induced MSC alignment as a response to different scaffold fabrication methods and patterns was demonstrated and evaluated both *in vitro* and *in vivo*. Our results showed that MSCs exhibited more controlled and organized attachment on printed scaffolds compared to casted scaffolds. The nanoscale polymer molecule alignment is believed to be the major determining factor for cell alignment, although the overall cell distribution could be affected by the micropatterning of the printed scaffold. In one aspect, the aligned polymer molecules caused attached cells to align, where we saw most of the cells aligned along the printed fiber with a pure parallel pattern, with and without a space in between the printed fibers. However, this effect can be compromised by the scaffold patterns that have crossed fibers, so that the level of alignment was weakened as the randomness degree of the polymer fibers increased. These findings will provide useful insight surrounding cell-material interactions, in particular in the context of 3D-printing approaches. The results will help to develop scaffolds with desired cell distribution in complex tissue engineering applications such as engineered zonal cartilage.

SAXS is a useful way to determine the material internal structure since the interference pattern is characteristic to the material structure. The intensity of the interfering waves is a result of distance of the particles and their orientations with respect to the incidence beam, so that the detector can record brightness and darkness based on whether the scattered waves arrive in phase or out of phase. In our case with a solid polymer sample, the orientation of polymer molecules and their degrees can be revealed by the 2D scattering pattern. In SAXS, where the purpose is to reveal the material intrinsic structure properties, only Thomson scattering is concerned as this type of photon collision is strictly synchronous to create coherent scattering that carries structural information. [238] Therefore, only the ratio of intensity distribution on each direction tells the particle or molecule orientation, not the overall intensity of each sample. In the casted samples, the scattering pattern has equal intensities around the incident beam, which indicated randomly oriented polymer molecules. As a contrast, the compressed scatter pattern on the horizontal direction demonstrated a molecule partial orientation along the vertical direction. We hypothesize that this phenomenon is caused by the shear force during high temperature and high pressure printing when polymer undergoes glass transition because similar partial orientation patterns are commonly seen in sheared liquids or spun fibers. [239] In another aspect, such alignment was not observed in our ongoing low temperature and low pressure printing project using the same polymer.

The cell organization on the printed scaffold was investigated. Our results demonstrated that the overall cell distribution combines the effect of aligned polymer molecules and printed fiber orientation. As a major factor during extrusion, sheered polymer “fluid” generated an organized micro-environment of aligned polymer molecules that had an impact on cell alignment. As the polymer molecules and polymer chains align, it may influence the regional wettability chemogradient and thus have an impact on the cell adhesion and organization. [240] However, it was noticed that cells also have an intension to bridge into small gaps (**Figure**

5.1B). This bridging feature has been found to be favored by cells during settlement because it reduces the unfavorable energy barriers by increases the tension along the unsupported cell membrane as well as reducing the overall adhesion strength. [241] Therefore, on parallel printed scaffolds, cells appeared highly aligned along each printed fiber because in this case, the molecule alignment is the only dominating factor as all printed fibers were separated from each other. For the crosshatch pattern or random pattern, where fibers crossed each other, the resulted small gaps in crossed regions served as another driving force for cell to settle besides the aligned polymer molecules. As a result, when the degree of randomness of the fiber angle increased (**Figure 5.1B, 2B**), attached MSCs were found to be less aligned, due to the effect of alignment caused by polymer molecule alignment was compromised by the gaps between crossed fibers favored by cells to reduce the attachment energy. The later driving force became more and more dominating as there were more connections between fibers present. To exclude the effect that the relatively high cell seeding density (10^7 cells/ml, equivalent to 10^6 cells/scaffold, with a yield attachment efficiency of 15%) may have a potential to encourage cells to grow in a certain direction as they were packed, lower seeding densities at 10^6 cells/ml and 10^5 cells/ml were performed, where same degree of alignment was demonstrated. Such alignment was based on cell adhesion through ECM. The demonstrated alignment phenomenon is believed to apply to other synthetic polymers going through comparable extrusion process. In fact, similar alignment effect was also achieved using scaffolds printed during our ongoing study using poly (L-lactide-co-caprolactone) (PLCL). After treating with an actin inhibitor cytochalasin D to interrupt the focal adhesion, the aligned pattern was completed lost and resulted random cell organization on the printed scaffold.

Next we expanded the cell alignment study in an *in vivo* rat model by implanting pre-seeded casted and parallel printed scaffolds subcutaneously. The demonstration of maintaining the

desired cell orientation *in vivo* is an essential step before future pre-clinical investigation, so that such potential was assessed in this study. Besides similar cell orientation observed as the *in vitro* studies, the anisotropic shape of cells on printed scaffold and the more rounded shape on casted scaffold indicated cellular function difference. These results demonstrated that the cell shape and alignment can be maintained or achieved in a *in vivo* model, which makes this approach very attractive to develop functional complex tissue with layered or controlled cell behavior such as creating zonal cartilage by printing a scaffold containing different patterns in each zonal.

It was previously discovered that the MSC shape as it adhered to a micro-patterned surface affects differentiation, wherein cellular anisotropy was indicated to have an impact on the lineage commitment of MSCs. [242] Although the full mechanism remains unclear, relevant progress made in the past decade indicated that the attached cellular shape might be a result of cytoskeletal tension. [243-245] In this study, we observed variable cell morphology among different printed patterns and printed vs. casted samples, which we hypothesize to be a result of the initial cellular adhesion response to surface environment (**Figure 5.1B, Figure 5.3B**). The cell shape can further influence differentiation capacity. [246-248] In our evaluation of chondrogenic gene expression, variable levels of chondrogenic differentiation of MSCs was demonstrated in the PCR results (**Figure 5.4**). We observed that attached MSCs appeared more elongated and aligned on the parallel patterned scaffolds and had enhanced chondrogenic gene marker expression. In particular, the zonal specific marker PRG4 expression associated with the superficial zone, was significantly higher in the parallel scaffold group where chondrocytes aligned parallel to one another. The recapitulation of articular cartilage zonal structure has been a great challenge in the field. The achievement of zonal marker expression as a result of cell alignment is an important step to develop functional cartilage tissue by engineering the cellular microenvironment. Although future

steps of more quantitative analysis and further comprehensive research is needed to understand more about how and why MSC morphology has an impact on differentiation, our demonstrated results will help open a new way to create and control such desired cell organization by using 3D printing techniques. Research in the field will greatly benefit the understanding of cell-cell and cell-material interactions and thus provides new concepts and techniques to develop advanced biomaterials for tissue regeneration.

5.5 Conclusions

The results indicated that PLGA molecules can be forced to align in the extruded direction at high shear conditions (e.g. high pressure and temperature, small needle). This phenomenon further induced the attached cells to align along the extruded fiber, which we propose could be a result of aligned polymer molecules on scaffold surface involved in cell attachment. However, the overall cell distribution on the scaffold can be influenced by the printed fiber organization as well. With the parallel printed pattern, molecule alignment dominates the cell alignment, where with the random pattern, such alignment can be altered as the cells are bridging the small gaps. The cell orientation was maintained *in vivo* in a subcutaneous implant, making this approach promising for combining with surgical procedures that release native stem cells for improved cartilage repair. The results on the effect of printed pattern on cell organization and differentiation demonstrated that this approach is promising to create scaffolds with controlled cell and ECM arrangement to achieve desired biological function required for chondrogenesis. Furthermore, the polymer molecule and cell alignment achieved by 3D extrusion will have a significant impact on regenerating biomimetic cartilage tissue in a cost and labor effective way, as well as providing a fundamental understanding of cell-material interactions.

5.6 Acknowledgements

Ting Guo was responsible for the experiment design, experiment performance, and data analysis. This work was supported by National Science Foundation grant CBET 1264517, CBET 1604742, National Institute of Biomedical Imaging and Bioengineering, Center for Engineering Complex Tissues (CECT, P41 EB023833), and University of Maryland Graduate School Fellowships. The quantitative analysis Image J plugin package Orientation J was provided by Dr. Michael Unser's Biomedical Imaging Group at Swiss federal Institute of Technology in Lausanne (EPFL) for free. The authors thank Dr. Feng Gao for his help on quantitative cell alignment data analysis and programming. We would also like to acknowledge the X-ray Crystallographic Center at University of Maryland for conducting SAXS. The animal surgery was performed by Dr. Laura Bracaglia, Dr. Hannah Baker, Casey Lim, and Douglas Powell.

Chapter 6: Bioactive Scaffold in Combination with Microfracture to Enhance Cartilage Regeneration

6.1 Introduction

Osteoarthritis is the most common cause of disability in adults.[232] To 2016, there are approximately 14 million individuals in the United States that experience symptomatic knee osteoarthritis. [249] Whether caused by trauma or pathological change, this degenerative disease is resulted from the breakdown of articular cartilage between joints. Articular cartilage is the highly specialized connective tissue surrounding surfaces at joints. Its primary function is to protect these surfaces by providing smooth, low friction contact and enabling smooth load transfers at the joints. Articular cartilage has a unique and distinct structure, despite the fact that it is innervated and lacks blood vessels, nerves, and lymphatics. Articular cartilage is composed of one cell type, chondrocytes, surrounded by a dense extracellular matrix (ECM) composed of water, collagen, hyaluronic acid, and proteoglycans.[250] Articular cartilage can be broken up into 3 zones, superficial, transitional, and deep zones that correspond to the cartilage depth. The distinct alignment of cells and collagen fibers in each zone provides specific support again mechanical loadings. ECM composes more than 90% of dry weight of articular cartilage and it also has an impact to maintain the water content of the tissue. Therefore, it is essential to understand and restore the ECM function in cartilage tissue engineering. The ECM of cartilage can be divided into 3 regions, pericelluar, territorial, and interterritorial, based on its composition and properties that it lends to cartilage.[251] The pericellular matrix composes the thin layer surrounding the chondrocytes. It is composed of mainly proteoglycans as well as other proteins and is responsible for transducing signals to the cell when the cartilage undergoes load bearing. It is theorized that the territorial matrix contributes to protecting chondrocytes from mechanical stresses and strains caused and

providing strength to the cartilage to endure loading. The final region of the ECM is the interterritorial region that composes the largest percentage of the ECM and supplies most of its mechanical properties. Large collagen fibers with the highest concentration of proteoglycans are randomly oriented throughout this region to provide compressive strength. Proteoglycans play an essential role in the ECM because the overall negative charge retains water molecules; so the resulted swelling pressure allows the tissue to resist compressive force.[252] The most abundant proteoglycan that composes the ECM of articular cartilage is aggrecan. It is decorated with several types of sulfated glycosaminoglycans (GAGs), including chondroitin sulfate and keratan sulfate. Multiple aggrecan monomers self-assemble into large molecules by covalently bond to hyaluronic acid forming large aggregated proteoglycans which carry a negative charge, resulting in significant amounts of water being retained by the tissue.[253, 254]

The most common surgical treatment for cartilage defects are microfracture and Autologous Chondrocyte Implantation (ACI). ACI is usually recommended for defects greater that 2 cm^2 in size and requires an extensive recovery time. It is also difficult to harvest and cultivate a large enough number of chondrocytes for implantation due to low proliferation rate and potential to dedifferentiate during culture.[255, 256] The recently FDA approved product Matrix-Induced Autologous Chondrocyte Implantation (MACI) showed improved treatment results.[257] However, it has the same drawbacks including the dual-surgery procedures and less abundant cell source. The most common surgical technique to treat cartilage defects is microfracture considering its well established standard procedure and lower cost. During the surgery, small holes are drilled into the subchondral bone underlying a cartilage defect to trigger the release of stem cells from bone marrow which differentiate into chondrocytes to regenerate articular cartilage tissue.[258] However, stem cells lack the guided cell

microenvironment to orient in the correct alignment that mimics native articular cartilage so the regenerated tissue is generally more fibrous and weaker than native tissue.

At the research stage, tissue engineering techniques have allowed scientists to attempt to regenerate biomimetic cartilage tissue, for example, by utilizing various levels of collagen II.[214] Other researchers have also attempted to isolate chondrocytes from the different zones of cartilage before seeding them onto 3D scaffolds in an effort to replicate the various zones in native articular cartilage.[259] However, besides the limited biological complexity and cell characterization involved in the design, the success of these approaches largely depend on the responses of the cells seeded on the scaffold, which is very challenging and not well-understood till now. An acellular scaffold with biological activities can be an attractive alternative for the cell-laden scaffold considering the potential manufacturing, preservation as a clinical product. To enhance the cartilage healing process, the acellular scaffold can be combined with the standard microfracture procedure without a second surgery.[260, 261] MSCs and growth factors released from bone marrow migrated to the defect site can initiate the tissue regeneration process. The goal of this study is to improve the cartilage tissue quality regenerated by microfracture by incorporating 3D printed scaffold functionalized with aggrecan. As the main proteoglycan component of native articular cartilage tissue, aggrecan provides binding sites to better recruit stem cells and growth factors to aggregate on the scaffold surface and increase cell attachment. Its function of trapping water in the cartilage microenvironment will also enhance the physiological environment for the stem cells released from microfracture. The first aim of the study is to design and verify the scaffold surface modification of aggrecan. We seeded the scaffold with bone marrow and analyzed the attached cell population using a customized centrifugation assay. After *in vitro* evaluation, we tested the scaffold function in a lapine model with microfracture, in comparison with the non-

functionalized scaffold and the standard procedure. The moving ability and regenerated tissue quality were assessed.

6.2 Materials and Methods

6.2.1 Scaffold Fabrication

Poly(L-lactide-co-caprolactone) (PLCL, PolySciTech, West Lafayette, IN) with lactic acid:caprolactone ratio of 70:30 and molecular weight of 45kD to 55kD was purchased for 3D printing. PLCL-amine scaffold material was made by combining PLCL with 15% poly(lactic-co-glycolic acid) (PLGA, PolySciTech, West Lafayette, IN) by weight and grinding the polymers together to form a homogeneous mixture. 3D printed scaffolds were fabricated using the 3D Bioplotter (EnvisionTEC, Gladbeck, Germany) using direct melt extrusion technique.[234] The scaffold inner pattern was programmed using the provided EnvisionTEC software. For printing, material was loaded in the printing cartridge and melted at 155°C for extrusion at 6.5 bar with an average speed of 4 mm/s using a 0.2 mm inner diameter stainless steel needle. Scaffolds had dimensions of 4 mm (length) x 4 mm (width) x 0.8 mm (height).

6.2.2 Aggrecan Functionalization of Scaffolds Through Covalent Bonding

Covalent bonding of aggrecan to the printed scaffold was achieved through the covalent bonding of EDC and sulfo-NHS. EDC acts as a zero-space linker and covalently binds the glycolic group on aggrecan molecules to the amine group on the printed PLCL scaffolds. PLCL-amine scaffolds were soaked in 0.1M 2-[morpholino]ethanesulfonic acid buffer (MES, Sigma-Aldrich, St. Louis, MO) buffer for 15 minutes prior to aggrecan functionalization. For each scaffold, a functionalization solution was composed of 0.5 mg lyophilized bovine

aggrecan (Sigma-Aldrich, St. Louis, MO), 1 mL MES buffer, 1.6 mg 1-ethyl-3-[3-dimethlaminopropyl] carbodiimide (EDC, Thermo Fisher Scientific Waltham, MA), and 4.4 mg N-hydroxysulfosuccinimide (sulfo-NHS, Thermo Fisher Scientific Waltham, MA) and allowed to react for 15 minutes based on the EDC-NHS reaction manufacturer protocol. Scaffolds were placed in the functionalization solution and placed on the shaker to react for 2 hours. Scaffolds were washed with phosphate-buffered saline (PBS, Sigma-Aldrich, St. Louis, MO).

6.2.3 Nuclear Magnetic Resonance Spectroscopy

Bruker Advance III 600 NMR spectrometer with BBFO gradient probe was used for the ^{1}H NMR experiments. Polymer samples were dissolved in Dimethyl Sulfoxide-d_6 (CD_3SOCD_3). The internal solvent signal δ (CD_3SOCD_3) = 2.5 ppm was used as reference. Aggrecan was dissolved in D_2O at 1mg/ml. Printed scaffold functionalized with aggrecan (PLCL-aggrecan) was dissolved in CD_3SOCD_3 / D_2O at 2:1 ratio for better solubility. Solvent suppression pulse sequence was used to suppress solvent ^{1}H signal for Aggrecan and PLCL-aggrecan samples to achieve the optimum sample signals. A total of 64, and 128 scans were used for ^{1}H, solvent suppression experiments, respectively.

6.2.4 Cell Culture and Seeding

Human mesenchymal stem cells (hMSCs, RoosterBio, Frederick, MD) were expanded in RoosterNourish high performance MSC media (RoosterBio, Frederick, MD). Cells were maintained according to the manufacturer's recommendation and grew 10X within 7 days of culturing. After reaching the recommended cell density provided by RoosterBio, cells were lifted with trypsin-EDTA (Gibco-LifeSciences, Gaithersburg, MD) and centrifuged at 200xg

for 10 minutes to form a cell pellet. Cells collected in a cell pellet were re-suspended in RoosterNourish media at a concentration of 10 million cells/mL of media. Approximately 1 million cells were seeded onto each scaffold by adding 100 µL of concentration cell solution to cover each scaffold. Scaffolds were kept at 37 ºC for 4 hours to allow for attachment to the scaffold surface. Cell culture media was changed every other day for cell maintenance.

6.2.5 Live/Dead Staining and Confocal Imaging

Live/dead assays were used to determine cell viability and morphology. Scaffolds were washed with Hank's buffered saline solution (HBSS, Life Technologies, Carlsbad, CA) for 5 minutes to remove excess media and other reagents. Cells on the scaffolds were stained with 2 µM ethidium homodimer and 4 µM calcein AM (Life Technologies, Carlsbad, CA) combined with HBSS and incubated for 30 minutes in the dark. Scaffolds were then washed with HBSS, soaked in 200 µL of 4% paraformaldehyde for each scaffold, and left to incubate for 15 minutes. Scaffolds were washed with 200 µL of phosphate-buffered saline (PBS) and stored in PBS until they could be imaged using a confocal microscope.

6.2.6 DNA Quantification

Human mesenchymal stem cells (hMSCs) were lifted from scaffolds using trypsin and centrifuged into a cell pellet. DNA was isolated from hMSCs using a DNeasy Plus MiniKit (Qiagen, Frederick, MD). DNA was quantified using a PicoGreen dsDNA Assay Kit (Quanti-iT, ThermoFisher Scientific, Waltham, MA). DNA isolates from the DNeasy kit were normalized to standard curve generated from the PicoGreen Assay to quantify DNA amounts.

6.2.7 Centrifugation Device Fabrication

A lid was designed in SolidWorks (Dassault Systémes, Vélizy-Villacoublay, France) for a slight press fit into the inner wells of a standard 24 well plate, allowing the assembly to be

flipped upside down and centrifuged. The designed device was intended to capture the scaffolds and cell solution during centrifugation. The lid was fabricated using an EnvisionTec Perfactory 4 Mini Multilens (Gladbeck Germany) using E-Shell 300, a clear, biocompatible acrylate-based resin (envisionTEC, Inc., Dearborn, MI). Excess resin was removed by submerging printed objects in 99% isopropanol (Pharmco-Aaper, Shelbyville, KY) for 5 minutes and blowing the interior dry with air. Complete resin curing was achieved with 1000 flashes of broad spectrum light (Otoflash, envisionTEC, Inc., Dearborn, MI). Scaffolds were cleaned in 100% ethanol (Pharmco-Aaper, Shelbyville, KY) for >30 minutes to leach any remaining soluble contaminants. Scaffolds were sterilized under fresh 100% ethanol and UV light for 20 minutes. Scaffolds were rehydrated in a serial dilution of ethanol to pH 7.4 sterile PBS (principal chemicals sourced from Sigma-Aldrich St. Louis, MO) in 4 steps (75:25, 50:50, 25:75, and 0:100 ethanol:PBS), with each intermediary step allowed to soak for 5 minutes.

6.2.8 Bone Marrow Seeding

Human whole unprocessed bone marrow (Lonza, MD) was seeded onto the printed scaffolds placed in ultra-low attachment 24-well plate (ThermoFisher). Equal amount of Dulbecco's modified Eagle's medium (DMEM; Life Technologies, MD) supplemented with 1.0% v/v penicillin/streptomycin (Life Technologies) and 0.1 mM nonessential amino acids (Life Technologies) was added to each well. The plate was incubated at 37°C, 5% CO_2, and 80% humidity for 24 hours to allow attachment.

6.2.9 Centrifugation Assay Set Up

The centrifugation assay set up is shown in Figure. The concept and determination of the centrifugal force were based on previously established protocol [262]. Upon test, the original lid of the 24-well plate was removed and the 3D printed cover (SmartLid)was applied to air-seal

the wells. The plates were centrifuged upside down at a relative centrifugal force (RCF) of 50 g for 5 min at 22°C to separate the adhered cells and non-adhered cells. After first centrifugation, the supernatant at the bottom of the SmartLid containing non-adhered cells were collected for cell counting. Tripsin-EDTA (Gibco) was then added to lift the adhered cells following a second centrifugation to harvest the adhered cells. The scaffolds and wells were washed once with PBS.

6.2.10 Evaluation of hMSCs Isolated from Whole Bone Marrow

Flow cytometry analysis was conducted to analyze the cell population isolated from the bone marrow. The cells were re-suspended at a concentration of approximately 5 million/mL. Cells and controls were stained using Human MSC Analysis Kit (BD Stemflow; BD, NJ) following the manufacturer's instruction. The data was analyzed using FlowJo for gating and population differentiation. Briefly, 100 μL of sample was mixed with 20 μL of the hMSC Positive Cocktail (CD90 FITC, CD73 APC, and CD105 PerCP-Cy5.5) and 20 μL of the hMSC Negative Cocktail (CD34 PE, CD45 PE, CD11b PE, CD19 PE, and HLA-DR PE) and incubated at 4°C in the dark for 30 min. After incubation, the mixed cell suspensions were washed twice with 500 μL of PBS containing 1% bovine serum albumin (BSA). The final cell pellet was suspended in 500 μL of PBS containing 1% BSA and analyzed using a BD FACSCanto II. The positive control using hMSCs (Lonza) and the negative isotype controls was used to set up the gate for all samples. The samples were running at medium rate for 90 second.

6.2.11 Animal Surgery and Tissue Harvest

Total of 14 New Zealand White Rabbit (7-9 lb) (Covance Inc., NJ) were included in this study. Anesthesia was induced by the veterinary resource staff with Ketamine (35-40

mg/kg)/Xylazine (2-5 mg/kg). Post sedation Isoflurane delivered from a precision vaporizer (1.5-3%) in 100 % O_2 was administered via face mask during the surgery. In this unilateral defect model, the right hind leg was served as defect leg while the left hind leg was treated as healthy control. Bupivacaine 0.25 % (up to 2 mg/kg) was injected to the trochlear grove prior to patella dislocation as local analgesia. The patella was dislocated laterally to expose the articular surface. A full thickness cartilage defect was then created on the trochlear grove with a size of 3 mm in length and width in the center of the trochlear groove. For groups with microfracture, the procedure was carried out by drilling with 0.75 mm K-wire. After debridement of the calcified cartilage layer, small holes (0.75 mm diameter holes approximately 2 mm deep equidistant from the created patellar groove defect) were made using K-wire at the four corners and the middle of the defect in the exposed bone of the chondral defect. Modified or unmodified polymer constructs were inserted into the cartilage defect site for two experiment groups and immediately thereafter the exposed patellar groove was reverted and the injury site was closed using resorbable sutures (**Figure 6.3A**).

The joints from both knees were harvested after 8 weeks. Euthanasia was performed with Beuthasol (Pentobarbital iv, 100 mg/kg) in auricular vein after a ketamine 20-40 mg/kg and 2-5 mg/kg xylazine subcutaneous injection. After euthanasia, the bilateral rabbit knee joints (femur end and chondyle) were then harvested for further analysis. The animal study including the following locomotion test (protocol #0717009) was approved by Institutional Animal Care and Use Committee (IACUC) at University of Maryland, School of Medicine.

6.2.12 Animal Locomotion Test and Evaluation

After two weeks (recovered from the surgery based on veterinarian's advice), the rabbits taken to an open field restricted by a 1.4 m × 0.5 m fence to allow for locomotion evaluation. Videos were recorded of rabbit test subjects from the top and side view on week 3, 4, 5, 6 and

8 post-surgery implantation of the scaffold. Videos were analyzed and test subjects were evaluated by Basso, Beattie, Bresnahan (BBB) Locomotor Rating Scale to quantify the subjects' movement, coordination, and weight bearing abilities post scaffold implantation. The BBB scale was slightly modified to fit the rabbit moving habits (**Table 1**). The score was averaged from three evaluators in a single blind study.

0	No observable movement of the hindlimbs.
1	Slight (limited) movement of one or two joints, usually hip and/or knee.
2	Extensive movement of one joint or extensive movement of one joint and slight movement of the other.
3	Extensive movement of two joints.
4	Slight movement of all three joints of the hindlimbs.
5	Slight movement of two joints and extensive movement of the third joint.
6	Extensive movement of two joints and slight movement of the third joint.
7	Extensive movement of the three joints in the hindlimbs.
8	Sweeping without weight bearing or plantar support of the paw without weight bearing.
9	Plantar support of the paw with weight bearing only in the support stage (i.e., when static) or occasional, frequent or inconsistent dorsal stepping with weight bearing and no plantar stepping.
10	Plantar stepping with occasional weight bearing and no forelimb-hindlimb coordination.
11	Plantar stepping with frequent to consistent weight bearing and no forelimb-hindlimb coordination.
12	Plantar stepping with frequent to consistent weight bearing and occasional forelimb-hindlimb coordination.
13	Plantar stepping with frequent to consistent weight bearing and frequent forelimb-hindlimb coordination.
14	Plantar stepping with consistent weight support, consistent forelimb-hindlimb coordination and predominantly rotated paw position (internally or externally) during locomotion both at the instant of initial contact with the surface or frequent plantar stepping, consistent forelimb-hindlimb coordination and occasional dorsal stepping.
15	Consistent plantar stepping, consistent forelimb-hindlimb coordination; predominant paw position is parallel to the body at the time of initial contact.
16	Consistent plantar stepping and forelimb-hindlimb coordination during gait; the predominant paw position is parallel to the body at the time of initial contact and curved at the instant of movement.
17	Consistent plantar stepping and forelimb-hindlimb coordination during gait; the predominant paw position is parallel to the body at the time of initial contact and at the instant of movement.

18	Consistent plantar stepping and forelimb-hindlimb coordination during gait; the predominant paw position is parallel to the body at the time of initial contact and curved during movement. The animal presents partial standing.
19	Consistent plantar stepping and forelimb-hindlimb coordination during gait; the predominant paw position is parallel to the body at the instant of contact and at the time of movement, and the animal presents occasionally full standing.
20	Consistent plantar stepping and forelimb-hindlimb coordination during gait; the predominant paw position is parallel to the body at the instant of contact and at the time of movement, and the animal presents frequent full standing.
21	Consistent plantar stepping and coordinated gait, consistent movement; paw position is predominantly parallel to the body during the whole support stage; consistent full standing.
	DEFINITIONS
	Slight: partial joint movement through less than half the range of joint motion. Extensive: movement through more than half of the range of joint motion. Sweeping: rhythmic movement of HL in which all three joints are extended, then fully flex and extend again; animal is usually side lying, the plantar surface of paw may or may not contact the ground; no weight support across the HL is evident. No Weight Support: no contraction of the extensor muscles of the HL during plantar placement of the paw; or no elevation of the hindquarter Weight Support: contraction of the extensor muscles of the HL during plantar placement of the paw, or elevation of the hindquarter. Plantar Stepping: The paw is in plantar contact with weight support then the HL is advanced forward and plantar contact with weight support is reestablished. Dorsal Stepping: weight is supported through the dorsal surface of the paw at some point in the step cycle. FL-HL Coordination: for every FL step an HL step is taken and the HLs alternate. Occasional: less than or equal to half. Frequent: more than half but not always; 51-94%. Consistent: nearly always or always; 95-100%. Partial standing: lifting the forelimb off the ground but with trouble holding the body straight for more than 1 second. Full standing: lifting the forelimb off the ground with a full support provided by the hindlimb.

Table 6. 1. Modified BBB Locomotor Rating Scale for Rabbits after Orthopedic Surgery

6.2.13 Optical Coherence Tomography

The frequency-domain OCT imaging system utilized in this study was equipped with a wavelength-swept laser as light source which was centered at 1310 nm with 100 nm

bandwidth [263]. The wavelength-swept frequency was 16 kHz and the output power was 17 mW. 3% of the laser output power went into a Mach-Zehnder interferometer (MZI) and generated a frequency-clock signal with uniformly spaced optical frequency to trigger the sampling of the OCT signal. The system applied a fiber-based Michelson interferometer and about 97% of the laser power was split evenly to the sample and reference arms of the interferometer. The signals reflected from the sample and reference arms encountered at the fiber couple (FC) and formed interference fringes, which encoded with different frequencies and then received by a balanced detector (BD). Depth-resolved tomography was achieved by performing fast Fourier transform of the interference fringes [264]. The scanning field of view (FOV) was set at 5 mm x 5 mm to cover the entire defect area with 800 pixels in each direction. During imaging, the tissue was irrigated by phosphate buffer saline (PBS) to prevent dehydration. For cartilage thickness analysis on the acquired images, 10 random sections were picked on the X-axis (cross-section from top of trochlea groove) and the thickness of each section was calculated from a random point on Y-axis. The average thickness of each group was calculated from all biological samples of that group.

6.2.14 Histological Staining and Image Analysis

After harvesting and OCT scanning, the tissue samples were fixed in buffered 4% paraformaldehyde solution containing 1% sucrose. After decalcification, followed by a standard series of dehydration, the samples were embedded in paraffin. The samples were sectioned to 5mm thick slices and placed on positively charged glass slides. For H&E staining, the samples were stained by hematoxylin, followed by counterstaining of eosin. For Alcian Blue staining, samples were stained by Alcian Blue for 30 minutes, then counterstained under nuclear fast red for 5 minutes. The pictures were taken using Nikon Ti2 microscope (Nikon, Tokyo, Japan) mounted with Nikon DS Ri2 camera. The images were analyzed using the automatic measurement tools built in the microscope software.

Chondrocytes number was counted in the H&E images by thresholding the RGB color. Circularity (0.33-1.00) and area (≥3.93) were applied as restrictions to determine cell nuclei. The binary area of Alcian Blue stained GAGs was quantified by adjusting HSI value (Hue, Saturation, Intensity). Area (0.05-13807 μm^2) was applied as a restriction factor to eliminate noise and background. In both cases, the healthy control image was used to set up the threshold and restrictions. The same settings were applied to all images.

6.3 Results and Discussion

Aggrecan functionalization and evaluation of cell adhesion

An EDC-NHS chemistry was performed to covalently bind the carboxyl groups on the side chains of aggrecan and the amine groups on the printed PLCL-amine scaffold (**Figure 6.1A**). After chemical reaction, the modified scaffold sample was compared to PLCL and PLCL-amine samples using NMR. First of all, by comparing the spectra of printed plain PLCL sample, raw PLGA-amine, and printed PLCL-amine sample (blended with 85% PLCL and 15% PLGA-amine), we demonstrated that the amine group can be preserved through the printing process (**Figure 6.1D**). Amine shift at 0.93 and 2.61 were observed in the PLCL-amine sample. Further analysis on PLCL-amine sample, pure aggrecan sample, and the functionalized sample revealed matching peaks to confirm the presence of aggrecan (**Figure 6.1D**). Because of the complex structure of aggrecan, the acquisition of separate peaks was challenging. The ^1H signal was relatively low due to low solubility of aggrecan as a large proteoglycan molecule. After solvent suppression, the match peaks were primarily observed at 3.94 resulted by sulfate shift and 1.5 resulted by carboxylic ester, since these two groups are the most abundant side chains of aggrecan.

The biological function of the modified sample was evaluated in the next steps. We seeded hMSCs onto PLCL scaffold, PLCL-amine scaffold, fibronectin coated PLCL scaffold, aggrecan coated scaffold, and aggrecan modified scaffold, respectively. The cells were stained with calcium AM (live) and EH (dead) after 24 hours. While all groups showed great cell viability, the cell attachment efficiency on PLCL and PLCL-amine scaffold is significantly lower than the other three groups, indicating that the proteins on the scaffold played an important role in improving the cell attachment (**Figure 6.1C**). The DNA quantification data after 7 days confirmed the live/dead imaging conclusion. The aggrecan modified scaffold showed three times more DNA content than the unmodied scaffold (**Figure 6.1B**). Note that although the PLCL-amine group appeared higher DNA content in the presented graph, the repeated experiment demonstrated that this difference is not significant between PLCL and PLCL-amine groups.

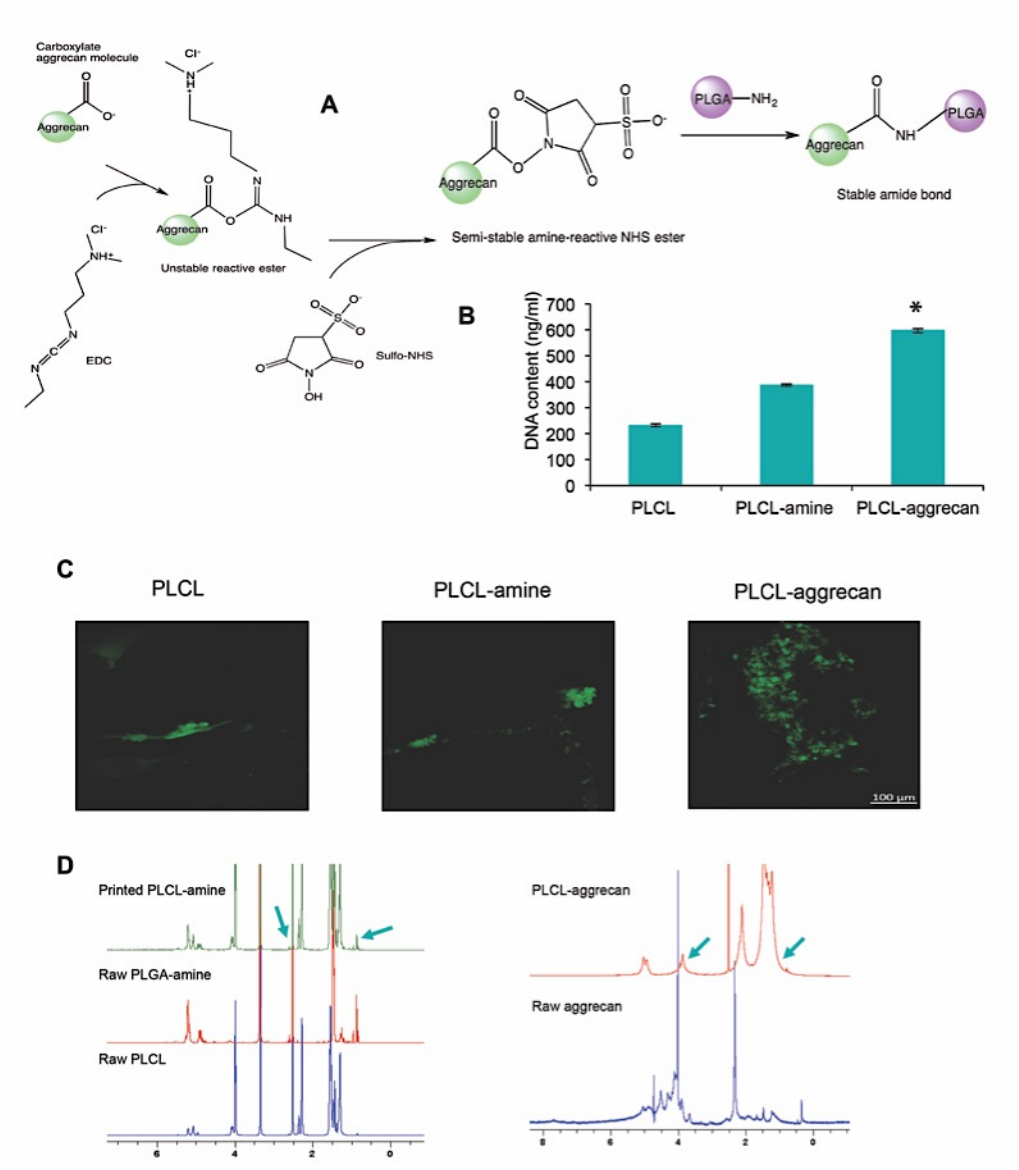

Figure 6. 1. Design and characterization of aggrecan functionalization on PLCL scaffold. A. Schematic diagram of chemical reaction between aggrecan and PLCL-amine scaffold using EDC and sulfo-NHS. **B.** DNA quantification of hMSCs seeded on PLCL, PLCL-amine, and PLCL-aggrecan scaffold after 7 days. **C.** Cell viability and attachment efficiency of hMSCs adhered on scaffolds after 24 hours. Live cells were stained green and dead cells were stained red. **D.** NMR spectrum confirming the presence of amine group after printing the blended PLCL and PLGA-amine material and the aggrecan modification.

A cell centrifugation assay to isolate the adhered cells from whole bone marrow was followed in order to analyzed the cell phenotype through flow cytometry (**Figure 6.2A**). By incorporating a 3D printed lid that can air seal the 24-well plate with designed features for

this experiment as demonstrated in the Method section, the non-adhered and adhered cell population were separated for further analysis. A hMSC cocktail was used in the flow cytometry to identify the hMSCs population (CD105+, CD90+, CD73+, CD11b-, CD19-, CD45-, HLA-DR-). The adhered population is approximately 0.1% of all cells in the whole bone marrow, according to both flow counting and hemocytometer counting. The aggrecan modified scaffold had approximately 10 times more adhered cells than the control groups. The adhered/attached cell count in controlled 90 second flow for aggrecan modified scaffold, PLCL scaffold and PLCL-amine scaffold was 286377, 21113, and 32551, respectively (**Figure 6.2B**). Among the adhered cells, after gating with isotype controls, the positive hMSCs count in 90 second flow for aggrecan modified scaffold and the two controls are 387, 200 and 214, which yields a positive hMSCs percentile of 0.1-1% among the adhered cells in the whole bone marrow (**Figure 6.2B**).

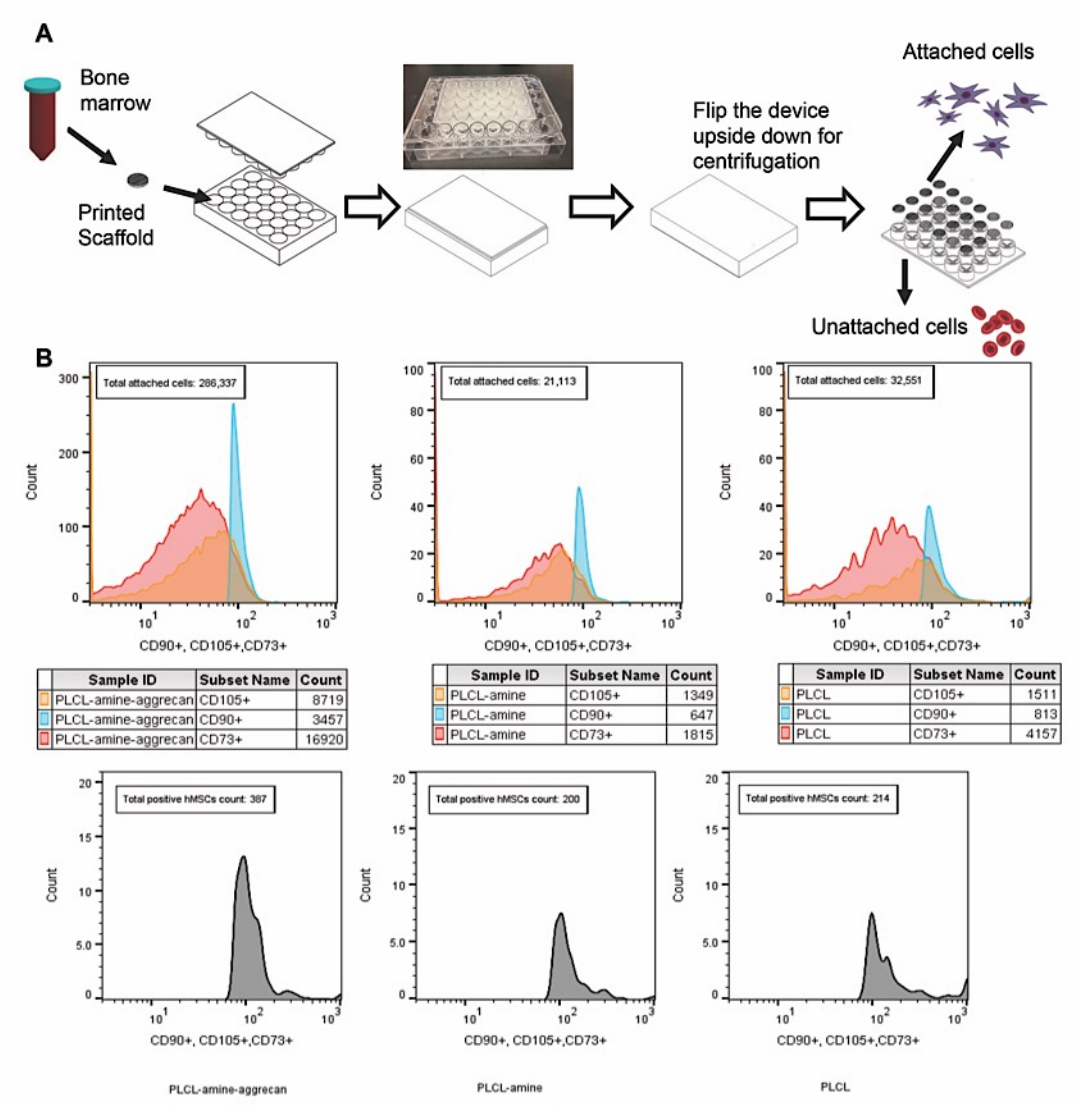

Figure 6. 2. Centrifugation assay to evaluate cell adhesion and adhered cell phenotype. **A.** Set up of the centrifugation assay for scaffolds seeded with whole bone marrow. A 3D printed lid was applied to separate the adhered and non-adhered cells. **B.** Flow cytometry analysis of the adhered cell population. Total attached cell number and positive hMSCs number were quantified.

In vivo assessment of scaffold function

NZW rabbits were used as an animal model to further evaluate the scaffold biofunctionality. NZW rabbit is a well-established small animal model for orthopedic surgeries because the condyle of mature rabbits is large enough to incorporate scaffold treatment with feasible surgical procedures. The thickness of the cartilage layer is also enough to prevent the

potential intrinsic repair compared to mouse or rat model.[265] Since cartilage regeneration process varies by gender, for example, the sexual hormones play a role in regulating chondrocytes function and collagen contents. In particular, female sex is strongly associated with higher incidences of OA.[266] Therefore, female rabbit has been used as a standard model in cartilage repair studies in existing literature, for the purpose of (1) consistent cartilage physiology properties and (2) a model associated with the disease prevalence. The animal surgery was completely successful following the approved protocol. All 14 rabbits survived with an overall good health condition until the termination of the study. The knee joints were harvested after 8 weeks for further analysis including tissue evaluation, OCT scanning and histology. The implanted scaffolds were mostly degraded after 8 weeks. A thin layer of regenerated cartilage tissue visibly appeared to cover the defect area in the experimental groups. With the additional scaffold, especially when functionalized scaffold, the newly regenerated cartilage tissue showed a healthier appearance (**Figure 6.3B**).

In the locomotion test, rabbit movement was recorded at each time point from both side view and top view throughout the eight week observations. The locomotion behavior was evaluated using a modified BBB score scale. While the defect control group appeared a waved shape, indicating no movement improvement over the course of study, all experimental groups showed an increasing trend of scores over time. Rabbits treated with aggrecan functionalized scaffold or plain scaffold had comparable scores with the rabbits treated with clinical procedure microfracture. BBB score was initially developed to evaluate locomotion test after spinal cord injury for rats.[267] The application in rabbit model has also been reported.[268] In this study of orthopaedic surgery, we modified the score to better represent the rabbit locomotion behavior. All the rabbits received a score higher than 13. Considering the relatively good recovery in regard to the movement ability with treatments, no significant difference among the experimental groups were observed at each time point.

All experimental groups with treatments had an average score of around 19 on week eight (**Figure 6.3C**). In addition, images at the moment of moving straight were captured to assess the foot pointing angle to their body. If the rabbits movement were affected by pain or the joint function, they would apply unbalanced force on their hind limb or even dragging the surgical site limb when walking, which can be reflected by the angle of the surgical site hind limb to their body. From the analysis, all groups with treatment show significantly small angle than the defect control group, indicating a healthier walking pattern (**Figure 6.3D**). The groups with implantation showed similar small angle (less than 10 degree) compared to the microfracture group, demonstrating that the scaffold didn't cause discomfort during movement.

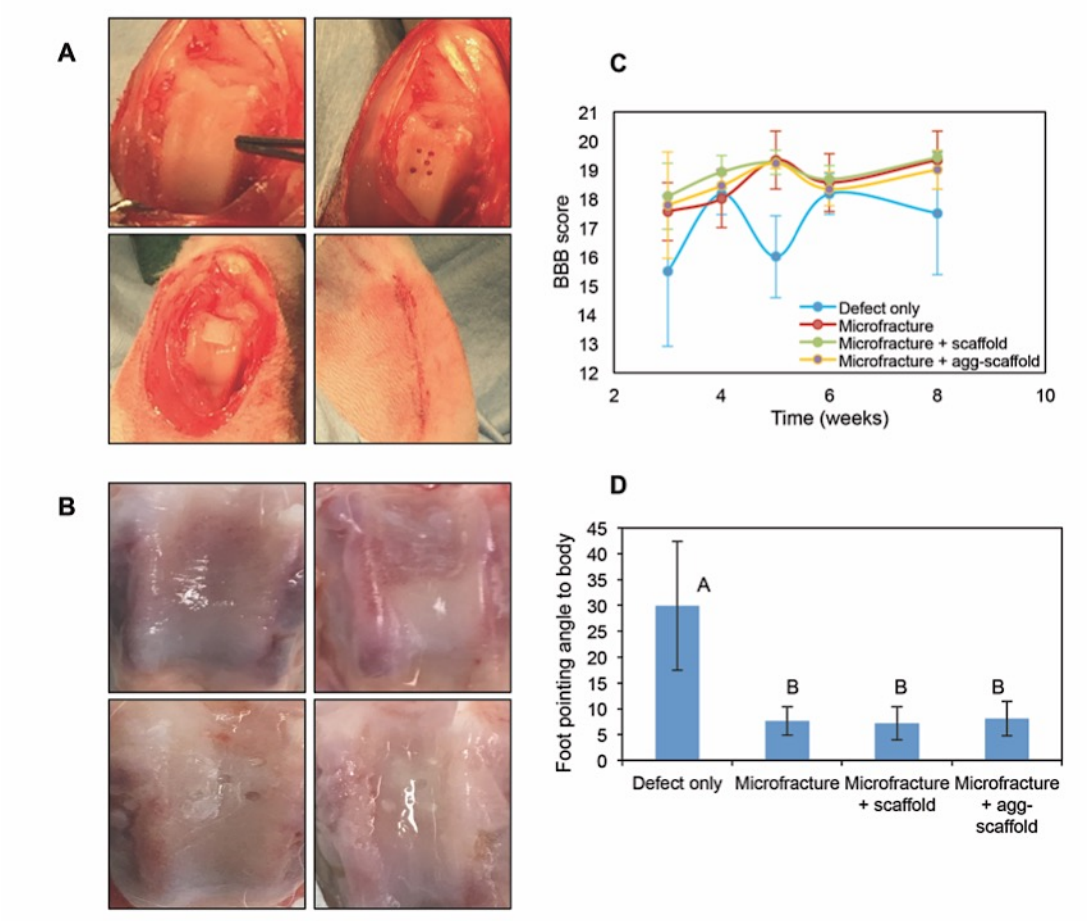

Figure 6. 3. Animal surgery and locomotion evaluation. A. Surgical procedure of microfracture and scaffold implantation. A 3 mm×3 mm full thickness defect was made in the

center of the trochlear groove (top left); 5 small holes (0.75mm) were drill at the four corner and the center of the defect on the subchondral bone (top right); scaffold with the defect size was covered the defect area (bottom left); the exposed patellar groove was reverted and the wound was closed by buried absorbable suture (bottom right). **B.** Harvested joints after 8 weeks showing regenerated cartilage tissue. Top left: defect without treatment; top right: defect treated by microfracture; bottom left: defect treated by microfracture and PLCL scaffold; bottom right: defect treated by microfracture and PLCL-aggrecan scaffold. **C.** BBB score evaluation over the 8 weeks of post-surgery observation in open field locomotion test. **D.** Measurement of foot alignment during movement.

The joints (femur end) were harvested for OCT scanning and histological analysis. The samples were scanned by OCT immediately after harvesting. A 5mm x 5mm scanning area was used to ensure the coverage of the entire defect area. Clinically, cartilage thickness is an important judgment of degree of osteoarthritis. In this study, it was measured as an important factor to evaluate the regeneration potential of different treatments. OCT, known as an analogous to ultrasound but presents advantages on resolution by measuring the intensity of backreflected infrared light instead of sound, has been used as an non-invasive method to assess the tissue both qualitatively and quantitatively including study on rabbit cartilage.[269, 270] The bone and cartilage boundary can be determined by the reflected light contrast due to different tissue structures.[269] The healthy control sample was used as a reference to determine the scan settings, and the outer and inner boundary of cartilage tissue. From the scanning, aggrecan functionalized scaffold resulted a more homogenous thickness distribution (**Figure 6.4**). This difference compared to the non-treated scaffold indicated a better integration with the newly regenerated tissue as a result of the biological function provided by aggrecan. The released cells and growth factors from bone marrow were better preserved through the proteoglycan support in this case. Furthermore, the average regenerated cartilage thickness of samples in the aggrecan-PLCL treatment group was 264 ± 80 μm, which is significantly higher than all other groups. The samples from defect control group, microfracture treatment group and PLCL scaffold group showed regenerated thickness of 47 ± 41 μm, 139 ± 72 μm, and 155 ± 80 μm, respectively (**Figure 6.4**). These resulted demonstrated the therapeutic

effect of biological functionalized scaffold using aggrecan. The combination of microfracture and this acellular bioactive scaffold resulted greatly improved cartilage regeneration in 8 weeks.

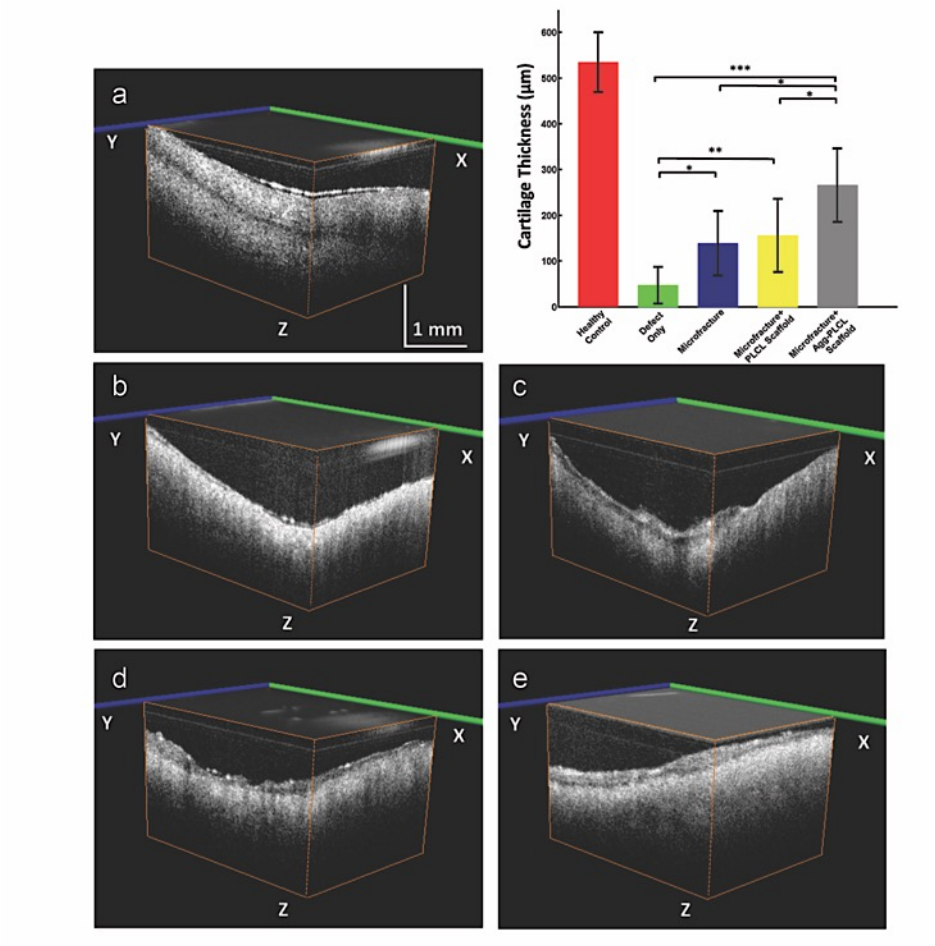

Figure 6. 4. 3D OCT images of cartilages and thickness quantification. The representative images of groups were listed: (a) Healthy control group, (b) Defect control group, (c) Microfracture group, (d) Microfracture and PLCL scaffold group and (e) Microfracture and Agg-PLCL scaffold group. Cartilage thickness was calculated from 10 randomly selected sections along y-axis. On each section, a random position on x-axis was selected for calculation. The average and standard deviation of the thickness in the plot was calculated from all samples in each group.

We performed histological staining for the harvested joints after embedding and decalcification. In the H&E staining, the nuclei were stained dark purple by hematoxylin and the eosinophilic structures mainly composed of intracellular and extracellular proteins were

counterstained by eosin Y as pink. The regenerated cartilage tissue appeared as lighter pink compared to the subchondral bone tissue (**Figure 6.5B**). Chondrocytes number in the cartilage layer was quantified using the Nikon Ti2 built-in analysis tool. The healthy control was used to set the color threshold and restrictions (circularity and area) to identify the cell nuclei. The defect control group showed very limited regenerated tissue with only 55 ± 26 chondrocytes in the imaging area. The microfracture treated group and the PLCL scaffold group showed similar amount of newly formed tissue with a chondrocytes count of 112 ± 26 and 134 ± 95, respectively. The slightly improved regeneration with non-treated scaffold might be caused by the initial support provided the implant, however, the poor integration with the local tissue limited the positive effect. With the addition of aggrecan, the tissue formation was significantly improved with almost three times more (366 ± 95) cell present in the cartilage layer. The alcian blue staining further confirmed the therapeutic effect of the functionalized scaffold (**Figure 6.5A**). As a major component of native cartilage, the produce of GAG by the chondrocytes have been used as a common way to assess the chondrogenesis or cartilage tissue regeneration. The GAG contents stained by alcian blue were greatly enhanced with the support of scaffold. The GAG expression was quantified as binary area (μm^2) in each image. The calculated average GAG contents of samples from defect group, microfracture group, PLCL scaffold group and aggrecan-PLCL scaffold group were 4412 ± 940 μm^2, 21052 ± 22064 μm^2, 380120 ± 32307 μm^2, and 92603 ± 30177 μm^2, respectively. The aggrecan functionalization resulted 20 times more GAG production than non-treated group and 4.4 times more GAG production compared to microfracture treatment.

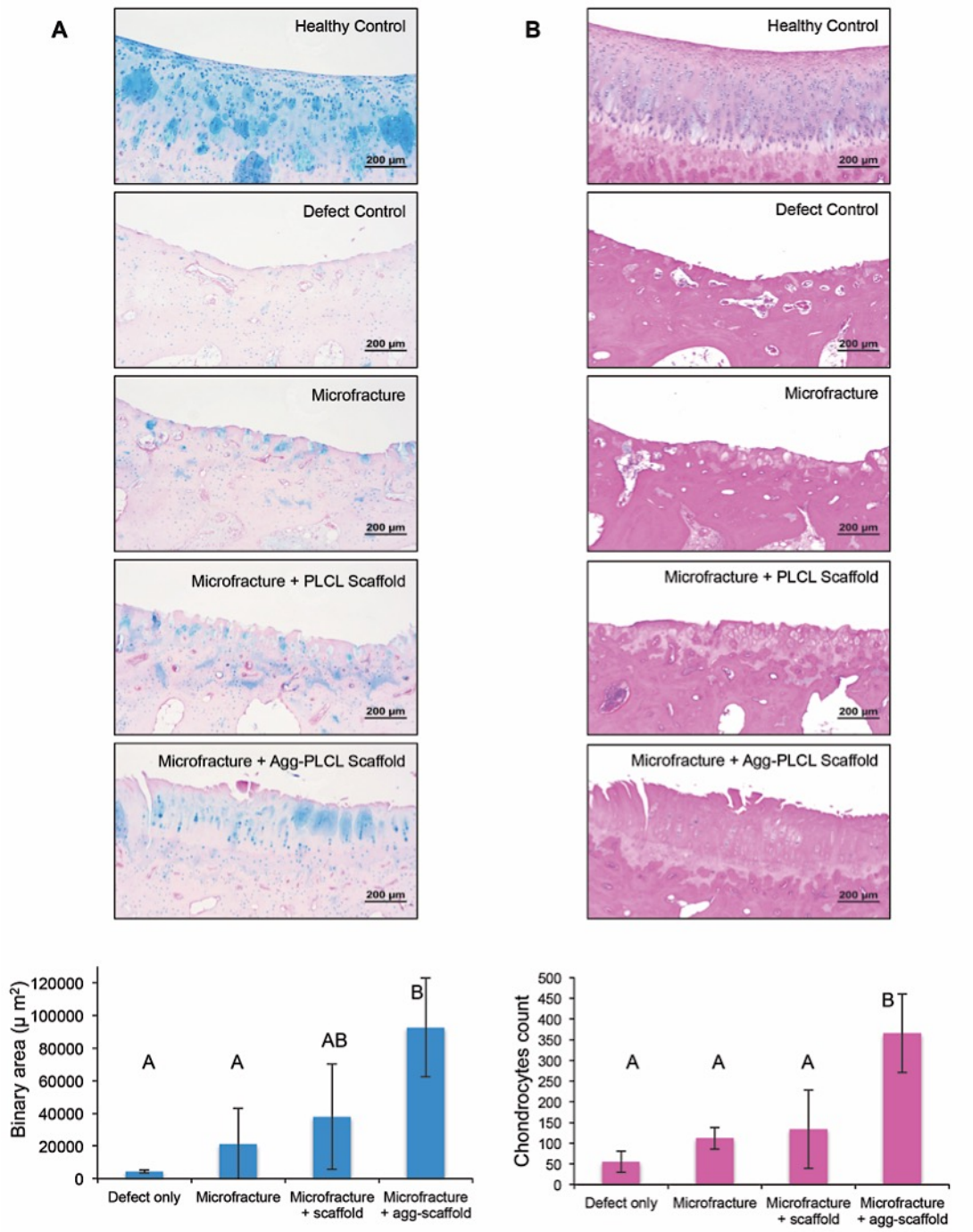

Figure 6. 5. Histological staining of regenerated cartilage tissue. A. Alcian Blue staining showing the GAGs production in different groups. Cell nuclei were stained purple and surrounding GAGs were stained blue. The GAGs expression level was quantified by binary area. **B.** H&E staining showing newly regenerated cartilage tissue. Cell nuclei were stained purple and the background tissue was stained pink. The cartilage layer presents a lighter pink than the bone tissue. The chondrocytes number was calculated and compared among groups. * Groups that do not share a letter are significantly different.

A major concern of microfracture is the success variance among different cases because the released stem cell and biomolecules have limited guidance and support in the defect area. The three rabbits in the microfracture group also showed relatively big standard deviation in multiple assessments. However, such variance seems to be reduced by incorporating the aggrecan-PLCL scaffold. All rabbits in this group showed similar recovery results both in locomotion test and histology evaluation, demonstrating the consistency of the treatment effect.

6.4 Conclusions

This study developed an effective method to regenerate critical articular defect by combining a 3D printed bioactive scaffold with the microfracture surgical procedure. The surface of 3D printed polymer scaffold was covalently modified with aggrecan to improve cell adhere and maintain cell function at the scaffold surface. With the functionalized scaffold, the microfracture outcome was significantly enhanced by providing extra support to the stem cells and growth factors released from bone marrow during the healing process. The additional aggrecan scaffold treatment resulted thicker and healthier regenerated cartilage layer. This biofunctionalized acellular scaffold combining with microfracture will have a great potential and impact on the future clinical solutions to improve the quality of repaired cartilage tissue for the demonstrated therapeutic effect without additional surgeries and the relative low cost compared to cell treatments.

6.5 Acknowledgements

My responsibilities in this study include but not limited to designing the experiment, writing the animal protocol, conducting the in vitro experiment, coordinating the animal study, and analyzing the data. The orthopedic surgeries were performed by Dr. Jonathan Packer and Dr.

Sean Meredith from University of Maryland School of Medicine. Dr. Hannah Baker, Evin Taskoy, and Maeesha Noshin contributed significantly in the animal surgeries and post-operational observations. We would like to thank the staffs, especially Dr. Ned Kriel and Theresa Nolan from the Veterinary Resources University of Maryland School of Medicine for assisting the surgeries and tissue harvest. The OCT analysis was performed by Dr. Qinggong Tang from the Biophotonic Imaging Lab at University of Maryland, College Park. The authors would also like to thank Dr. Fu Chen from the Analytical NMR Service & Research Center, University of Maryland for his help on NMR experiments.

Chapter 7: Summary and Future Directions

7.1 Summary

The overall objective of this thesis work was to develop new solutions for effective cartilage regeneration by engineering the favored cellular microenvironment. This goal was achieved by investigating the key components of tissue engineering in several steps including understanding the cell function, environment stimuli, cell-scaffold interaction. The 3D printed scaffold with biofunctionality was finally combined with the standard surgical procedure in a pre-clinical model to demonstrate the therapeutic potential in cartilage repair.

The first aim was to understand the impact of external mechanical stimuli to MSC proliferation and differentiation. We developed a bioreactor that can apply both shear and compressive forces to engineered tissues in dynamic culture. In our system, alginate hydrogel scaffolds with encapsulated hMSCs were cultured under different dynamic conditions while subjected to periodic, compressive force. Compared to static culture, dynamic culture can maintain a higher cell population throughout the study. With the application of only shear stress, qRT-PCR and immunohistochemistry revealed that hMSCs experienced less chondrogenic differentiation than the static group. The second study showed that chondrogenic differentiation was enhanced by additional mechanical compression. After 14 days, Alcian blue staining showed more extracellular matrix formed in the compression group. The upregulation of the positive chondrogenic markers such as Sox 9, aggrecan, and type II collagen were demonstrated by qPCR. Our bioreactor provides a novel approach to apply mechanical forces to engineered cartilage. Results suggest that a combination of dynamic culture with proper mechanical stimulation may promote efficient progenitor cell expansion *in vitro*, thereby allowing the culture of clinically relevant articular chondrocytes for the treatment of articular cartilage defects.

This first work showed the importance of external signals for cartilage regeneration, which inspired a more comprehensive approach to incorporate novel material and physical signals for cartilage scaffold design. In the second aim, we utilized 3D printing technology to fabricate the cartilaginous scaffold for its potential capability to meet specific patient need and the controlled manufacturing conditions. Although many studies have contributed to this emerging field of additive manufacturing, which includes material development and computer-aided scaffold design, current quantitative analyses do not correlate material properties, printing parameters, and printing outcomes to a great extent. A model that correlates these properties has tremendous potential to standardize 3D printing for tissue engineering and biomaterial science. In Chapter 4, we printed poly(lactic-*co*-glycolic acid) (PLGA) utilizing a direct melt extrusion technique without additional ingredients. We investigated PLGA with various lactic acid:glycolic acid (LA:GA) molecular weight ratios and end caps to demonstrate the dependence of the extrusion process on the polymer composition. Micro-computed tomography (microCT) was then used to evaluate printed scaffolds containing different LA:GA ratios, composed of different fiber patterns, and processed under different printing conditions. We built a statistical model to reveal the correlation and predominant factors that determine printing precision. Our model showed a strong linear relationship between the actual and predicted precision under different combinations of printing conditions and material compositions. This quantitative examination establishes a significant foreground to 3D print biomaterials following a systematic fabrication procedure. Additionally, our proposed statistical models can be applied to couple specific biomaterials and 3D printing applications for patient implants with particular requirements.

With the developed techniques to achieve high resolution in patterning the scaffold, in the third aim, we focused on the cell-material interaction since it's critical to remain cell function for further tissue regeneration. Many fabrication processes have been developed to create microenvironments to control cell attachment and organization on a 3D scaffold. However, these approaches often involve heavy engineering and only the surface layer can be patterned. We found that 3D extrusion based printing at high temperature and pressure will result an aligned effect on the polymer molecules, and this molecular arrangement will further induce the cell alignment and different differentiation capacities. In particular, articular cartilage tissue is known to have zonal collagen fiber and cell orientation to support different functions, where collagen fibers and chondrocytes align parallel, randomly, and perpendicular, respectively, to the surface of the joint. We used small angle X-ray scattering analysis to substantiate the polymer molecule alignment phenomenon. The cellular response was evaluated both in vitro and in vivo. Seeded mesenchymal stem cells showed different morphology and orientation on scaffolds, as a combined result of polymer molecule alignment and printed scaffold patterns. Gene expression results showed improved superficial zonal chondrogenic marker expression in parallel-aligned group. The cell alignment was successfully maintained in the animal model after 7 days with distinct MSC morphology between the casted and parallel printed scaffolds. This 3D printing induced polymer and cell alignment will have a significant impact on developing scaffold with controlled cell-material interactions for complex tissue engineering while avoiding complicated surface treatment, and therefore provides new concept for effective tissue repairing in future clinical applications.

In the last aim, we developed a strategy to combine our engineered scaffold with the clinical surgical procedure, microfracture, where local stem cells and growth factors can be released from the bone marrow to cover the cartilage defect area. To better represent the mechanical

properties of native cartilage, we changed the PGA component in the co-polymer PLGA to PCL and used co-polymer PLCL as our carrier scaffold in the lapine cartilage defect model. The aggrecan functionalization on the scaffold surface was proven to overcome the drawbacks associated with regular microfracture treatment. Both the animal locomotion test and histology evaluation showed more consistent successful recovery in all subjects in the aggrecan-PLCL treated group in regard of higher BBB score and improved tissue quality.

In conclusion, the use of acellular scaffold with bioactivity can serve as an additional therapeutic approach to microfracture, to achieve enhanced cartilage tissue regeneration by guiding the local cells and biomolecules organization and signaling. The simple fabrication and single surgery procedure make this approach very practical in future clinical treatment.

7.2 Future Directions

In the present work, we have accomplished effective methods to recapitulating the cartilage environment and demonstrated the promising tissue regeneration capability. Described below are some thoughts that may bring the current design closer to future realities.

In Chapter 2, we suggested a combined culture conditions to expand chondrocytes to a clinical relevant amount, as well as suggested the mechanical stimuli to improve MSC chondrogenesis. Notably, the combined effects of growth factors and mechanical stimuli on chondrogenesis have not been well understood. Future studies to evaluate different combinations of growth factor loading and mechanical loading would be necessary to better address the complex consequence. For both shear only dynamic culture and dynamic compression culture, we observed a trend increased of chondrogenic marker expression towards the end of the study. A study with longer time points to reveal the further

differentiation process and cell phenotype will be beneficial to understand the behavior of hMSCs undergoing chondrogenic differentiation in this complex culture system. Detailed effects such as hypertrophic phenotype prevention induced by the compression dynamic culture will be further evaluated in future studies. The small dimension and moderate mechanical loading in this study tried to minimize the possible heterogeneity, but further investigation into forces distribution and cellular response will help us better understand this bioreactor system.

The quantitative study on how material composition and printing conditions impact the printing resolution we discussed in Chapter 4 has brought in an important concern in using 3D printed scaffold for clinical treatment. Although many materials with various mechanical properties have been reported in different regenerative medicine areas, most of these materials are very specific to a certain application. The lack of standards in material composition choices and manufacturing specifications would potentially hinder the process to transit most of 3D printing concept into clinical reality. Future work on creating a material library and standard operating procedure would be very beneficial and meaningful to help researchers and clinicians to better utilize this advanced technology.

Our findings on the induced molecule and cell alignment in Chapter 5 provide an effective way to recapture the detailed cellular organization in native cartilage tissues. This concept can also be applied to further studies that require controlled cell organization. However, this pilot study could be strengthened by incorporating more comprehensive characterization of the molecule alignment. Although engineering approaches have created the many solutions for current clinical problems, the understanding of the biological mechanism is always essential to break the bottleneck of tissue engineering development. The detailed biological

process involved in the cellular organization and response to their microenvironment needs to be better understood in order to accomplish success in the regenerative medicine field.

In the last objective (Chapter 6), we proposed to combine our engineered scaffold with the standard clinical procedure microfracture. The aggrecan functionalized scaffold showed promising results as a therapeutic material. For the limited cartilage thickness in our lapine model, our current scaffold fabrication only allowed 2 layers of material deposition. Therefore, the microstructure of the zonal cartilage was not well presented. Future studies with more details included in the scaffold design that recapitulates the cell alignment and ECM formation would greatly improve the ability to direct in situ cellular behavior. For example, a surface structural modification using aligned nanofibers to mimic the thin layer of superficial zone of native cartilage would be helpful to improve the complexity of the scaffold. Considering the complicated structure of cartilage tissue, as well as a weight bearing tissue, it will be beneficial to use a larger pre-clinical model to test the treatment outcome because the scaffold can be better integrated with more local tissue and the mechanical loading is more similar to human body.

7.3 Contributions

The work presented in this dissertation has resulted in five first author publications, along with two manuscripts in preparation. I was also listed as co-authors in 3 additional publications. I have also presented the related work at six international conferences. My research was partially supported by the Ann G. Wylie Dissertation Fellowship and the Graduate School Summer Research Fellowship. The use of patterned scaffold for cartilage regeneration has been filed for a provisional patent.

Multiple techniques developed in this thesis work will have a broad impact to the society in advancing the healthcare products and research devices.

The cell culture system featuring static and dynamic conditions at different stages will provide a favored way to expand cells *in vitro* to the clinical relevant amount while maintaining cell phenotype for cartilage regeneration and help solve the problems associated with the current cell-based treatments.

The concept of establishing a systematic printing library of biocompatible material will greatly facilitate the transition of 3D printing technologies from bench work to future clinical applications with standardized manufacturing procedures.

The acellular therapeutic scaffold we developed in combination with the microfracture will provide a cost-effective method to improve the treatment outcome of the current standard clinical surgery for cartilage repair. The fabrication process and the one step procedure make it a feasible and promising approach to achieve a fast clinical transition.

Last but not least, the tools we invented during assay development have a great potential to benefit other researchers. For example, the 3D printed lid (invention disclosure in progress) for centrifugation assay provides a convenient way to separate attached and non-attached cells on 3D scaffolds, which can be marketed as an assay product for many laboratory uses.

Bibliography

1. Demoor, M.; Ollitrault, D.; Gomez-Leduc, T.; Bouyoucef, M.; Hervieu, M.; Fabre, H.; Lafont, J.; Denoix, J. M.; Audigie, F.; Mallein-Gerin, F.; Legendre, F.; Galera, P., Cartilage tissue engineering: molecular control of chondrocyte differentiation for proper cartilage matrix reconstruction. *Biochimica et biophysica acta* **2014,** 1840, (8), 2414-40.
2. Becerra, J.; Andrades, J. A.; Guerado, E.; Zamora-Navas, P.; Lopez-Puertas, J. M.; Reddi, A. H., Articular cartilage: structure and regeneration. *Tissue engineering. Part B, Reviews* **2010,** 16, (6), 617-27.
3. Li, S. W.; Prockop, D. J.; Helminen, H.; Fassler, R.; Lapvetelainen, T.; Kiraly, K.; Peltarri, A.; Arokoski, J.; Lui, H.; Arita, M.; et al., Transgenic mice with targeted inactivation of the Col2 alpha 1 gene for collagen II develop a skeleton with membranous and periosteal bone but no endochondral bone. *Genes Dev* **1995,** 9, (22), 2821-30.
4. Triche, R.; Mandelbaum, B. R., Overview of cartilage biology and new trends in cartilage stimulation. *Foot Ankle Clin* **2013,** 18, (1), 1-12.
5. Coates, E. E.; Fisher, J. P., Phenotypic variations in chondrocyte subpopulations and their response to in vitro culture and external stimuli. *Ann Biomed Eng* **2010,** 38, (11), 3371-88.
6. Klein, T. J.; Malda, J.; Sah, R. L.; Hutmacher, D. W., Tissue engineering of articular cartilage with biomimetic zones. *Tissue Eng Part B Rev* **2009,** 15, (2), 143-57.
7. Kempson, G. E.; Muir, H.; Pollard, C.; Tuke, M., The tensile properties of the cartilage of human femoral condyles related to the content of collagen and glycosaminoglycans. *Biochimica et biophysica acta* **1973,** 297, (2), 456-72.
8. Huber, M.; Trattnig, S.; Lintner, F., Anatomy, biochemistry, and physiology of articular cartilage. *Investigative radiology* **2000,** 35, (10), 573-80.
9. Schinagl, R. M.; Gurskis, D.; Chen, A. C.; Sah, R. L., Depth-dependent confined compression modulus of full-thickness bovine articular cartilage. *Journal of orthopaedic research : official publication of the Orthopaedic Research Society* **1997,** 15, (4), 499-506.
10. Ulrich-Vinther, M.; Maloney, M. D.; Schwarz, E. M.; Rosier, R.; O'Keefe, R. J., Articular cartilage biology. *J Am Acad Orthop Surg* **2003,** 11, (6), 421-30.
11. Aydelotte, M. B.; Kuettner, K. E., Differences between sub-populations of cultured bovine articular chondrocytes. I. Morphology and cartilage matrix production. *Connect Tissue Res* **1988,** 18, (3), 205-22.
12. Klein, T. J.; Schumacher, B. L.; Schmidt, T. A.; Li, K. W.; Voegtline, M. S.; Masuda, K.; Thonar, E. J.; Sah, R. L., Tissue engineering of stratified articular cartilage from chondrocyte subpopulations. *Osteoarthritis Cartilage* **2003,** 11, (8), 595-602.
13. Klein, T. J.; Rizzi, S. C.; Reichert, J. C.; Georgi, N.; Malda, J.; Schuurman, W.; Crawford, R. W.; Hutmacher, D. W., Strategies for Zonal Cartilage Repair using Hydrogels. *Macromol Biosci* **2009,** 9, (11), 1049-1058.
14. Zheng, Z. H.; Li, X. Y.; Ding, J.; Jia, J. F.; Zhu, P., Allogeneic mesenchymal stem cell and mesenchymal stem cell-differentiated chondrocyte suppress the responses of type II collagen-reactive T cells in rheumatoid arthritis. *Rheumatology* **2008,** 47, (1), 22-30.
15. Ng, K. W.; Wang, C. C.; Mauck, R. L.; Kelly, T. A.; Chahine, N. O.; Costa, K. D.; Ateshian, G. A.; Hung, C. T., A layered agarose approach to fabricate depth-dependent inhomogeneity in chondrocyte-seeded constructs. *J Orthop Res* **2005,** 23, (1), 134-41.
16. Gleghorn, J. P.; Lee, C. S.; Cabodi, M.; Stroock, A. D.; Bonassar, L. J., Adhesive properties of laminated alginate gels for tissue engineering of layered structures. *Journal of biomedical materials research. Part A* **2008,** 85, (3), 611-8.
17. Nguyen, L. H.; Kudva, A. K.; Guckert, N. L.; Linse, K. D.; Roy, K., Unique biomaterial compositions direct bone marrow stem cells into specific chondrocytic

phenotypes corresponding to the various zones of articular cartilage. *Biomaterials* **2011,** 32, (5), 1327-1338.
18. Thorpe, S. D.; Nagel, T.; Carroll, S. F.; Kelly, D. J., Modulating Gradients in Regulatory Signals within Mesenchymal Stem Cell Seeded Hydrogels: A Novel Strategy to Engineer Zonal Articular Cartilage. *Plos One* **2013,** 8, (4).
19. Spitters, T. W. G. M.; Mota, C. M. D.; Uzoechi, S. C.; Slowinska, B.; Martens, D. E.; Moroni, L.; Karperien, M., Glucose Gradients Influence Zonal Matrix Deposition in 3D Cartilage Constructs. *Tissue Eng Pt A* **2014,** 20, (23-24), 3270-3278.
20. Chen, R. R.; Mooney, D. J., Polymeric growth factor delivery strategies for tissue engineering. *Pharm Res* **2003,** 20, (8), 1103-12.
21. Mierisch, C. M.; Cohen, S. B.; Jordan, L. C.; Robertson, P. G.; Balian, G.; Diduch, D. R., Transforming growth factor-beta in calcium alginate beads for the treatment of articular cartilage defects in the rabbit. *Arthroscopy* **2002,** 18, (8), 892-900.
22. Kim, S. E.; Park, J. H.; Cho, Y. W.; Chung, H.; Jeong, S. Y.; Lee, E. B.; Kwon, I. C., Porous chitosan scaffold containing microspheres loaded with transforming growth factor-beta1: implications for cartilage tissue engineering. *J Control Release* **2003,** 91, (3), 365-74.
23. Benders, K. E.; van Weeren, P. R.; Badylak, S. F.; Saris, D. B.; Dhert, W. J.; Malda, J., Extracellular matrix scaffolds for cartilage and bone regeneration. *Trends Biotechnol* **2013,** 31, (3), 169-76.
24. Gilbert, T. W.; Sellaro, T. L.; Badylak, S. F., Decellularization of tissues and organs. *Biomaterials* **2006,** 27, (19), 3675-83.
25. Coburn, J. M.; Gibson, M.; Monagle, S.; Patterson, Z.; Elisseeff, J. H., Bioinspired nanofibers support chondrogenesis for articular cartilage repair. *Proc Natl Acad Sci U S A* **2012,** 109, (25), 10012-7.
26. Choi, B.; Kim, S.; Fan, J.; Kowalski, T.; Petrigliano, F.; Evseenko, D.; Lee, M., Covalently conjugated transforming growth factor-β1 in modular chitosan hydrogels for the effective treatment of articular cartilage defects. *Biomater. Sci.* **2015**.
27. Kang, S. W.; Bada, L. P.; Kang, C. S.; Lee, J. S.; Kim, C. H.; Park, J. H.; Kim, B. S., Articular cartilage regeneration with microfracture and hyaluronic acid. *Biotechnol Lett* **2008,** 30, (3), 435-9.
28. Doral, M. N.; Bilge, O.; Batmaz, G.; Donmez, G.; Turhan, E.; Demirel, M.; Atay, O. A.; Uzumcugil, A.; Atesok, K.; Kaya, D., Treatment of osteochondral lesions of the talus with microfracture technique and postoperative hyaluronan injection. *Knee surgery, sports traumatology, arthroscopy : official journal of the ESSKA* **2012,** 20, (7), 1398-403.
29. Hoemann, C. D.; Hurtig, M.; Rossomacha, E.; Sun, J.; Chevrier, A.; Shive, M. S.; Buschmann, M. D., Chitosan-glycerol phosphate/blood implants improve hyaline cartilage repair in ovine microfracture defects. *J Bone Joint Surg Am* **2005,** 87, (12), 2671-86.
30. Lee, C. H.; Cook, J. L.; Mendelson, A.; Moioli, E. K.; Yao, H.; Mao, J. J., Regeneration of the articular surface of the rabbit synovial joint by cell homing: a proof of concept study. *Lancet* **2010,** 376, (9739), 440-8.
31. Burdick, J. A.; Mauck, R. L.; Gorman, J. H., 3rd; Gorman, R. C., Acellular biomaterials: an evolving alternative to cell-based therapies. *Sci Transl Med* **2013,** 5, (176), 176ps4.
32. Wilson, C. J.; Clegg, R. E.; Leavesley, D. I.; Pearcy, M. J., Mediation of biomaterial-cell interactions by adsorbed proteins: a review. *Tissue Eng* **2005,** 11, (1-2), 1-18.
33. Yuan, L.; Yu, Q.; Li, D.; Chen, H., Surface modification to control protein/surface interactions. *Macromol Biosci* **2011,** 11, (8), 1031-40.
34. Sridhar, B. V.; Doyle, N. R.; Randolph, M. A.; Anseth, K. S., Covalently tethered TGF-beta1 with encapsulated chondrocytes in a PEG hydrogel system enhances extracellular matrix production. *Journal of biomedical materials research. Part A* **2014,** 102, (12), 4464-72.

35. Atala, A.; Kasper, F. K.; Mikos, A. G., Engineering complex tissues. *Science translational medicine* **2012,** 4, (160), 160rv12.
36. Sridhar, B. V.; Brock, J. L.; Silver, J. S.; Leight, J. L.; Randolph, M. A.; Anseth, K. S., Development of a cellularly degradable PEG hydrogel to promote articular cartilage extracellular matrix deposition. *Adv Healthc Mater* **2015,** 4, (5), 702-13.
37. Skaalure, S. C.; Chu, S.; Bryant, S. J., An enzyme-sensitive PEG hydrogel based on aggrecan catabolism for cartilage tissue engineering. *Adv Healthc Mater* **2015,** 4, (3), 420-31.
38. Shah, R. N.; Shah, N. A.; Del Rosario Lim, M. M.; Hsieh, C.; Nuber, G.; Stupp, S. I., Supramolecular design of self-assembling nanofibers for cartilage regeneration. *Proceedings of the National Academy of Sciences of the United States of America* **2010,** 107, (8), 3293-8.
39. Chawla, K.; Yu, T. B.; Stutts, L.; Yen, M.; Guan, Z., Modulation of chondrocyte behavior through tailoring functional synthetic saccharide-peptide hydrogels. *Biomaterials* **2012,** 33, (26), 6052-60.
40. Yang, Z.; Wu, Y.; Li, C.; Zhang, T.; Zou, Y.; Hui, J. H.; Ge, Z.; Lee, E. H., Improved mesenchymal stem cells attachment and in vitro cartilage tissue formation on chitosan-modified poly(L-lactide-co-epsilon-caprolactone) scaffold. *Tissue Eng Part A* **2012,** 18, (3-4), 242-51.
41. Kim, H. D.; Heo, J.; Hwang, Y.; Kwak, S. Y.; Park, O. K.; Kim, H.; Varghese, S.; Hwang, N. S., Extracellular-matrix-based and Arg-Gly-Asp-modified photopolymerizing hydrogels for cartilage tissue engineering. *Tissue engineering. Part A* **2015,** 21, (3-4), 757-66.
42. Luo, Z.; Jiang, L.; Xu, Y.; Li, H.; Xu, W.; Wu, S.; Wang, Y.; Tang, Z.; Lv, Y.; Yang, L., Mechano growth factor (MGF) and transforming growth factor (TGF)-beta3 functionalized silk scaffolds enhance articular hyaline cartilage regeneration in rabbit model. *Biomaterials* **2015,** 52, 463-75.
43. Shi, C.; Zhu, Y.; Ran, X.; Wang, M.; Su, Y.; Cheng, T., Therapeutic potential of chitosan and its derivatives in regenerative medicine. *J Surg Res* **2006,** 133, (2), 185-92.
44. Madihally, S. V.; Matthew, H. W., Porous chitosan scaffolds for tissue engineering. *Biomaterials* **1999,** 20, (12), 1133-42.
45. Suh, J. K.; Matthew, H. W., Application of chitosan-based polysaccharide biomaterials in cartilage tissue engineering: a review. *Biomaterials* **2000,** 21, (24), 2589-98.
46. Correia, C. R.; Moreira-Teixeira, L. S.; Moroni, L.; Reis, R. L.; van Blitterswijk, C. A.; Karperien, M.; Mano, J. F., Chitosan Scaffolds Containing Hyaluronic Acid for Cartilage Tissue Engineering. *Tissue Eng Part C-Me* **2011,** 17, (7), 717-730.
47. Yan, L. P.; Wang, Y. J.; Ren, L.; Wu, G.; Caridade, S. G.; Fan, J. B.; Wang, L. Y.; Ji, P. H.; Oliveira, J. M.; Oliveira, J. T.; Mano, J. F.; Reis, R. L., Genipin-cross-linked collagen/chitosan biomimetic scaffolds for articular cartilage tissue engineering applications. *J Biomed Mater Res A* **2010,** 95A, (2), 465-475.
48. Bhat, S.; Tripathi, A.; Kumar, A., Supermacroprous chitosan-agarose-gelatin cryogels: in vitro characterization and in vivo assessment for cartilage tissue engineering. *J R Soc Interface* **2011,** 8, (57), 540-54.
49. Neves, S. C.; Moreira Teixeira, L. S.; Moroni, L.; Reis, R. L.; Van Blitterswijk, C. A.; Alves, N. M.; Karperien, M.; Mano, J. F., Chitosan/poly(epsilon-caprolactone) blend scaffolds for cartilage repair. *Biomaterials* **2011,** 32, (4), 1068-79.
50. Naderi-Meshkin, H.; Andreas, K.; Matin, M. M.; Sittinger, M.; Bidkhori, H. R.; Ahmadiankia, N.; Bahrami, A. R.; Ringe, J., Chitosan-based injectable hydrogel as a promising in situ forming scaffold for cartilage tissue engineering. *Cell Biol Int* **2014,** 38, (1), 72-84.
51. Yan, J. H.; Yang, L.; Wang, G. R.; Xiao, Y.; Zhang, B. H.; Qi, N. M., Biocompatibility Evaluation of Chitosan-based Injectable Hydrogels for the Culturing Mice Mesenchymal Stem Cells In Vitro. *J Biomater Appl* **2010,** 24, (7), 625-637.

52. Li, J.; Kong, M.; Cheng, X. J.; Li, J. J.; Liu, W. F.; Chen, X. G., A facile method for preparing biodegradable chitosan derivatives with low grafting degree of poly(lactic acid). *Int J Biol Macromol* **2011,** 49, (5), 1016-21.
53. Coates, E. E.; Riggin, C. N.; Fisher, J. P., Matrix molecule influence on chondrocyte phenotype and proteoglycan 4 expression by alginate-embedded zonal chondrocytes and mesenchymal stem cells. *J Orthop Res* **2012,** 30, (12), 1886-97.
54. LeRoux, M. A.; Guilak, F.; Setton, L. A., Compressive and shear properties of alginate gel: effects of sodium ions and alginate concentration. *J Biomed Mater Res* **1999,** 47, (1), 46-53.
55. Wang, C. C.; Yang, K. C.; Lin, K. H.; Liu, H. C.; Lin, F. H., A highly organized three-dimensional alginate scaffold for cartilage tissue engineering prepared by microfluidic technology. *Biomaterials* **2011,** 32, (29), 7118-26.
56. Wang, C. C.; Yang, K. C.; Lin, K. H.; Liu, Y. L.; Liu, H. C.; Lin, F. H., Cartilage regeneration in SCID mice using a highly organized three-dimensional alginate scaffold. *Biomaterials* **2012,** 33, (1), 120-7.
57. Awad, H. A.; Wickham, M. Q.; Leddy, H. A.; Gimble, J. M.; Guilak, F., Chondrogenic differentiation of adipose-derived adult stem cells in agarose, alginate, and gelatin scaffolds. *Biomaterials* **2004,** 25, (16), 3211-22.
58. Mauck, R. L.; Soltz, M. A.; Wang, C. C.; Wong, D. D.; Chao, P. H.; Valhmu, W. B.; Hung, C. T.; Ateshian, G. A., Functional tissue engineering of articular cartilage through dynamic loading of chondrocyte-seeded agarose gels. *J Biomech Eng* **2000,** 122, (3), 252-60.
59. Hascall, V. C.; Heinegard, D., Aggregation of cartilage proteoglycans. I. The role of hyaluronic acid. *J Biol Chem* **1974,** 249, (13), 4232-41.
60. Burdick, J. A.; Chung, C.; Jia, X.; Randolph, M. A.; Langer, R., Controlled degradation and mechanical behavior of photopolymerized hyaluronic acid networks. *Biomacromolecules* **2005,** 6, (1), 386-91.
61. Plaas, A.; Li, J.; Riesco, J.; Das, R.; Sandy, J. D.; Harrison, A., Intraarticular injection of hyaluronan prevents cartilage erosion, periarticular fibrosis and mechanical allodynia and normalizes stance time in murine knee osteoarthritis. *Arthritis Res Ther* **2011,** 13, (2), R46.
62. Wang, Y. Z.; Blasioli, D. J.; Kim, H. J.; Kim, H. S.; Kaplan, D. L., Cartilage tissue engineering with silk scaffolds and human articular chondrocytes. *Biomaterials* **2006,** 27, (25), 4434-4442.
63. Kim, H. J.; Kim, U. J.; Vunjak-Novakovic, G.; Min, B. H.; Kaplan, D. L., Influence of macroporous protein scaffolds on bone tissue engineering from bone marrow stem cells. *Biomaterials* **2005,** 26, (21), 4442-52.
64. Chao, P. H.; Yodmuang, S.; Wang, X.; Sun, L.; Kaplan, D. L.; Vunjak-Novakovic, G., Silk hydrogel for cartilage tissue engineering. *J Biomed Mater Res B Appl Biomater* **2010,** 95, (1), 84-90.
65. Bhardwaj, N.; Kundu, S. C., Silk fibroin protein and chitosan polyelectrolyte complex porous scaffolds for tissue engineering applications. *Carbohydrate Polymers* **2011,** 85, (2), 325-333.
66. Daniels, A. U.; Chang, M. K.; Andriano, K. P., Mechanical properties of biodegradable polymers and composites proposed for internal fixation of bone. *J Appl Biomater* **1990,** 1, (1), 57-78.
67. Cui, L.; Wu, Y. H.; Cen, L.; Zhou, H.; Yin, S.; Liu, G. P.; Liu, W.; Cao, Y. L., Repair of articular cartilage defect in non-weight bearing areas using adipose derived stem cells loaded polyglycolic acid mesh. *Biomaterials* **2009,** 30, (14), 2683-2693.
68. Lohan, A.; Marzahn, U.; El Sayed, K.; Haisch, A.; Kohl, B.; Muller, R. D.; Ertel, W.; Schulze-Tanzil, G.; John, T., In vitro and in vivo neo-cartilage formation by heterotopic chondrocytes seeded on PGA scaffolds. *Histochem Cell Biol* **2011,** 136, (1), 57-69.

69. Ishaug-Riley, S. L.; Okun, L. E.; Prado, G.; Applegate, M. A.; Ratcliffe, A., Human articular chondrocyte adhesion and proliferation on synthetic biodegradable polymer films. *Biomaterials* **1999,** 20, (23-24), 2245-56.
70. Moran, J. M.; Pazzano, D.; Bonassar, L. J., Characterization of polylactic acid-polyglycolic acid composites for cartilage tissue engineering. *Tissue Eng* **2003,** 9, (1), 63-70.
71. Zhang, Y.; Yang, F.; Liu, K.; Shen, H.; Zhu, Y.; Zhang, W.; Liu, W.; Wang, S.; Cao, Y.; Zhou, G., The impact of PLGA scaffold orientation on in vitro cartilage regeneration. *Biomaterials* **2012,** 33, (10), 2926-35.
72. Wu, X.; Liu, Y.; Li, X.; Wen, P.; Zhang, Y.; Long, Y.; Wang, X.; Guo, Y.; Xing, F.; Gao, J., Preparation of aligned porous gelatin scaffolds by unidirectional freeze-drying method. *Acta Biomater* **2010,** 6, (3), 1167-77.
73. M. L. Alves da Silva, A. M., A. R. Costa-Pinto, P. Costa, S. Faria, M. Gomes, R. L. Reis, N. M. Neves, Cartilage Tissue Engineering Using Electrospun PCL Nanofiber Meshes and MSCs. *Biomacromolecules* **2010,** 11, (12), 3228-3236.
74. Christensen, B. B.; Foldager, C. B.; Hansen, O. M.; Kristiansen, A. A.; Le, D. Q.; Nielsen, A. D.; Nygaard, J. V.; Bunger, C. E.; Lind, M., A novel nano-structured porous polycaprolactone scaffold improves hyaline cartilage repair in a rabbit model compared to a collagen type I/III scaffold: in vitro and in vivo studies. *Knee Surg Sports Traumatol Arthrosc* **2012,** 20, (6), 1192-204.
75. Riley, S. L.; Dutt, S.; De La Torre, R.; Chen, A. C.; Sah, R. L.; Ratcliffe, A., Formulation of PEG-based hydrogels affects tissue-engineered cartilage construct characteristics. *J Mater Sci Mater Med* **2001,** 12, (10-12), 983-90.
76. Bryant, S. J.; Anseth, K. S., Controlling the spatial distribution of ECM components in degradable PEG hydrogels for tissue engineering cartilage. *J Biomed Mater Res A* **2003,** 64, (1), 70-9.
77. Bryant, S. J.; Anseth, K. S.; Lee, D. A.; Bader, D. L., Crosslinking density influences the morphology of chondrocytes photoencapsulated in PEG hydrogels during the application of compressive strain. *J Orthop Res* **2004,** 22, (5), 1143-9.
78. Cui, X.; Breitenkamp, K.; Finn, M. G.; Lotz, M.; D'Lima, D. D., Direct human cartilage repair using three-dimensional bioprinting technology. *Tissue Eng Part A* **2012,** 18, (11-12), 1304-12.
79. Lanza, R. P.; Langer, R. S.; Vacanti, J., *Principles of tissue engineering*. 2nd ed.; Academic Press: San Diego, CA, 2000; p xli, 995 p.
80. Jackson, D. W.; Simon, T. M., Chondrocyte transplantation. *Arthroscopy* **1996,** 12, (6), 732-8.
81. Gupta, P. K.; Das, A. K.; Chullikana, A.; Majumdar, A. S., Mesenchymal stem cells for cartilage repair in osteoarthritis. *Stem Cell Res Ther* **2012,** 3, (4), 25.
82. Noel, D.; Djouad, F.; Jorgense, C., Regenerative medicine through mesenchymal stem cells for bone and cartilage repair. *Curr Opin Investig Drugs* **2002,** 3, (7), 1000-4.
83. Lee, K. B.; Hui, J. H.; Song, I. C.; Ardany, L.; Lee, E. H., Injectable mesenchymal stem cell therapy for large cartilage defects--a porcine model. *Stem Cells* **2007,** 25, (11), 2964-71.
84. Kupcsik, L.; Stoddart, M. J.; Li, Z.; Benneker, L. M.; Alini, M., Improving chondrogenesis: potential and limitations of SOX9 gene transfer and mechanical stimulation for cartilage tissue engineering. *Tissue Eng Part A* **2010,** 16, (6), 1845-55.
85. Angele, P.; Schumann, D.; Angele, M.; Kinner, B.; Englert, C.; Hente, R.; Fuchtmeier, B.; Nerlich, M.; Neumann, C.; Kujat, R., Cyclic, mechanical compression enhances chondrogenesis of mesenchymal progenitor cells in tissue engineering scaffolds. *Biorheology* **2004,** 41, (3-4), 335-46.
86. Larsson, T.; Aspden, R. M.; Heinegard, D., Effects of mechanical load on cartilage matrix biosynthesis in vitro. *Matrix* **1991,** 11, (6), 388-94.

87. Yeatts, A. B.; Fisher, J. P., Tubular perfusion system for the long-term dynamic culture of human mesenchymal stem cells. *Tissue Eng Part C Methods* **2011,** 17, (3), 337-48.
88. Yu, L.; Ferlin, K. M.; Nguyen, B. N.; Fisher, J. P., Tubular perfusion system for chondrocyte culture and superficial zone protein expression. *Journal of biomedical materials research. Part A* **2015,** 103, (5), 1864-74.
89. Yoon, D. M.; Hawkins, E. C.; Francke-Carroll, S.; Fisher, J. P., Effect of construct properties on encapsulated chondrocyte expression of insulin-like growth factor-1. *Biomaterials* **2007,** 28, (2), 299-306.
90. Pelaez, D.; Charles Huang, C.-Y.; Cheung, H. S., Cyclic Compression Maintains Viability and Induces Chondrogenesis of Human Mesenchymal Stem Cells in Fibrin Gel Scaffolds. *Stem Cells and Development* **2009,** 18, (1), 93-102.
91. Bae, H.; Yu, M., Miniature Fabry-Perot pressure sensor created by using UV-molding process with an optical fiber based mold. *Opt Express* **2012,** 20, (13), 14573-14583.
92. Yoon, D. M.; Curtiss, S.; Reddi, A. H.; Fisher, J. P., Addition of Hyaluronic Acid to Alginate Embedded Chondrocytes Interferes with Insulin-like Growth Factor-1 Signaling In Vitro and In Vivo. *Tissue Eng Pt A* **2009,** 15, (11), 3449-3459.
93. Yeatts, A. B.; Gordon, C. N.; Fisher, J. P., Formation of an Aggregated Alginate Construct in a Tubular Perfusion System. *Tissue Eng Part C-Me* **2011,** 17, (12), 1171-1178.
94. Zhang, Z. Y.; Teoh, S. H.; Chong, W. S.; Foo, T. T.; Chng, Y. C.; Choolani, M.; Chan, J., A biaxial rotating bioreactor for the culture of fetal mesenchymal stem cells for bone tissue engineering. *Biomaterials* **2009,** 30, (14), 2694-704.
95. Zhao, F.; Pathi, P.; Grayson, W.; Xing, Q.; Locke, B. R.; Ma, T., Effects of oxygen transport on 3-d human mesenchymal stem cell metabolic activity in perfusion and static cultures: experiments and mathematical model. *Biotechnol Prog* **2005,** 21, (4), 1269-80.
96. Chen, X.; Xu, H.; Wan, C.; McCaigue, M.; Li, G., Bioreactor expansion of human adult bone marrow-derived mesenchymal stem cells. *Stem Cells* **2006,** 24, (9), 2052-9.
97. King, J. A.; Miller, W. M., Bioreactor development for stem cell expansion and controlled differentiation. *Curr Opin Chem Biol* **2007,** 11, (4), 394-8.
98. Xie, Y.; Hardouin, P.; Zhu, Z.; Tang, T.; Dai, K.; Lu, J., Three-dimensional flow perfusion culture system for stem cell proliferation inside the critical-size beta-tricalcium phosphate scaffold. *Tissue Eng* **2006,** 12, (12), 3535-43.
99. Noriega, S.; Mamedov, T.; Turner, J. A.; Subramanian, A., Intermittent applications of continuous ultrasound on the viability, proliferation, morphology, and matrix production of chondrocytes in 3D matrices. *Tissue Eng* **2007,** 13, (3), 611-8.
100. Kock, L. M.; Malda, J.; Dhert, W. J.; Ito, K.; Gawlitta, D., Flow-perfusion interferes with chondrogenic and hypertrophic matrix production by mesenchymal stem cells. *J Biomech* **2014,** 47, (9), 2122-9.
101. Kanichai, M.; Ferguson, D.; Prendergast, P. J.; Campbell, V. A., Hypoxia promotes chondrogenesis in rat mesenchymal stem cells: a role for AKT and hypoxia-inducible factor (HIF)-1alpha. *J Cell Physiol* **2008,** 216, (3), 708-15.
102. Adesida, A. B.; Mulet-Sierra, A.; Jomha, N. M., Hypoxia mediated isolation and expansion enhances the chondrogenic capacity of bone marrow mesenchymal stromal cells. *Stem Cell Res Ther* **2012,** 3, (2), 9.
103. Smith, R. L.; Carter, D. R.; Schurman, D. J., Pressure and shear differentially alter human articular chondrocyte metabolism: a review. *Clin Orthop Relat Res* **2004**, (427 Suppl), S89-95.
104. Quinn, T. M.; Grodzinsky, A. J.; Buschmann, M. D.; Kim, Y. J.; Hunziker, E. B., Mechanical compression alters proteoglycan deposition and matrix deformation around individual cells in cartilage explants. *J Cell Sci* **1998,** 111, 573-583.
105. Takahashi, I.; Nuckolls, G. H.; Takahashi, K.; Tanaka, O.; Semba, I.; Dashner, R.; Shum, L.; Slavkin, H. C., Compressive force promotes sox9, type II collagen and aggrecan

and inhibits IL-1beta expression resulting in chondrogenesis in mouse embryonic limb bud mesenchymal cells. *J Cell Sci* **1998,** 111 (Pt 14), 2067-76.
106. Angele, P.; Yoo, J. U.; Smith, C.; Mansour, J.; Jepsen, K. J.; Nerlich, M.; Johnstone, B., Cyclic hydrostatic pressure enhances the chondrogenic phenotype of human mesenchymal progenitor cells differentiated in vitro. *J Orthop Res* **2003,** 21, (3), 451-7.
107. Lucchinetti, E.; Adams, C. S.; Horton, W. E., Jr.; Torzilli, P. A., Cartilage viability after repetitive loading: a preliminary report. *Osteoarthritis Cartilage* **2002,** 10, (1), 71-81.
108. Kong, D.; Zheng, T.; Zhang, M.; Wang, D.; Du, S.; Li, X.; Fang, J.; Cao, X., Static mechanical stress induces apoptosis in rat endplate chondrocytes through MAPK and mitochondria-dependent caspase activation signaling pathways. *Plos One* **2013,** 8, (7), e69403.
109. Thorpe, S. D.; Buckley, C. T.; Vinardell, T.; O'Brien, F. J.; Campbell, V. A.; Kelly, D. J., The response of bone marrow-derived mesenchymal stem cells to dynamic compression following TGF-beta3 induced chondrogenic differentiation. *Ann Biomed Eng* **2010,** 38, (9), 2896-909.
110. Mouw, J. K.; Connelly, J. T.; Wilson, C. G.; Michael, K. E.; Levenston, M. E., Dynamic compression regulates the expression and synthesis of chondrocyte-specific matrix molecules in bone marrow stromal cells. *Stem Cells* **2007,** 25, (3), 655-63.
111. Langer, R.; Vacanti, J. P., Tissue engineering. *Science* **1993,** 260, (5110), 920-6.
112. Kim, T. K.; Sharma, B.; Williams, C. G.; Ruffner, M. A.; Malik, A.; McFarland, E. G.; Elisseeff, J. H., Experimental model for cartilage tissue engineering to regenerate the zonal organization of articular cartilage. *Osteoarthritis and cartilage / OARS, Osteoarthritis Research Society* **2003,** 11, (9), 653-64.
113. Woodfield, T. B.; Malda, J.; de Wijn, J.; Peters, F.; Riesle, J.; van Blitterswijk, C. A., Design of porous scaffolds for cartilage tissue engineering using a three-dimensional fiber-deposition technique. *Biomaterials* **2004,** 25, (18), 4149-61.
114. Lansdown, A. B.; Payne, M. J., An evaluation of the local reaction and biodegradation of calcium sodium alginate (Kaltostat) following subcutaneous implantation in the rat. *J R Coll Surg Edinb* **1994,** 39, (5), 284-8.
115. Kim, I. L.; Mauck, R. L.; Burdick, J. A., Hydrogel design for cartilage tissue engineering: a case study with hyaluronic acid. *Biomaterials* **2011,** 32, (34), 8771-82.
116. Bian, L.; Zhai, D. Y.; Mauck, R. L.; Burdick, J. A., Coculture of human mesenchymal stem cells and articular chondrocytes reduces hypertrophy and enhances functional properties of engineered cartilage. *Tissue Eng Part A* **2011,** 17, (7-8), 1137-45.
117. Wang, Y.; Bella, E.; Lee, C. S.; Migliaresi, C.; Pelcastre, L.; Schwartz, Z.; Boyan, B. D.; Motta, A., The synergistic effects of 3-D porous silk fibroin matrix scaffold properties and hydrodynamic environment in cartilage tissue regeneration. *Biomaterials* **2010,** 31, (17), 4672-81.
118. Wang, Y.; Blasioli, D. J.; Kim, H. J.; Kim, H. S.; Kaplan, D. L., Cartilage tissue engineering with silk scaffolds and human articular chondrocytes. *Biomaterials* **2006,** 27, (25), 4434-42.
119. Mahmoudifar, N.; Doran, P. M., Tissue engineering of human cartilage in bioreactors using single and composite cell-seeded scaffolds. *Biotechnology and Bioengineering* **2005,** 91, (3), 338-355.
120. Richardson, S. M.; Curran, J. M.; Chen, R.; Vaughan-Thomas, A.; Hunt, J. A.; Freemont, A. J.; Hoyland, J. A., The differentiation of bone marrow mesenchymal stem cells into chondrocyte-like cells on poly-L-lactic acid (PLLA) scaffolds. *Biomaterials* **2006,** 27, (22), 4069-4078.
121. Noth, U.; Tuli, R.; Osyczka, A. M.; Danielson, K. G.; Tuan, R. S., In vitro engineered cartilage constructs produced by press-coating biodegradable polymer with human mesenchymal stem cells. *Tissue Engineering* **2002,** 8, (1), 131-144.

122. Bryant, S. J.; Anseth, K. S., Hydrogel properties influence ECM production by chondrocytes photoencapsulated in poly(ethylene glycol) hydrogels. *J Biomed Mater Res* **2002,** 59, (1), 63-72.
123. Uematsu, K.; Hattori, K.; Ishimoto, Y.; Yamauchi, J.; Habata, T.; Takakura, Y.; Ohgushi, H.; Fukuchi, T.; Sato, M., Cartilage regeneration using mesenchymal stem cells and a three-dimensional poly-lactic-glycolic acid (PLGA) scaffold. *Biomaterials* **2005,** 26, (20), 4273-4279.
124. Chen, G. P.; Sato, T.; Ushida, T.; Ochiai, N.; Tateishi, T., Tissue engineering of cartilage using a hybrid scaffold of synthetic polymer and collagen. *Tissue Engineering* **2004,** 10, (3-4), 323-330.
125. da Silva, M. L. A.; Martins, A.; Costa-Pinto, A. R.; Costa, P.; Faria, S.; Gomes, M.; Reis, R. L.; Neves, N. M., Cartilage Tissue Engineering Using Electrospun PCL Nanofiber Meshes and MSCs. *Biomacromolecules* **2010,** 11, (12), 3228-3236.
126. Casper, M. E.; Fitzsimmons, J. S.; Stone, J. J.; Meza, A. O.; Huang, Y.; Ruesink, T. J.; O'Driscoll, S. W.; Reinholz, G. G., Tissue engineering of cartilage using poly-epsilon-caprolactone nanofiber scaffolds seeded in vivo with periosteal cells. *Osteoarthr Cartilage* **2010,** 18, (7), 981-991.
127. Woodfield, T. B. F.; Malda, J.; de Wijn, J.; Peters, F.; Riesle, J.; van Blitterswijk, C. A., Design of porous scaffolds for cartilage tissue engineering using a three-dimensional fiber-deposition technique. *Biomaterials* **2004,** 25, (18), 4149-4161.
128. Lansdown, A. B.; Payne, M. J., An evaluation of the local reaction and biodegradation of calcium sodium alginate (Kaltostat) following subcutaneous implantation in the rat. *Journal of the Royal College of Surgeons of Edinburgh* **1994,** 39, (5), 284-8.
129. Bian, L.; Zhai, D. Y.; Mauck, R. L.; Burdick, J. A., Coculture of human mesenchymal stem cells and articular chondrocytes reduces hypertrophy and enhances functional properties of engineered cartilage. *Tissue Eng Part A* **2011,** 17, (7-8), 1137-45.
130. Bryant, S. J.; Anseth, K. S., Hydrogel properties influence ECM production by chondrocytes photoencapsulated in poly(ethylene glycol) hydrogels. *Journal of biomedical materials research* **2002,** 59, (1), 63-72.
131. Schnabel, M.; Marlovits, S.; Eckhoff, G.; Fichtel, I.; Gotzen, L.; Vecsei, V.; Schlegel, J., Dedifferentiation-associated changes in morphology and gene expression in primary human articular chondrocytes in cell culture. *Osteoarthritis Cartilage* **2002,** 10, (1), 62-70.
132. Hollister, S. J., Porous scaffold design for tissue engineering. *Nature materials* **2005,** 4, (7), 518-24.
133. Lee, K. Y.; Mooney, D. J., Hydrogels for tissue engineering. *Chemical reviews* **2001,** 101, (7), 1869-79.
134. Seda Tigli, R.; Ghosh, S.; Laha, M. M.; Shevde, N. K.; Daheron, L.; Gimble, J.; Gumusderelioglu, M.; Kaplan, D. L., Comparative chondrogenesis of human cell sources in 3D scaffolds. *Journal of tissue engineering and regenerative medicine* **2009,** 3, (5), 348-60.
135. Li, W. J.; Tuli, R.; Okafor, C.; Derfoul, A.; Danielson, K. G.; Hall, D. J.; Tuan, R. S., A three-dimensional nanofibrous scaffold for cartilage tissue engineering using human mesenchymal stem cells. *Biomaterials* **2005,** 26, (6), 599-609.
136. Mironov, V.; Boland, T.; Trusk, T.; Forgacs, G.; Markwald, R. R., Organ printing: computer-aided jet-based 3D tissue engineering. *Trends in Biotechnology* **2003,** 21, (4), 157-161.
137. Hutmacher, D. W., Scaffold design and fabrication technologies for engineering tissues--state of the art and future perspectives. *Journal of biomaterials science. Polymer edition* **2001,** 12, (1), 107-24.
138. Chia, H. N.; Wu, B. M., High-resolution direct 3D printed PLGA scaffolds: print and shrink. *Biofabrication* **2015,** 7, (1), 015002.

139. Kai, H.; Wang, X.; Madhukar, K. S.; Qin, L.; Yan, Y.; Zhang, R., Fabrication of a two-level tumor bone repair biomaterial based on a rapid prototyping technique. *Biofabrication* **2009,** 1, (2), 025003.
140. Hutmacher, D. W., Scaffolds in tissue engineering bone and cartilage. *Biomaterials* **2000,** 21, (24), 2529-2543.
141. Brama, P. A.; Holopainen, J.; van Weeren, P. R.; Firth, E. C.; Helminen, H. J.; Hyttinen, M. M., Effect of loading on the organization of the collagen fibril network in juvenile equine articular cartilage. *J Orthop Res* **2009,** 27, (9), 1226-34.
142. Schuurman, W.; Klein, T. J.; Dhert, W. J. A.; van Weeren, P. R.; Hutmacher, D. W.; Malda, J., Cartilage regeneration using zonal chondrocyte subpopulations: a promising approach or an overcomplicated strategy? *J Tissue Eng Regen M* **2015,** 9, (6), 669-678.
143. Yeong, W. Y.; Chua, C. K.; Leong, K. F.; Chandrasekaran, M., Rapid prototyping in tissue engineering: challenges and potential. *Trends in biotechnology* **2004,** 22, (12), 643-52.
144. Cheah, C. M.; Chua, C. K.; Leong, K. F.; Cheong, C. H.; Naing, M. W., Automatic algorithm for generating complex polyhedral scaffold structures for tissue engineering. *Tissue Engineering* **2004,** 10, (3-4), 595-610.
145. Peltola, S. M.; Melchels, F. P.; Grijpma, D. W.; Kellomaki, M., A review of rapid prototyping techniques for tissue engineering purposes. *Ann Med* **2008,** 40, (4), 268-80.
146. Bose, S.; Vahabzadeh, S.; Bandyopadhyay, A., Bone tissue engineering using 3D printing. *Mater Today* **2013,** 16, (12), 496-504.
147. Fedorovich, N. E.; Dewijn, J. R.; Verbout, A. J.; Alblas, J.; Dhert, W. J. A., Three-dimensional fiber deposition of cell-laden, viable, patterned constructs for bone tissue printing. *Tissue Eng Pt A* **2008,** 14, (1), 127-133.
148. Cooke, M. N.; Fisher, J. P.; Dean, D.; Rimnac, C.; Mikos, A. G., Use of stereolithography to manufacture critical-sized 3D biodegradable scaffolds for bone ingrowth. *Journal of Biomedical Materials Research Part B-Applied Biomaterials* **2003,** 64B, (2), 65-69.
149. Boland, T.; Xu, T.; Damon, B.; Cui, X., Application of inkjet printing to tissue engineering. *Biotechnology journal* **2006,** 1, (9), 910-7.
150. Landers, R.; Hubner, U.; Schmelzeisen, R.; Mulhaupt, R., Rapid prototyping of scaffolds derived from thermoreversible hydrogels and tailored for applications in tissue engineering. *Biomaterials* **2002,** 23, (23), 4437-47.
151. Fedorovich, N. E.; Swennen, I.; Girones, J.; Moroni, L.; van Blitterswijk, C. A.; Schacht, E.; Alblas, J.; Dhert, W. J., Evaluation of photocrosslinked Lutrol hydrogel for tissue printing applications. *Biomacromolecules* **2009,** 10, (7), 1689-96.
152. Hutmacher, D. W.; Schantz, T.; Zein, I.; Ng, K. W.; Teoh, S. H.; Tan, K. C., Mechanical properties and cell cultural response of polycaprolactone scaffolds designed and fabricated via fused deposition modeling. *J Biomed Mater Res* **2001,** 55, (2), 203-16.
153. Sun, W.; Lal, P., Recent development on computer aided tissue engineering--a review. *Comput Methods Programs Biomed* **2002,** 67, (2), 85-103.
154. Guilak, F.; Jones, W. R.; Ting-Beall, H. P.; Lee, G. M., The deformation behavior and mechanical properties of chondrocytes in articular cartilage. *Osteoarthritis Cartilage* **1999,** 7, (1), 59-70.
155. Moroni, L.; de Wijn, J. R.; van Blitterswijk, C. A., 3D fiber-deposited scaffolds for tissue engineering: influence of pores geometry and architecture on dynamic mechanical properties. *Biomaterials* **2006,** 27, (7), 974-85.
156. Zein, I.; Hutmacher, D. W.; Tan, K. C.; Teoh, S. H., Fused deposition modeling of novel scaffold architectures for tissue engineering applications. *Biomaterials* **2002,** 23, (4), 1169-85.
157. Sun, H.; Mei, L.; Song, C.; Cui, X.; Wang, P., The in vivo degradation, absorption and excretion of PCL-based implant. *Biomaterials* **2006,** 27, (9), 1735-40.

158. Dounchis, J. S.; Bae, W. C.; Chen, A. C.; Sah, R. L.; Coutts, R. D.; Amiel, D., Cartilage repair with autogenic perichondrium cell and polylactic acid grafts. *Clin Orthop Relat Res* **2000**, (377), 248-64.
159. Hsu, S. H.; Yen, H. J.; Tseng, C. S.; Cheng, C. S.; Tsai, C. L., Evaluation of the growth of chondrocytes and osteoblasts seeded into precision scaffolds fabricated by fused deposition manufacturing. *J Biomed Mater Res B Appl Biomater* **2007,** 80, (2), 519-27.
160. Woodfield, T. B.; Van Blitterswijk, C. A.; De Wijn, J.; Sims, T. J.; Hollander, A. P.; Riesle, J., Polymer scaffolds fabricated with pore-size gradients as a model for studying the zonal organization within tissue-engineered cartilage constructs. *Tissue Eng* **2005,** 11, (9-10), 1297-311.
161. Lim, J. Y.; Kim, N. A.; Lim, D. G.; Kim, K. H.; Jeong, S. H., Effects of thermal and mechanical stress on the physical stability of human growth hormone and epidermal growth factor. *Arch Pharm Res* **2015,** 38, (8), 1488-98.
162. Liu, L.; Xiong, Z.; Zhang, R. J.; Jin, L.; Yan, Y. N., A Novel Osteochondral Scaffold Fabricated via Multi-nozzle Low-temperature Deposition Manufacturing. *J Bioact Compat Pol* **2009,** 24, 18-30.
163. Saito, E.; Liao, E. E.; Hu, W. W.; Krebsbach, P. H.; Hollister, S. J., Effects of designed PLLA and 50:50 PLGA scaffold architectures on bone formation in vivo. *J Tissue Eng Regen M* **2013,** 7, (2), 99-111.
164. He, Y.; Wildman, R. D.; Tuck, C. J.; Christie, S. D.; Edmondson, S., An Investigation of the Behavior of Solvent based Polycaprolactone ink for Material Jetting. *Sci Rep* **2016,** 6, 20852.
165. Hung, K. C.; Tseng, C. S.; Hsu, S. H., Synthesis and 3D printing of biodegradable polyurethane elastomer by a water-based process for cartilage tissue engineering applications. *Adv Healthc Mater* **2014,** 3, (10), 1578-87.
166. Hung, K. C.; Tseng, C. S.; Hsu, S. H., Synthesis and 3D printing of biodegradable polyurethane elastomer by a water-based process for cartilage tissue engineering applications. *Adv Healthc Mater* **2014,** 3, (10), 1578-87.
167. Censi, R.; Schuurman, W.; Malda, J.; di Dato, G.; Burgisser, P. E.; Dhert, W. J. A.; van Nostrum, C. F.; di Martino, P.; Vermonden, T.; Hennink, W. E., A Printable Photopolymerizable Thermosensitive p(HPMAm-lactate)-PEG Hydrogel for Tissue Engineering. *Adv Funct Mater* **2011,** 21, (10), 1833-1842.
168. Skardal, A.; Zhang, J. X.; McCoard, L.; Xu, X. Y.; Oottamasathien, S.; Prestwich, G. D., Photocrosslinkable Hyaluronan-Gelatin Hydrogels for Two-Step Bioprinting. *Tissue Eng Pt A* **2010,** 16, (8), 2675-2685.
169. Sun, J. Y.; Zhao, X.; Illeperuma, W. R.; Chaudhuri, O.; Oh, K. H.; Mooney, D. J.; Vlassak, J. J.; Suo, Z., Highly stretchable and tough hydrogels. *Nature* **2012,** 489, (7414), 133-6.
170. Stampfl, J.; Baudis, S.; Heller, C.; Liska, R.; Neumeister, A.; Kling, R.; Ostendorf, A.; Spitzbart, M., Photopolymers with tunable mechanical properties processed by laser-based high-resolution stereolithography. *J Micromech Microeng* **2008,** 18, (12).
171. Lee, S. J.; Kang, H. W.; Park, J. K.; Rhie, J. W.; Hahn, S. K.; Cho, D. W., Application of microstereolithography in the development of three-dimensional cartilage regeneration scaffolds. *Biomed Microdevices* **2008,** 10, (2), 233-41.
172. Schuller-Ravoo, S.; Teixeira, S. M.; Feijen, J.; Grijpma, D. W.; Poot, A. A., Flexible and elastic scaffolds for cartilage tissue engineering prepared by stereolithography using poly(trimethylene carbonate)-based resins. *Macromol Biosci* **2013,** 13, (12), 1711-9.
173. Weiss, T.; Hildebrand, G.; Schade, R.; Liefeith, K., Two-Photon polymerization for microfabrication of three-dimensional scaffolds for tissue engineering application. *Engineering in Life Sciences* **2009,** 9, (5), 384-390.

174. Dobratz, E. J.; Kim, S. W.; Voglewede, A.; Park, S. S., Injectable cartilage: using alginate and human chondrocytes. *Arch Facial Plast Surg* **2009,** 11, (1), 40-7.
175. Cohen, D. L.; Lipton, J. I.; Bonassar, L. J.; Lipson, H., Additive manufacturing for in situ repair of osteochondral defects. *Biofabrication* **2010,** 2, (3), 035004.
176. Cohen, D. L.; Malone, E.; Lipson, H.; Bonassar, L. J., Direct freeform fabrication of seeded hydrogels in arbitrary geometries. *Tissue Eng* **2006,** 12, (5), 1325-35.
177. Fedorovich, N. E.; Schuurman, W.; Wijnberg, H. M.; Prins, H. J.; van Weeren, P. R.; Malda, J.; Alblas, J.; Dhert, W. J., Biofabrication of osteochondral tissue equivalents by printing topologically defined, cell-laden hydrogel scaffolds. *Tissue Eng Part C Methods* **2012,** 18, (1), 33-44.
178. Roberts, S.; Weightman, B.; Urban, J.; Chappell, D., Mechanical and biochemical properties of human articular cartilage in osteoarthritic femoral heads and in autopsy specimens. *J Bone Joint Surg Br* **1986,** 68, (2), 278-88.
179. Cloyd, J. M.; Malhotra, N. R.; Weng, L.; Chen, W.; Mauck, R. L.; Elliott, D. M., Material properties in unconfined compression of human nucleus pulposus, injectable hyaluronic acid-based hydrogels and tissue engineering scaffolds. *Eur Spine J* **2007,** 16, (11), 1892-1898.
180. Schuurman, W.; Khristov, V.; Pot, M. W.; van Weeren, P. R.; Dhert, W. J.; Malda, J., Bioprinting of hybrid tissue constructs with tailorable mechanical properties. *Biofabrication* **2011,** 3, (2), 021001.
181. Izadifar, Z.; Chang, T.; Kulyk, W.; Chen, X.; Eames, B. F., Analyzing Biological Performance of 3D-Printed, Cell-Impregnated Hybrid Constructs for Cartilage Tissue Engineering. *Tissue Eng Part C Methods* **2016**.
182. Kundu, J.; Shim, J. H.; Jang, J.; Kim, S. W.; Cho, D. W., An additive manufacturing-based PCL-alginate-chondrocyte bioprinted scaffold for cartilage tissue engineering. *J Tissue Eng Regen Med* **2015,** 9, (11), 1286-97.
183. Kesti, M.; Muller, M.; Becher, J.; Schnabelrauch, M.; D'Este, M.; Eglin, D.; Zenobi-Wong, M., A versatile bioink for three-dimensional printing of cellular scaffolds based on thermally and photo-triggered tandem gelation. *Acta Biomater* **2015,** 11, 162-72.
184. Markstedt, K.; Mantas, A.; Tournier, I.; Martinez Avila, H.; Hagg, D.; Gatenholm, P., 3D Bioprinting Human Chondrocytes with Nanocellulose-Alginate Bioink for Cartilage Tissue Engineering Applications. *Biomacromolecules* **2015,** 16, (5), 1489-96.
185. Gao, G.; Schilling, A. F.; Hubbell, K.; Yonezawa, T.; Danh, T.; Hong, Y.; Dai, G.; Cui, X., Improved properties of bone and cartilage tissue from 3D inkjet-bioprinted human mesenchymal stem cells by simultaneous deposition and photocrosslinking in PEG-GelMA. *Biotechnol Lett* **2015,** 37, (11), 2349-2355.
186. Xu, T.; Binder, K. W.; Albanna, M. Z.; Dice, D.; Zhao, W.; Yoo, J. J.; Atala, A., Hybrid printing of mechanically and biologically improved constructs for cartilage tissue engineering applications. *Biofabrication* **2013,** 5, (1), 015001.
187. Sharma, B.; Williams, C. G.; Kim, T. K.; Sun, D.; Malik, A.; Khan, M.; Leong, K.; Elisseeff, J. H., Designing zonal organization into tissue-engineered cartilage. *Tissue Eng* **2007,** 13, (2), 405-14.
188. Hwang, N. S.; Varghese, S.; Lee, H. J.; Theprungsirikul, P.; Canver, A.; Sharma, B.; Elisseeff, J., Response of zonal chondrocytes to extracellular matrix-hydrogels. *FEBS Lett* **2007,** 581, (22), 4172-8.
189. Coates, E.; Fisher, J. P., Gene expression of alginate-embedded chondrocyte subpopulations and their response to exogenous IGF-1 delivery. *J Tissue Eng Regen Med* **2012,** 6, (3), 179-92.
190. Reed, S.; Lau, G.; Delattre, B.; Lopez, D. D.; Tomsia, A. P.; Wu, B. M., Macro- and micro-designed chitosan-alginate scaffold architecture by three-dimensional printing and directional freezing. *Biofabrication* **2016,** 8, (1), 015003-015003.

191. Castro, N. J.; O'Brien, J.; Zhang, L. G., Integrating biologically inspired nanomaterials and table-top stereolithography for 3D printed biomimetic osteochondral scaffolds. *Nanoscale* **2015,** 7, (33), 14010-22.
192. Goldstein, T. A.; Smith, B. D.; Zeltsman, D.; Grande, D.; Smith, L. P., Introducing a 3-dimensionally Printed, Tissue-Engineered Graft for Airway Reconstruction: A Pilot Study. *Otolaryngology-Head and Neck Surgery* **2015,** 153, (6), 1001-1006.
193. Mannoor, M. S.; Jiang, Z.; James, T.; Kong, Y. L.; Malatesta, K. A.; Soboyejo, W. O.; Verma, N.; Gracias, D. H.; McAlpine, M. C., 3D printed bionic ears. *Nano Lett* **2013,** 13, (6), 2634-9.
194. Hinton, T. J.; Jallerat, Q.; Palchesko, R. N.; Park, J. H.; Grodzicki, M. S.; Shue, H. J.; Ramadan, M. H.; Hudson, A. R.; Feinberg, A. W., Three-dimensional printing of complex biological structures by freeform reversible embedding of suspended hydrogels. *Sci Adv* **2015,** 1, (9), e1500758.
195. Pati, F.; Ha, D. H.; Jang, J.; Han, H. H.; Rhie, J. W.; Cho, D. W., Biomimetic 3D tissue printing for soft tissue regeneration. *Biomaterials* **2015,** 62, 164-75.
196. Mazza, G.; Rombouts, K.; Rennie Hall, A.; Urbani, L.; Vinh Luong, T.; Al-Akkad, W.; Longato, L.; Brown, D.; Maghsoudlou, P.; Dhillon, A. P.; Fuller, B.; Davidson, B.; Moore, K.; Dhar, D.; De Coppi, P.; Malago, M.; Pinzani, M., Decellularized human liver as a natural 3D-scaffold for liver bioengineering and transplantation. *Sci Rep* **2015,** 5, 13079.
197. Di Bella, C.; Fosang, A.; Donati, D. M.; Wallace, G. G.; Choong, P. F., 3D Bioprinting of Cartilage for Orthopedic Surgeons: Reading between the Lines. *Front Surg* **2015,** 2, 39.
198. Hutmacher, D. W., Scaffolds in tissue engineering bone and cartilage. *Biomaterials* **2000,** 21, (24), 2529-43.
199. Trachtenberg J.E., P. J. K., Smith B.T., Piard C.M., Santoro M., Scott D.W., Fisher J.P., and Mikos A.G., Extrusion-Based 3D Printing of Poly(propylene fumarate) in a Full-Factorial Design. *ACS Biomater. Sci. Eng* **2016**.
200. Pan, Z.; Ding, J., Poly(lactide-co-glycolide) porous scaffolds for tissue engineering and regenerative medicine. *Interface Focus* **2012,** 2, (3), 366-77.
201. Gentile, P.; Chiono, V.; Carmagnola, I.; Hatton, P. V., An overview of poly(lactic-co-glycolic) acid (PLGA)-based biomaterials for bone tissue engineering. *Int J Mol Sci* **2014,** 15, (3), 3640-59.
202. Seunarine, K.; Gadegaard, N.; Tormen, M.; Meredith, D. O.; Riehle, M. O.; Wilkinson, C. D., 3D polymer scaffolds for tissue engineering. *Nanomedicine (Lond)* **2006,** 1, (3), 281-96.
203. Roy, T. D.; Simon, J. L.; Ricci, J. L.; Rekow, E. D.; Thompson, V. P.; Parsons, J. R., Performance of degradable composite bone repair products made via three-dimensional fabrication techniques. *J Biomed Mater Res A* **2003,** 66, (2), 283-91.
204. Behrens, A. M.; Lee, N. G.; Casey, B. J.; Srinivasan, P.; Sikorski, M. J.; Daristotle, J. L.; Sandler, A. D.; Kofinas, P., Biodegradable-Polymer-Blend-Based Surgical Sealant with Body-Temperature-Mediated Adhesion. *Adv Mater* **2015,** 27, (48), 8056-61.
205. Wang, M. O.; Vorwald, C. E.; Dreher, M. L.; Mott, E. J.; Cheng, M. H.; Cinar, A.; Mehdizadeh, H.; Somo, S.; Dean, D.; Brey, E. M.; Fisher, J. P., Evaluating 3D-Printed Biomaterials as Scaffolds for Vascularized Bone Tissue Engineering. *Advanced Materials* **2015,** 27, (1), 138-144.
206. Chew, S. A.; Arriaga, M. A.; Hinojosa, V. A., Effects of surface area to volume ratio of PLGA scaffolds with different architectures on scaffold degradation characteristics and drug release kinetics. *Journal of biomedical materials research. Part A* **2016,** 104, (5), 1202-11.
207. Ozdil, D.; Aydin, H. M., Polymers for medical and tissue engineering applications. *Journal of Chemical Technology & Biotechnology* **2014,** 89, (12), 1793-1810.

208. Aho, J.; Boetker, J. P.; Baldursdottir, S.; Rantanen, J., Rheology as a tool for evaluation of melt processability of innovative dosage forms. *Int J Pharm* **2015,** 494, (2), 623-42.
209. Zhang, F.; Tuck, C.; Hague, R.; He, Y. F.; Saleh, E.; Li, Y.; Sturgess, C.; Wildman, R., Inkjet printing of polyimide insulators for the 3D printing of dielectric materials for microelectronic applications. *J. Appl. Polym. Sci.* **2016,** 133, (18), 11.
210. Aho, J.; Boetker, J. P.; Baldursdottir, S.; Rantanen, J., Rheology as a tool for evaluation of melt processability of innovative dosage forms. *Int J Pharmaceut* **2015,** 494, (2), 623-642.
211. Pfitzner, J., Poiseuille and his law. *Anaesthesia* **1976,** 31, (2), 273-5.
212. Makadia, H. K.; Siegel, S. J., Poly Lactic-co-Glycolic Acid (PLGA) as Biodegradable Controlled Drug Delivery Carrier. *Polymers (Basel)* **2011,** 3, (3), 1377-1397.
213. Cohen, N. P.; Foster, R. J.; Mow, V. C., Composition and dynamics of articular cartilage: structure, function, and maintaining healthy state. *J Orthop Sports Phys Ther* **1998,** 28, (4), 203-15.
214. Guo, T.; Lembong, J.; Zhang, L.; Fisher, J., Three-Dimensional Printing Articular Cartilage: Recapitulating the Complexity of Native Tissue. *Tissue Engineering Part B-Reviews* **2017,** 23, (3), 225-236.
215. Discher, D.; Mooney, D.; Zandstra, P., Growth Factors, Matrices, and Forces Combine and Control Stem Cells. *Science* **2009,** 324, (5935), 1673-1677.
216. Yang, Q.; Peng, J.; Guo, Q.; Huang, J.; Zhang, L.; Yao, J.; Yang, F.; Wang, S.; Xu, W.; Wang, A.; Lu, S., A cartilage ECM-derived 3-D porous acellular matrix scaffold for in vivo cartilage tissue engineering with PKH26-labeled chondrogenic bone marrow-derived mesenchymal stem cells. *Biomaterials* **2008,** 29, (15), 2378-2387.
217. Kaur, G.; Valarmathi, M.; Potts, J.; Jabbari, E.; Sabo-Attwood, T.; Wang, Q., Regulation of osteogenic differentiation of rat bone marrow stromal cells on 2D nanorod substrates. *Biomaterials* **2010,** 31, (7), 1732-1741.
218. Park, J.; Yang, H.; Woo, D.; Jeon, S.; Park, K., The promotion of chondrogenesis, osteogenesis, and adipogenesis of human mesenchymal stem cells by multiple growth factors incorporated into nanosphere-coated microspheres. *Biomaterials* **2011,** 32, (1), 28-38.
219. Discher, D.; Janmey, P.; Wang, Y., Tissue cells feel and respond to the stiffness of their substrate. *Science* **2005,** 310, (5751), 1139-1143.
220. Albrecht, D.; Underhill, G.; Wassermann, T.; Sah, R.; Bhatia, S., Probing the role of multicellular organization in three-dimensional microenvironments. *Nature Methods* **2006,** 3, (5), 369-375.
221. Reilly, G.; Engler, A., Intrinsic extracellular matrix properties regulate stem cell differentiation. *Journal of Biomechanics* **2010,** 43, (1), 55-62.
222. Boyan, B.; Hummert, T.; Dean, D.; Schwartz, Z., Role of material surfaces in regulating bone and cartilage cell response. *Biomaterials* **1996,** 17, (2), 137-146.
223. Flemming, R.; Murphy, C.; Abrams, G.; Goodman, S.; Nealey, P., Effects of synthetic micro- and nano-structured surfaces on cell behavior. *Biomaterials* **1999,** 20, (6), 573-588.
224. JULIANO, R.; HASKILL, S., SIGNAL TRANSDUCTION FROM THE EXTRACELLULAR-MATRIX. *Journal of Cell Biology* **1993,** 120, (3), 577-585.
225. Mousa, S.; Cheresh, D., Recent advances in cell adhesion molecules and extracellular matrix proteins: Potential clinical implications. *Drug Discovery Today* **1997,** 2, (5), 187-199.
226. Curtis, A.; Wilkinson, C., Nantotechniques and approaches in biotechnology. *Trends in Biotechnology* **2001,** 19, (3), 97-101.
227. Lizundia, E.; Saenz-Perez, M.; Patrocinio, D.; Aurrekoetxea, I.; Vivanco, M.; Vilas, J., Nanopatterned polystyrene-b-poly(acrylic acid) surfaces to modulate cell-material

interaction. *Materials Science & Engineering C-Materials For Biological Applications* **2017,** 75, 229-236.
228. Dalby, M.; Gadegaard, N.; Tare, R.; Andar, A.; Riehle, M.; Herzyk, P.; Wilkinson, C.; Oreffo, R., The control of human mesenchymal cell differentiation using nanoscale symmetry and disorder. *Nature Materials* **2007,** 6, (12), 997-1003.
229. Yim, E.; Pang, S.; Leong, K., Synthetic nanostructures inducing differentiation of human mesenchymal stem cells into neuronal lineage. *Experimental Cell Research* **2007,** 313, (9), 1820-1829.
230. Stevens, M. M.; George, J. H., Exploring and engineering the cell surface interface. *Science* **2005,** 310, (5751), 1135-8.
231. Klein, T.; Rizzi, S.; Reichert, J.; Georgi, N.; Malda, J.; Schuurman, W.; Crawford, R.; Hutmacher, D., Strategies for Zonal Cartilage Repair using Hydrogels. *Macromolecular Bioscience* **2009,** 9, (11), 1049-1058.
232. Lawrence, R.; Felson, D.; Helmick, C.; Arnold, L.; Choi, H.; Deyo, R.; Gabriel, S.; Hirsch, R.; Hochberg, M.; Hunder, G.; Jordan, J.; Katz, J.; Kremers, H.; Wolfe, F.; Workgrp, N. A. D.; Workgrp, N. A. D., Estimates of the prevalence of arthritis and other rheumatic conditions in the United States. *Arthritis and Rheumatism* **2008,** 58, (1), 26-35.
233. McCormick, F.; Harris, J. D.; Abrams, G. D.; Frank, R.; Gupta, A.; Hussey, K.; Wilson, H.; Bach, B.; Cole, B., Trends in the surgical treatment of articular cartilage lesions in the United States: an analysis of a large private-payer database over a period of 8 years. *Arthroscopy* **2014,** 30, (2), 222-6.
234. Guo, T.; Holzberg, T. R.; Lim, C. G.; Gao, F.; Gargava, A.; Trachtenberg, J. E.; Mikos, A. G.; Fisher, J. P., 3D printing PLGA: a quantitative examination of the effects of polymer composition and printing parameters on print resolution. *Biofabrication* **2017,** 9, (2), 024101.
235. Guo, T.; Yu, L.; Lim, C.; Goodley, A.; Xiao, X.; Placone, J.; Ferlin, K.; Nguyen, B.; Hsieh, A.; Fisher, J., Effect of Dynamic Culture and Periodic Compression on Human Mesenchymal Stem Cell Proliferation and Chondrogenesis. *Annals of Biomedical Engineering* **2016,** 44, (7), 2103-2113.
236. Vozzi, G.; Flaim, C.; Bianchi, F.; Ahluwalia, A.; Bhatia, S., Microfabricated PLGA scaffolds: a comparative study for application to tissue engineering. *Materials Science & Engineering C-Biomimetic and Supramolecular Systems* **2002,** 20, (1-2), 43-47.
237. Kim, S.; Utsunomiya, H.; Koski, J.; Wu, B.; Cima, M.; Sohn, J.; Mukai, K.; Griffith, L.; Vacanti, J., Survival and function of hepatocytes on a novel three-dimensional synthetic biodegradable polymer scaffold with an intrinsic network of channels. *Annals of Surgery* **1998,** 228, (1), 8-13.
238. Putnam, C.; Hammel, M.; Hura, G.; Tainer, J., X-ray solution scattering (SAXS) combined with crystallography and computation: defining accurate macromolecular structures, conformations and assemblies in solution. *Quarterly Reviews of Biophysics* **2007,** 40, (3), 191-285.
239. Somani, R.; Hsiao, B.; Nogales, A.; Srinivas, S.; Tsou, A.; Sics, I.; Balta-Calleja, F.; Ezquerra, T., Structure development during shear flow-induced crystallization of i-PP: In-situ small-angle X-ray scattering study. *Macromolecules* **2000,** 33, (25), 9385-9394.
240. Khang, G.; Lee, S. J.; Lee, J. H.; Kim, Y. S.; Lee, H. B., Interaction of fibroblast cells on poly(lactide-co-glycolide) surface with wettability chemogradient. *Biomed Mater Eng* **1999,** 9, (3), 179-87.
241. Carman, M.; Estes, T.; Feinberg, A.; Schumacher, J.; Wilkerson, W.; Wilson, L.; Callow, M.; Callow, J.; Brennan, A., Engineered antifouling microtopographies - correlating wettability with cell attachment. *Biofouling* **2006,** 22, (1), 11-21.

242. Peng, R.; Yao, X.; Ding, J., Effect of cell anisotropy on differentiation of stem cells on micropatterned surfaces through the controlled single cell adhesion. *Biomaterials* **2011,** 32, (32), 8048-8057.
243. Kilian, K.; Bugarija, B.; Lahn, B.; Mrksich, M., Geometric cues for directing the differentiation of mesenchymal stem cells. *Proceedings of the National Academy of Sciences of the United States of America* **2010,** 107, (11), 4872-4877.
244. Yim, E.; Darling, E.; Kulangara, K.; Guilak, F.; Leong, K., Nanotopography-induced changes in focal adhesions, cytoskeletal organization, and mechanical properties of human mesenchymal stem cells. *Biomaterials* **2010,** 31, (6), 1299-1306.
245. Thery, M.; Pepin, A.; Dressaire, E.; Chen, Y.; Bornens, M., Cell distribution of stress fibres in response to the geometry of the adhesive environment. *Cell Motility and the Cytoskeleton* **2006,** 63, (6), 341-355.
246. McBeath, R.; Pirone, D.; Nelson, C.; Bhadriraju, K.; Chen, C., Cell shape, cytoskeletal tension, and RhoA regulate stem cell lineage commitment. *Developmental Cell* **2004,** 6, (4), 483-495.
247. Ruiz, S.; Chen, C., Emergence of Patterned Stem Cell Differentiation Within Multicellular Structures. *Stem Cells* **2008,** 26, (11), 2921-2927.
248. Gao, L.; McBeath, R.; Chen, C., Stem Cell Shape Regulates a Chondrogenic Versus Myogenic Fate Through Rac1 and N-Cadherin. *Stem Cells* **2010,** 28, (3), 564-572.
249. Deshpande, B. R.; Katz, J. N.; Solomon, D. H.; Yelin, E. H.; Hunter, D. J.; Messier, S. P.; Suter, L. G.; Losina, E., Number of Persons With Symptomatic Knee Osteoarthritis in the US: Impact of Race and Ethnicity, Age, Sex, and Obesity. *Arthritis Care Res (Hoboken)* **2016,** 68, (12), 1743-1750.
250. Cohen, N.; Foster, R.; Mow, V., Composition and dynamics of articular cartilage: Structure, function, and maintaining healthy state. *Journal of Orthopaedic & Sports Physical Therapy* **1998,** 28, (4), 203-215.
251. Sophia Fox, A. J.; Bedi, A.; Rodeo, S. A., The basic science of articular cartilage: structure, composition, and function. *Sports Health* **2009,** 1, (6), 461-8.
252. YANAGISHITA, M., FUNCTION OF PROTEOGLYCANS IN THE EXTRACELLULAR-MATRIX. *Acta Pathologica Japonica* **1993,** 43, (6), 283-293.
253. Kiani, C.; Chen, L.; Wu, Y.; Yee, A.; Yang, B., Structure and function of aggrecan. *Cell Research* **2002,** 12, (1), 19-32.
254. Guo, T.; Ferlin, K.; Kaplan, D.; Fisher, J., Engineering Niches for Cartilage Tissue Regeneration. In *Biology and Engineering of Stem Cell Niches*, 1 ed.; Vishwakarma, A.; Karp, J., Eds. Elsevier: 2017.
255. Jones, D.; Peterson, L., Autologous chondrocyte implantation. *Journal of Bone and Joint Surgery-American Volume* **2006,** 88A, (11), 2502-2520.
256. Hinckel, B. B.; Gomoll, A. H., Autologous Chondrocytes and Next-Generation Matrix-Based Autologous Chondrocyte Implantation. *Clin Sports Med* **2017,** 36, (3), 525-548.
257. Kon, E.; Filardo, G.; Di Martino, A.; Marcacci, M., ACI and MACI. *Journal of Knee Surgery* **2012,** 25, (1), 17-22.
258. Hurst, J.; Steadman, J.; O'Brien, L.; Rodkey, W.; Briggs, K., Rehabilitation Following Microfracture for Chondral Injury in the Knee. *Clinics in Sports Medicine* **2010,** 29, (2), 257-+.
259. Mainil-Varlet, P.; Rieser, F.; Grogan, S.; Mueller, W.; Saager, C.; Jakob, R., Articular cartilage repair using a tissue-engineered cartilage-like implant: an animal study. *Osteoarthritis and Cartilage* **2001,** 9, S6-S15.
260. Erggelet, C.; Endres, M.; Neumann, K.; Morawietz, L.; Ringe, J.; Haberstroh, K.; Sittinger, M.; Kaps, C., Formation of cartilage repair tissue in articular cartilage defects

pretreated with microfracture and covered with cell-free polymer-based implants. *J Orthop Res* **2009,** 27, (10), 1353-60.
261. Yang, H. S.; La, W. G.; Bhang, S. H.; Kim, H. J.; Im, G. I.; Lee, H.; Park, J. H.; Kim, B. S., Hyaline cartilage regeneration by combined therapy of microfracture and long-term bone morphogenetic protein-2 delivery. *Tissue Eng Part A* **2011,** 17, (13-14), 1809-18.
262. Ferlin, K. M.; Kaplan, D. S.; Fisher, J. P., Separation of Mesenchymal Stem Cells Through a Strategic Centrifugation Protocol. *Tissue Engineering Part C-Methods* **2016,** 22, (4), 348-359.
263. Tang, Q.; Wang, J.; Frank, A.; Lin, J.; Li, Z.; Chen, C.-w.; Jin, L.; Wu, T.; Greenwald, B. D.; Mashimo, H.; Chen, Y., Depth-resolved imaging of colon tumor using optical coherence tomography and fluorescence laminar optical tomography. *Biomedical optics express* **2016,** 7, (12), 5218-5232.
264. Tang, Q.; Liang, C.-P.; Wu, K.; Sandler, A.; Chen, Y., Real-time epidural anesthesia guidance using optical coherence tomography needle probe. *Quantitative Imaging in Medicine and Surgery* **2014,** 5, (1), 118-124.
265. Chu, C. R.; Szczodry, M.; Bruno, S., Animal models for cartilage regeneration and repair. *Tissue Eng Part B Rev* **2010,** 16, (1), 105-15.
266. Garstang, S. V.; Stitik, T. P., Osteoarthritis: epidemiology, risk factors, and pathophysiology. *Am J Phys Med Rehabil* **2006,** 85, (11 Suppl), S2-11; quiz S12-4.
267. BASSO, D.; BEATTIE, M.; BRESNAHAN, J., A SENSITIVE AND RELIABLE LOCOMOTOR RATING-SCALE FOR OPEN-FIELD TESTING IN RATS. *Journal of Neurotrauma* **1995,** 12, (1), 1-21.
268. Yoshil, S.; Ito, S.; Shima, M.; Taniguchi, A.; Akagi, M., Functional restoration of rabbit spinal cord using collagen-filament scaffold. *Journal of Tissue Engineering and Regenerative Medicine* **2009,** 3, (1), 19-25.
269. Rogowska, J.; Bryant, C. M.; Brezinski, M. E., Cartilage thickness measurements from optical coherence tomography. *Journal of the Optical Society of America a-Optics Image Science and Vision* **2003,** 20, (2), 357-367.
270. Han, C. W.; Chu, C. R.; Adachi, N.; Usas, A.; Fu, F. H.; Huard, J.; Pan, Y., Analysis of rabbit articular cartilage repair after chondrocyte implantation using optical coherence tomography. *Osteoarthritis and Cartilage* **2003,** 11, (2), 111-121.